TECHNISCHE UNIVERSITÄT WIEN

# Master Thesis

## RAFT Polymers for Tissue Regeneration

Performed at the Institute of Applied Synthetic Chemistry

Technische Universität Wien

Under the Supervision of

Univ.Prof. Dipl.-Ing. Dr.techn. Robert Liska

and

Projektass. Dipl.-Ing. Dr.techn. Stefan Baudis

by

Patrick Steinbauer, BSc.

Vorgartenstraße 134-138/2/43, 1020 Wien

Vienna, January 18, 2018

‘‘Today progress happens so fast that when someone declares a problem to be completely impracticable and unsolvable in the next moment he is interrupted by someone else who has already solved and realized the problem.’’

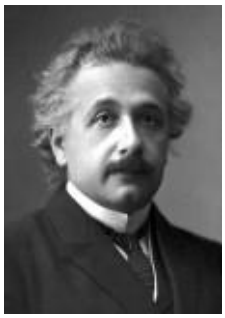

**Albert Einstein**[1]

1879-1955

# Danksagung

In erster Linie möchte ich mich Dr. Robert Liska bedanken, dass er mir die Möglichkeit gegeben hat, meine Diplomarbeit in seiner Arbeitsgruppe zu verfassen. Nicht nur das große Interesse an Polymerchemie war ausschlaggebend dafür, nach meiner Bachelorarbeit nun auch meine Diplomarbeit in deiner Gruppe zu schreiben, sondern auch der einzigartige Teamgeist dieser Gruppe und die offene und freundliche Art der Betreuung, mit der er diese Gruppe führt, waren entscheidende Beweggründe dafür.

Außerdem möchte ich mich bei Dr. Claudia Dworak und Dr. Stefan Baudis, für die Betreuung meiner Diplomarbeit, herzlich bedanken. Sie sind mir immer mit Rat und Tat zur Seite gestanden und hatten immer ein offenes Ohr für mich.

Ein herzliches Dankeschön gebührt auch den Kollegen vom ILSB. Allen voran möchte ich Dr. Philipp Thurner für die sehr kompetente Betreuung meiner Arbeit im Bereich der AFM erwähnen. Ein großes Dankeschön gilt auch Dr. Orestis Andriotis, der mich am AFM-Gerät eingelernt hat und mir stets geholfen hat, sei es bei den Messungen oder auch bei der Auswertung der Daten. Zuletzt auch noch vielen Dank an meinen „Funktionalisierungs-Kollegen“ Dipl. Ing. Andreas Rohatschek, mit dem ich viele Stunden vor dem AFM-Gerät verbracht habe und einige AFM-Chips funktionalisiert habe.

Hiermit möchte ich mich bei allen Personen der Arbeitsgruppe „MC“ für das tolle Arbeitsklima und auch für viele unvergessliche Momente Abseits der Arbeit bedanken. Ein großer Dank gebührt auch der „Jungen Garde“, die mich sofort in die Arbeitsgruppe integriert hat. Ich möchte mich auch bei Sebi, meinem Sitznachbarn, für das tolle Arbeitsklima bedanken.

Ganz speziell möchte ich Sascha danken. Wir haben uns im „Erstsemestrigen Tutorium“ kennengelernt und nun stehen wir beide zur selben Zeit, im selben Team, am Ende des Studiums. Vielen Dank für die gemeinsamen Jahre des Studiums und für die Freundschaft, die noch viele weitere Jahre dauern möge.

Zuletzt gilt mein Dank meiner Familie, meiner Freundin Karin und ganz speziell meinen Eltern. Sie haben immer an mich geglaubt und durch ihere bedingungslose Unterstützung, sowohl moralisch als auch finanziell, haben sie mir den Abschluss und die einzigartigen Jahre des Studiums ermöglicht. Dafür kann ich ihnen nicht genug danken!

# Abstract

The number of patients with minor and major accidents coming into accident and emergency care is steadily rising due to increasing life spans and the aging of our society. In order to ensure efficient care and health of human beings, medical methods need to be optimized. The fixation and adhesion between tissues, implants or scaffolds have to be refined, but the number and versatility of biomimetic and biocompatible adhesives that can be used for such purpose is limited.

In the last few years studies of phosphorus-based polymers have attracted attention because of their large variety of applications. In the field of adhesion promotors and tissue engineering they have been subject of great interest. These phosphorus-based materials are proved to be biodegradable, blood-compatible and led to strong interactions with bones, enamel or dentin.

The problem in measuring the adhesion properties of bone glue is to distinguish between cohesive and adhesive behavior and little information is known from processes at the molecular level.

In this thesis, new approach is to measure the adhesion via single molecule force microscopy (SMFM). Therefore, AFM tips had to be functionalized to investigate the adhesion of two amino acid sequences, of a dopamine compound and of the adhesive block copolymers on different substrates. We were interested in the development of such polymers for adhesion properties. Therefore, phosphorus-containing methacrylates were polymerized via reversible addition-fragmentation chain transfer (RAFT) polymerization. This polymerization technique had proved to be a highly versatile and widely applicable living radical polymerization method. It allows the synthesis of well-defined polymers with different architectures. Hence, it is possible to form a narrow distributed block copolymer. These block copolymers can bind to hydroxyl, carboxylic or amino groups of the organic collagen of a bone and form complexes with $Ca^{2+}$ ions in the inorganic components.

# Kurzfassung

Die Zahl der Patienten mit leichten und schweren Unfällen in der Unfall- und Notfallversorgung nimmt aufgrund der zunehmenden Lebenserwartung unserer Gesellschaft stetig zu. Die Fixierung und Adhäsion zwischen Geweben, Implantaten oder Gerüststrukturen muss verbessert werden, aber die Anzahl und Vielseitigkeit von biomimetischen und biokompatiblen Klebstoffen, die für einen solchen Zweck verwendet werden können, ist begrenzt.

In den letzten Jahren haben Studien von phosphorbasierten Polymeren aufgrund ihrer großen Anwendungsvielfalt viel Aufmerksamkeit auf sich gezogen (Adhäsions-Promotoren und der Gewebszüchtung). Diese phosphor-basierten Materialien erweisen sich als biologisch abbaubar, blutverträglich und führen zu starken Wechselwirkungen mit Knochen, Zahnschmelz oder Dentin. Das Problem bei der Messung der Adhäsionseigenschaften von Knochenklebern liegt in der Unterscheidung zwischen kohäsivem und adhäsivem Verhalten und der geringen Information in Prozessen auf molekularer Ebene. Ein neuer Ansatz in dieser Arbeit ist es die Adhäsion mittels Ein-Molekül-Rasterkraftmikroskopie (SMFM) zu messen. Um die Adhäsion zweier Aminosäuresequenzen, einer Dopamin Verbindung und der adhäsiven Blockcopolymere auf verschiedenen Substraten untersuchen zu können, wurden AFM-Spitzen mit diesen Proben funktionalisiert. Wir waren an der Entwicklung solcher Polymere für Adhäsionseigenschaften interessiert. Daher wurden phosphorhaltige Methacrylate über die RAFT-Polymerisation (Reversible Addition-Fragmentation chain Transfer) synthetisiert. Diese Polymerisationstechnik erweist sich als eine äußerst vielseitige und weithin anwendbare lebende radikalische Polymerisationsmethode. Diese Technik ermöglicht die Synthese von wohldefinierten Polymeren mit modifizierbaren Strukturen und Polymeren. Daher ist es möglich, eine enge Molekulargewichtsverteilung von Blockcopolymeren einzustellen und verschiedene Polymerarchitekturen herzustellen.Diese Blockcopolymere können an Hydroxyl-, Carboxyl- oder Aminogruppen des organischen Kollagens eines Knochens binden und Komplexe mit $Ca^{2+}$-Ionen in den anorganischen Komponenten bilden.

# Table of contents

# Introduction

## 1 Bone Structure and Bone Adhesives

### 1.1 Bone: Structure and Healing

Bone is a dynamic, mineralized and highly vascular tissue, characterized by its hardness, growth mechanisms and its capacity to heal and remodel itself.[2] Bone is responsible for several key functions within the body, such as protection of vital organs, maintenance of mineral homeostasis, generation of red and white blood cells for immune reaction and oxygenation of other tissues, and storage of calcium, phosphate and other important ions.[2]

Histologically, bones can be classified into two types according to their architecture: cortical bone, which is very dense and cancellous or trabecular bone, also known as spongy bone, which consists of a network of struts. The bone marrow is located inside this spongy structure and constantly reproduces our blood cells. The mechanical properties[2] of those two types of bone are shown in Table 1.

***Table 1: Mechanical properties of cortical and cancellous bone***

| | ***Porosity [%]*** | ***Young's modulus [GPa]*** | ***Tensile strength [MPa]*** | ***Compressive strength [MPa]*** | ***Bending strength [MPa]*** |
|---|---|---|---|---|---|
| ***Cortical bone*** | 5-30 | 15-20 | 50-150 | 100-200 | 250 |
| ***Cancellous bone*** | 30-90 | 0.1-2 | - | 2-20 | - |

A healthy adult human body consists of 206 bones of various shapes and sizes. About 80 wt% of an adult skeleton is made up of cortical bone and the remaining 20 wt% is formed of cancellous bone.[3]

Bone as an organ consists of the bone matrix, which provides mechanical strength, the bone cells, which are responsible for maintaining the structure of the matrix and the bone marrow with the vascular network.

Bone belongs to the group of connective tissues, which have small numbers of cells and much more extracellular matrix than other tissues.[4] The extracellular matrix is composed of an organic phase and an inorganic biomineral phase. The organic part of bone consists of 90% type I collagen, a fibrillary protein which provides the framework of the human skeleton. The remaining 10% are made up of other proteins and polysaccharides. The main inorganic phase within the bone matrix is a biological analogue of the mineral hydroxyapatite (HA) with the composition $Ca_5(PO_4)_3OH$ and a hexagonal crystal structure. These crystals are 20-80 nm long and 4-5 nm thick and together with collagen fibrils they organize first into parallel ordered layers (lamellae) and then into cylindrical structures called osteons.[5] A central neurovascular canal (Haversian canal) is running through these osteons (see Figure 1).[6]

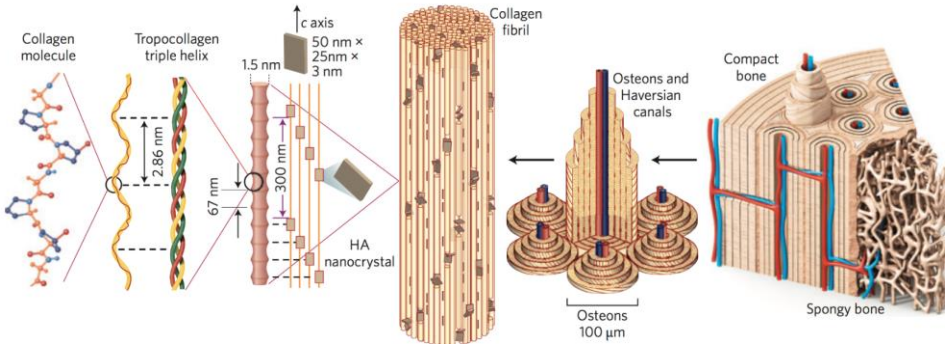


***Figure 1: Architecture of bone[7]***

The most prominent non-collagenous organic constituents of bone matrix are four proteins: bone sialoprotein (BSP), osteopontin (OP), osteocalcin (OC) and osteonectin (ON). These proteins were produced by bone cells and they are involved in regulating bone mineralization and remodelling.

Due to injuries, diseases and surgical interventions, defects in bone can occur, indeed bone has a unique capacity to heal and remodel without leaving a scar. Natural bone healing takes a long period of time, in consequence of the decrease in blood supply at the fracture site and the need of calcium and phosphorus to strengthen and harden new bone. The duration of bone regeneration can be affected by numerous factors, such as metabolic factors, hormones, nutrition, genetics, age, activity stress and other diseases.[8]

In order to promote **bone regeneration and healing** it is important to understand the process of bone remodelling. It allows bone to respond to

different biomechanical cues and stresses, to repair small damages and maintain the serum ion and mineral concentrations.[9-10] Bone remodelling is the continuous resorption of bone by osteoclasts followed by the deposition of new bone by osteoblasts. Bone resorption and formation are strictly regulated to prevent excessive bone resorption leading to osteoporosis.

Bone fractures typically heal and remodel via the following steps and processes (see Figure 2).[9, 11]

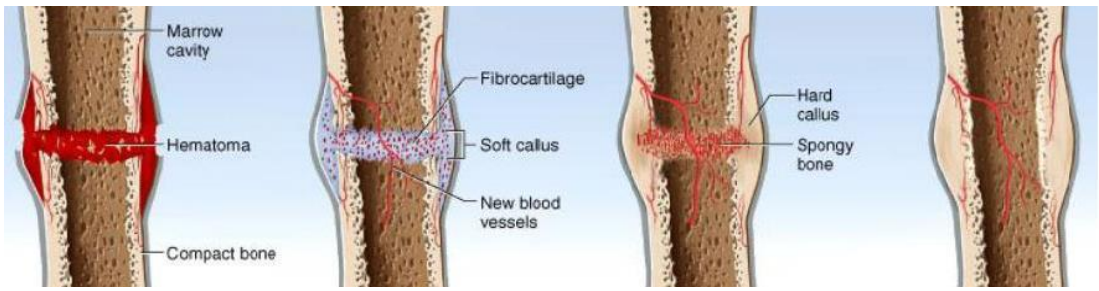


a) b) c) d)

***Figure 2: Processes of fracture healing[12]***

First a fracture clot and hematoma is formed at the side, leading to swelling and inflammation. Osteoclasts remove the debris and dead cells and the hematoma is converted to granulation tissue by invasion of cells and blood capillaries (Figure 2a). The infiltration of blood vessels forms a procallus, which is invaded by fibroblasts. These fibroblasts produce collagen fibrils to connect the broken ends of the bone. A soft callus is formed (Figure 2b). For the hard callus formation osteoblasts deposit a temporary bony collar around the fracture to unite the broken pieces while ossification occurs (Figure 2c). In the last step bone remodelling takes place (Figure 2d). Small bone fragments are removed by osteoclasts, while osteoblasts deposit trabecular bone and convert it to cortical bone.

## 1.2 Bone Adhesives

Nowadays, quality of life plays an important role in aging society, while suffering a variety of life-threatening diseases and accidents. In order to ensure efficient care and health of human beings medical methods need to be optimized. For example, fixation and adhesion between tissues, implants or

scaffolds have to be refined, but the number and versatility of biomimetic and biocompatible adhesives that can be used for such purpose is limited.

The development of adhesives and bone glues can be traced back many centuries.[13] The difficulties are special requirements[14] to bone glues and different fields of applications. Bone adhesives must be non-toxic and biocompatible to be eligible for clinical application in trauma and orthopedic surgery. Furthermore, they should not irritate the surrounding tissue, be biodegradable in a certain time and during polymerization heat development must be minimal. Of course the adhesive must bind in moist environment, so high bonding strength *in situ* is important. Moreover, easy preparation, practicability and applicability, minimal compression of volume, storage stability and efficiency are relevant facts.

Therefore, the actual applicability of bone adhesives is restricted to few specific indications so far. In the past, tested bone adhesives could not meet the requirements and failed either in biocompatibility, degradability or in poor composite strength. Bone adhesives can be classified in synthetic, biological, current and future developments (see Table 2).[14]

***Table 2: Classification of bone adhesives***

| | |
|---|---|
| **Synthetic bone adhesives** | Epoxy resins |
| | Polyurethane foams |
| | Cyanoacrylates |
| | Polymethylmethacrylates (PMMA) |
| **Biological bone adhesives** | Fibrin adhesives |
| | Gelatin-resorcin-aldehydes |
| | Protein-aldehyde-systems |
| **Current and future developments** | Adhesives based on peptides (mussels proteins) |
| | Alkylene bis(oligolactoyl) methacrylates |

As mentioned above **epoxy resins** belong to synthetic bone adhesives. In 1958 Bloch[15] reported the usage of Araldite (diclycidylether of epichlorhydrine and bisphenol-A, see Figure 3) as bone glue for fractures at the forelegs of twenty sheep. In eight cases inflammation or low adhesion on moist fragments occurred.

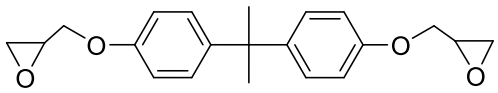

***Figure 3: Structure of Araldite***

In 1960 Nigst *et al.*[16] has glued tibia fractures of rabbits with epoxy resins.[17] In further studies done by Rietz[18] the weakness of this materials as exposed. Ritz found epoxy resins initiate fibrotic capsule around the adhesive, act as barrier to callus formation, do not adhere to the bone due to moisture, lipids or blood, and cause tissue necrosis because of polymerization heat.[13]

In 1959 a **polyurethane** foam, called Ostamer, was used for gap filling and splinting of fractured bones.[17, 19] The material is a segmented polyurethane from polycaprolactone (PCL) with MDI (4,4'-diphenylmethane diisocyanate) using 1,4-butanediol as chain extender (see Figure 4).

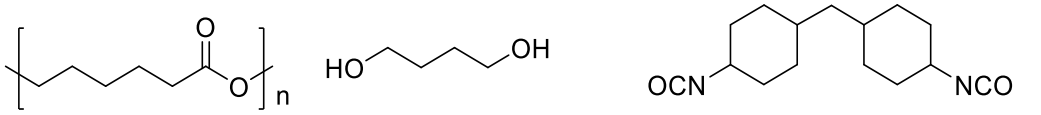


***Figure 4: Monomers of Ostamer***

Unfortunately, the material used in animal and human bodies was highly unsatisfactory.[20] Although Ostamer shows no toxicity in the surrounding tissue,[21-22, 23] studies showed too high polymerization temperature[18] as well as weak adhesion in moist milieu.[17] Furthermore, infections,[14] tissue necrosis[21] and delays in scar formation[24] were observed.

**Cyanoacrylate adhesives** were developed by Coover Jr[25] in 1959. Nowadays they are known as the commercial available instant glue. The longer the alkyl chain of 2-cyanoacrylate esters (see Figure 5), the lower is the bonding strength and the toxicity of the compound. In contrast, elasticity and polymerization time increase.[26] Thereby, n-octyl esters and n-butyl esters show lower toxicity, but for surgical adhesives they were not suitable due to their lower bonding strength.

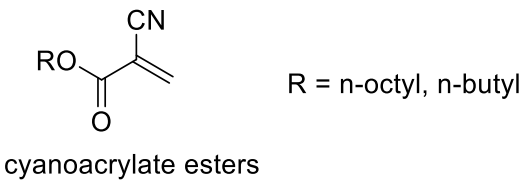


***Figure 5: Structure of cyanoacrylate esters***

In 1963 the former Soviet Union promoted the development of cyanoacrylate bone adhesives. Reports of displacement of the glued fracture ends were followed by reports of high infection rates and toxic by-products (cyanoacetic acid, formaldehyde).[27]

Since the 1930s **polymethylmethacrylates (PMMA)** (see Figure 6) has been widely used in dentistry.

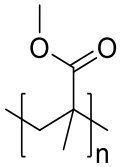


poly(methyl methacrylate)

***Figure 6: Structure of PMMA***

First, Charnley[28] has used PMMA for the fixation of total hip arthroplasty. Thereby, problems with polymerization heat and toxicity occurred. But Hulliger[20] has shown that cured methacrylate was well tolerated for cell cultures. Furthermore, significant dislocation at the glued fracture appeared on spines.[29-30]

However biopolymers were the first biodegradable materials to be used clinically. They possess several advantages such as bioactivity, the ability to present receptor-binding ligands to cells and natural remodeling.
The use of **fibrin adhesives** goes back to 1940 and now they are the most popular soft tissue adhesives.[30-31] The most popular fibrin sealant is called Tisseel.[32-33] The advantages are no heat development and fast curing time.[17]
The fibrin sealant consists of fibrinogen and thrombin which were applied to the tissue to stop blood clotting. The enzyme thrombin converts fibrinogen into fibrin monomers and after a few seconds it cross-links (see Figure 7).

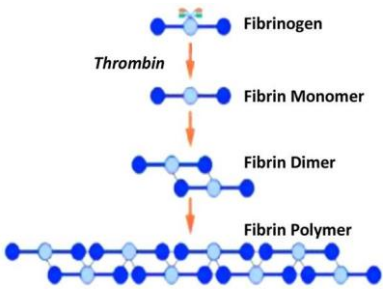


***Figure 7: Cross-linking of fibrin sealants through thrombin***

**Gelatin-Resorcinol-Aldehyde (GRF) adhesives** were developed by Cooper and Falb.[34] Resorcin and formaldehyde react to a 3D-network while gelatine was used as filler. Gelatin is cross-linked via the amines in the lysine side chains with formaldehyde (see Figure 8a), whereas the resorcinol groups are linked via electrophilic aromatic substitution (see Figure 8b).[35]

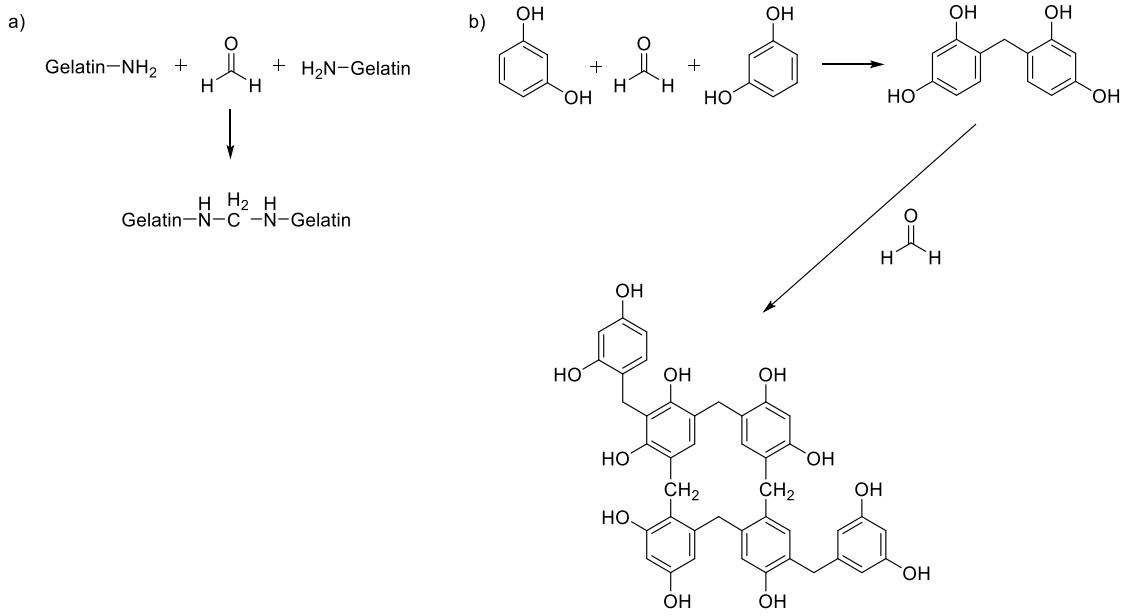


***Figure 8: The mechanism of the gelatin-resorcinol-aldehyde adhesive with a) the cross-linking of gelatin by formaldehyde and b) the formation of resorcinol networks by formaldehyde***

In further developments formaldehyde was replaced by glutaraldehyde or glyoxal. These adhesives were applied for reconstruction of aortic valves, but not for fracture treatment.

In GRF adhesives the proteins act as filling materials, while in **protein-aldehyde systems** they serve as reactive, cross-linking components.[36] The aldehyde molecules cross-link protein molecules to each other and create a flexible mechanical seal. These systems have not been tested for bone adhesion applications. In 1998 a protein-aldehyde system called BioGlue was tested for the repair of acute thoracic aortic dissection.[15] Nowadays, it is applied for surgical sutures.

The **current and future developments** are discussed in the State of the Art (chapter 1 in the General Part).

# 2 Free radical polymerization

Poly(methylmethacrylate) (PMMA) is widely used in dentistry as described before. In addition to that, is also used as bone cement for implant fixation in various orthopedic and trauma surgeries.[37] Generally, methylmethacrylate is polymerized via free radical polymerization (FRP).[38-39]

More than half of all commercially available polymers were synthesized by free radical polymerization. The reaction of this versatile method can be performed in bulk, solution or dispersed media like emulsion or suspension. A wide range of monomers (e.g. vinyl chlorines, vinyl acetates, styrenes, (meth)acrylates and acryl nitriles) is susceptible for this polymerization method.

A radical polymerization process includes four steps.[40] Once primary radicals $R_I^\bullet$ are formed (**initiation step**), the actual start of the polymerization occurs by the addition of $\mathbf{R_I^\bullet}$ to the double bond of a monomer **M**, leading to the formation of $\mathbf{M_1^\bullet}$, the chain-starting radical. The subsequent step is the propagation, where the polymer starts to grow by adding more and more monomer units **M** to the (polymeric) radical $\mathbf{P_1^\bullet}$. Thereby two types of addition are possible (**propagation step**). In general, the 1,3-addition (head-to-tail) is preferred over the 1,2-addition (head-to-head), so polymers obtained via FRP show a high amount of head-to-tail structures. **Termination** in radical polymerization processes is possible either by combination or disproportionation, depending on the type of monomer and the reaction temperature. At low temperatures, combination is more likely to happen, resulting in an increase of molecular weight. At higher temperatures disproportionation is favored, whereat the molecular weight stays unchanged. **Transfer reactions** of the radicals may occur during the polymerization process, which results in branching of the polymers. Depending on whether inter- or intramolecular transfer happens, long chain and short chain branching, respectively, can be observed.

Beside all the advantages of FRP, a major drawback occurs when it comes to the preparation of polymers with a complex structure and defined molecular weight as well as molecular weight distribution. Additionally, it is not possible to prepare copolymers with specific monomer composition. Therefore,

controlled radical polymerization techniques have been developed in the past decades.

# 3 Controlled radical polymerization

Controlled radical polymerization (CRP) techniques open up new ways in the field of polymer synthesis concerning functionality, topology and compositions.[41] In general, all CRP methods are based on a dynamic equilibrium between a dormant, which is unable to self-terminate or propagate, and an active species, present at low concentration, during polymerization. Further characteristics are a first-order kinetic plot, the pre-determination of the molecular weight by the initial concentration of monomer and controlling species and the possibility to synthesize telechelic polymers.[40] Figure 9 shows the difference of molecular weight distribution of FRP and Reversible Addition Fragmentation-chain transfer polymerization (RAFT), an important CRP technique.

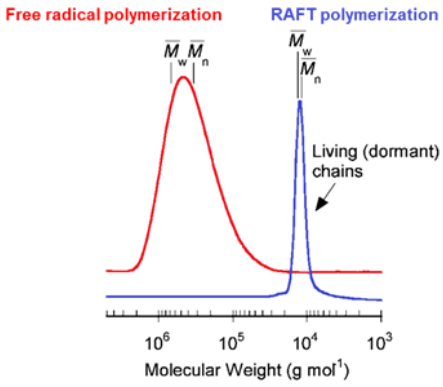


***Figure 9: Typical size exclusion chromatography traces and resulting molecular weight distributions for the polymerization of styrene via FRP (red) and via RAFT polymerization (blue)[42]***

The self-regulation of CRP can be guided either by a deactivation/activation process with a stable radical (Stable Free Radical Polymerization SFRP), an organometallic compound as in nitroxide mediated polymerizations (NMP) or in atom transfer radical polymerizations (ATRP). This type of polymerization kinetics is called **Persistent Radical Effect (PRE)**. The model is explained by Fischer[43-44] and describes the high selectivity in radical processes. The self-regulation of CRP can also be directed by a bimolecular degenerative transfer by the addition of transfer agents as in RAFT polymerization.

The living radical polymerization methods based on PRE stand in contrast to the techniques which work according to the principle of the **degenerative transfer (DT)** (see Figure 10).[41]

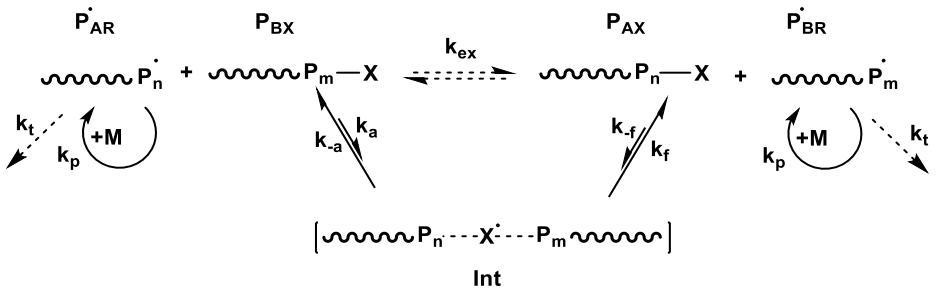


***Figure 10: Principle of the degenerative transfer[41]***

The DT is based on the exchange of the active center between the active and dormant species via reversible chain transfer.[45] Therefore, several mechanisms are possible, but the transfer has to proceed very fast compared to the propagation in order to obtain polymers with narrow molecular weight distribution.[46] The relocation can succeed directly or via short-lived intermediate (Int). Thereby, the radical is transferred from the active polymer chain $P_{AR}^{\bullet}$ to the dormant species $P_{BX}$, where $P_{AX}$ and $P_{BR}^{\bullet}$ are formed.

One of the polymerization techniques which follow the degenerative transfer is for example the **Iodine-Transfer Polymerization (ITP)**, where iodines are used to transfer the radical to the dormant species.[47] The most prominent type of these techniques is the Reversible Addition Fragmentation-chain Transfer polymerization (RAFT).

# 4 RAFT polymerization

Reversible Addition Fragmentation-chain Transfer polymerization (RAFT) is a quite young polymerization technique and it attracts more and more attention over the years.[48] This method was established by the Australian CSIRO group[49-50] in 1998 and French researchers in 1999.[51-52]

The RAFT polymerization technique opens new possibilities regarding reaction conditions and polymer architectures. The advantages of RAFT over CRP methods are: lower reaction temperatures can be applied in contrast to NMP and compared to ATRP, no transition metal catalyst is needed.[53]

The **RAFT mechanism** consists of several reaction steps.[54] As above mentioned RAFT polymerization relies on the DT mechanism, characterized by an addition-fragmentation step.[54]

The first step is the **initiation**, where radicals have to be formed in order to start the polymerization. These radicals can be formed by thermally triggered homolytic cleavage of a covalent bond of initiator molecules like azo compounds, by photoinitiators or redox initiator systems. The most common thermal initiators are azobis(isobutyronitrile) (AIBN) or 4,4'-azobis(4-cyano-valeric acid) (ACVA).[55-56] The formed radical is able to initiate the polymerization by addition to an olefinic group of a monomer. Successively a polymeric radical is formed (see Figure 11).[48]

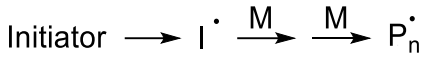


***Figure 11: Initiation step of radical induced polymerization[48]***

In order to control the reaction and the molecular weight distribution to perform controlled radical polymerization a specific molecule is needed. In RAFT polymerization the controlling molecule is called **RAFT agent** or chain transfer agent (CTA). The used CTAs are thiocarbonyl compounds, which contain a reactive double bond as well as a weak single bond (see Figure 12).[57]

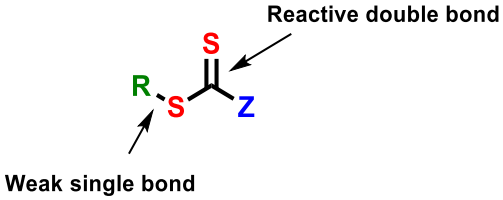


***Figure 12: General structure of RAFT agents[58]***

The suitability of the RAFT agent for a specific monomer type (e.g. acrylates, acrylamides) can be ensured by varying the R- (green) and Z-group (blue). Depending on the Z-group, the RAFT agent can be assigned to one of the four general structures (see Figure 13).[57]

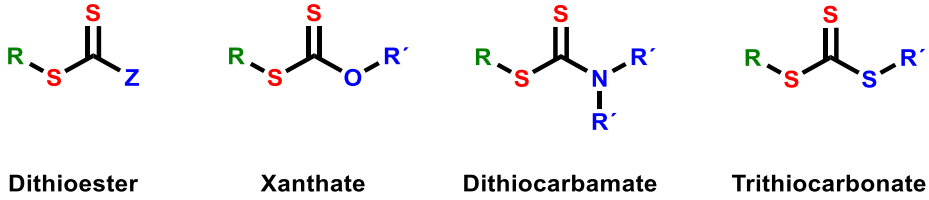


***Figure 13: Different structures of chain transfer agents***

The Z-group plays a very important role concerning the reactivity of the thiocarbonyl group and the role of the R-group has to show high capability of acting as a homolytic leaving group, being responsible for the re-initiation of the polymerization.[59]

In the **pre-equilibrium** reaction step the DT mechanism is involved. Due to the use of a RAFT agent (CTA), the $P_n^{\bullet}$ radical adds to the thiocarbonyl group and forms a intermediate radical, which decomposes subsequently into dormant species and a new radical with the leaving group $R^{\bullet}$ (see Figure 14).[48]

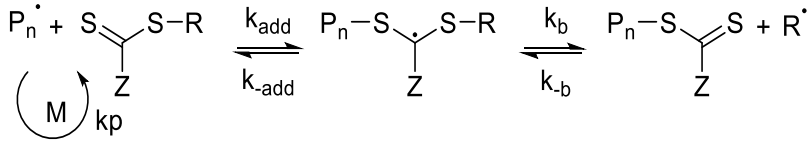


***Figure 14: Reversible chain transfer and propagation in RAFT polymerization[48]***

The next step is a **re-initiation** step. The $R^{\bullet}$ adds to the double bond of the monomer M and a new radical R-M$^{\bullet}$ is formed. By the addition of further monomer molecules the polymer radical $P_m^{\bullet}$ is generated(see Figure 15).[48]

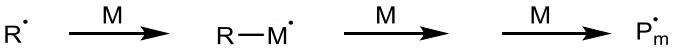


***Figure 15: Re-initiation step of the RAFT polymerization[48]***

In the **main equilibrium** the propagating radical $P_m^{\bullet}$ of the re-initiation step is able to react with the dormant species from the previous pre-equilibrium to form a new intermediate. The following fragmentation generates a dormant species and a new released radical $P_n^{\bullet}$, which is able to propagate again (see Figure 16).[54]

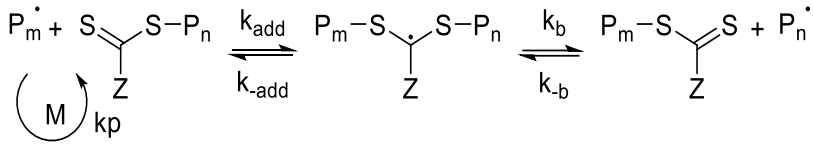


***Figure 16: Main equilibrium and propagation in RAFT polymerization[48]***

**Termination** processes may occur in RAFT polymerization as well as in free radical polymerization. When two polymeric radicals $P_n^{\bullet}$ and $P_m^{\bullet}$ react with each other they are called dead chains (see Figure 17). In order of low radical concentration, by the use of small amounts of radical initiator, these termination processes occur very infrequently. Furthermore, a higher amount of radicals is existent in the dormant state.[48]

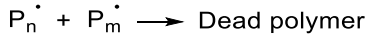


***Figure 17: Termination reaction in RAFT polymerization[48]***

RAFT polymerization can be used for the preparation of different polymer architectures (e.g. block copolymers[60-62], graft and comb polymers[63-64], star polymers[65-67], hyper branched[68-69] and dendritic polymers[70-71]) out of several types of monomers under various reaction conditions.

The **synthesis of block copolymers (BCP)** has attracted more and more attention over the past decades, because they show a high potential for usage in many different fields (e.g. biomedicine[72], nanotechnology[73]). In this chapter only the synthesis of block copolymers via RAFT polymerization is thematized. Generally, there are two possibilities for the synthesis of block copolymers via RAFT polymerization (see Figure 18).[53] The first one is a one pot synthesis. Thereby, the controlled polymerization of monomer A with RAFT agent is started by an initiator I. After the completion of the first block, the second monomer B and a small amount of initiator are added to the reaction mixture. The polymerization comes to an end when the formation of the block copolymer is finished. Due to this method it is not only possible to prepare diblock polymers, but also multi block copolymers.[74] Nevertheless, some requirements have to be fulfilled to allow the synthesis via this route. In order to avoid irregular propagating polymers, the crossover has to happen fast and in a quantitative way. Thereby, the order of added monomers has to be considered.

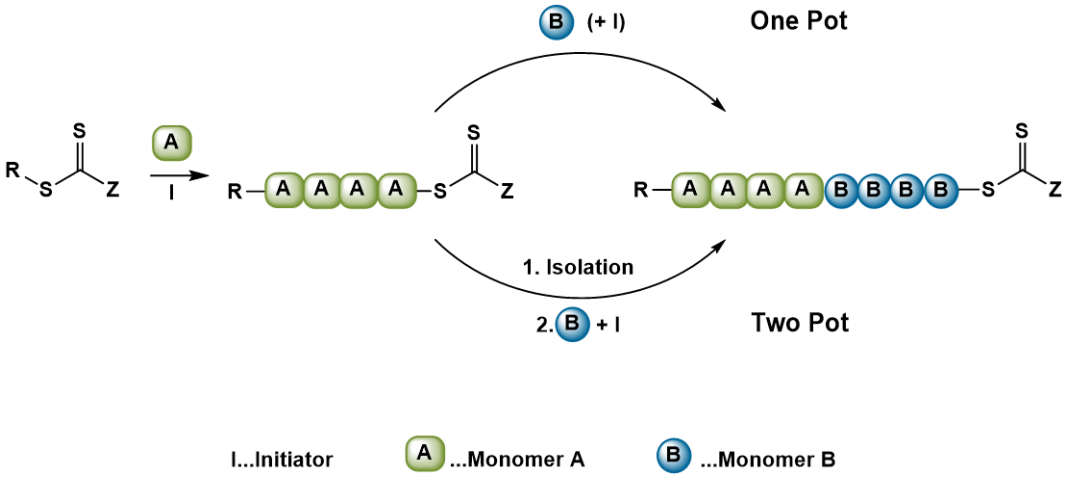


***Figure 18: Synthesis of a block copolymer via RAFT polymerization***

If the one pot pathway is not possible, the synthesis of block copolymers can also be performed in a two pot procedure. The first step, the synthesis of the homopolymer, is done in the same way as by choosing the one pot path. In contrast to that, the polymer is isolated (e.g. by precipitation) to obtain a so called macro RAFT agent, which can be used for the synthesis of the second block by mixing it with some more initiator and monomer B.

# 5 Atomic Force Microscopy

The adhesion properties of bone glues or adhesives in general can be determined via tensile tests or contact angle measurements. Moreover, pull-off experiments and macroscopic lap shear bond strength measurements can be done to obtain adhesion properties.[75] The problem in many cases is, to distinguish between cohesive and adhesive behavior and there is little information at the molecular level. This is where atomic force spectroscopy can be used to get more information microscopically.

## 5.1 The Atomic Force Microscope

The atomic force microscope (AFM), was first described in 1986 by Binnig *et al.*[76] and belongs to the scanning probe microscope (SPM) family.
The AFM was initially developed to measure sample topographies. Figure 19 shows the typical setup and basic principle of AFM.

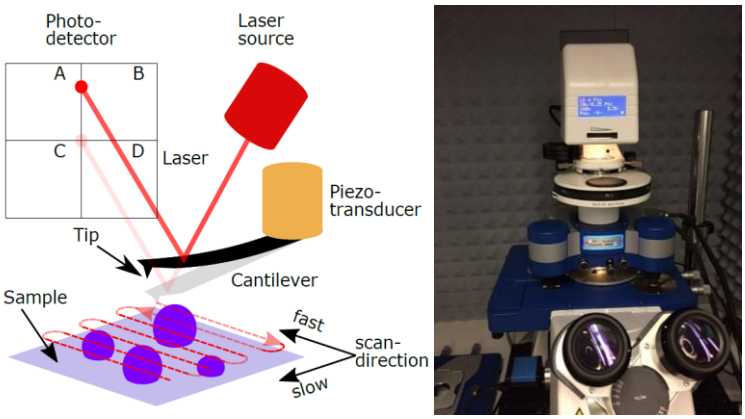


***Figure 19: Typical AFM setup[77]***

The AFM working principle is the measurement of force between a tip and the sample surface using special probes made by an elastic, spring-like cantilever with a sharp tip on the end. The cantilever is carried by a piezo element. The force applied to the tip by the surface, results in bending of the cantilever. By the measurement of the cantilever deflection, it is possible to determine the tip-surface interaction force. This technique allows mapping of the surface topography at sub-nanometer resolution. The fact that it is possible to modify the surface and manipulate individual molecules, makes AFM an ideal tool for biological applications.[78]

## 5.2 Technical requirements

The nowadays used **cantilevers** were invented by Wolter *et al.*[79] and C.F.Quate [80-82]. As mentioned above the cantilever with its tip is one of the major parts of the AFM and it can be seen as mechanical spring. The cantilevers are attached to the AFM chips. The commercial available materials for cantilevers are silicon, silicon nitride and gold coated silicon.[83] They are fabricated by micro-electro-mechanical-system (MEMS) technology which contains lithography and etching steps.[84] The AFM-chips are by convention 3.4 x 1.6 mm in size and about 0.5 mm thick,[85] so that probes from different manufacturers can be used in most probe holders. The cantilevers are available with different spring constants (e.g. stiffness) in the range of 0.005 N $m^{-1}$ to 450 N $m^{-1}$.[86-87] Furthermore, the cantilevers are also available in different shapes (e.g. V-shaped, rectangular, triangular) as it can be seen in Figure 20.

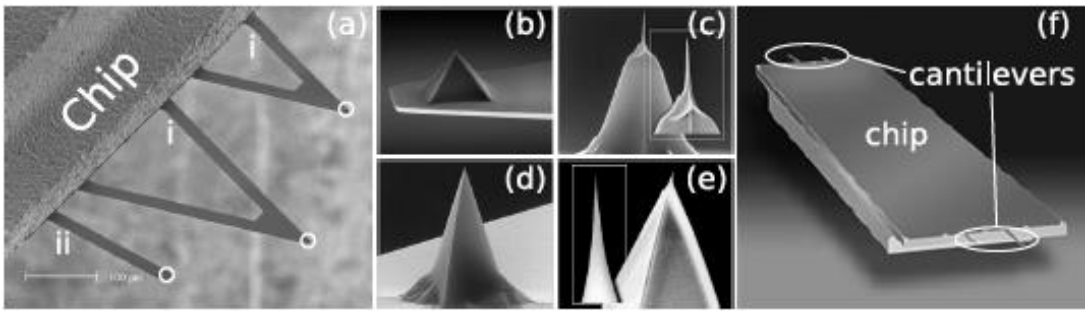


***Figure 20: (a) Different shapes of cantilevers: V-shape (i), rectangular (ii)[88], (b)-(e) different tips[89-92], (f) chip with four rectangular cantilevers[91]***

As mentioned above, the AFM-tip is brought into contact with the surface or close enough to recognize long- or short-range surface forces (e.g. Van der Waals forces). Afterwards the cantilever scans over the sample row-by-row. Thereby, the cantilever is bent with respect to the sample's topography. The bending can be translated into a high-resolution image of the surface using different detection methods like the optical lever-, the interferometry-, the capacitive sensor- and piezoresistive/piezoelectric method. The **optical lever technique** is the most commonly one[83] and relies on a laser beam which is reflected from the upper side of the cantilever towards a photodetector.

The deflection of the cantilever is proportional to the force. Once the deflection of the cantilever is known as a distance (D), the spring constant (k) is needed

to convert this value into force (F). Therefore, the well-known Hooke's law can be used (see Equation 1).

$$F = -kD$$

***Equation 1: Hooke's law - Calculation of force out of spring constant and deflection of the cantilever***

For quantitative force measurements, the spring constant of the cantilever must be calibrated, to determine the **stiffness of the cantilever**. The cantilever stiffness depends on the material properties and the shape with typical values of $10^1$-$10^5$ pN $nm^{-1}$. The calibration is necessary as manufacturers provide them with large fluctuation margins. There are several different possibilities to calibrate the spring constants of cantilevers. These can be obtained through comparison with a reference cantilever of known stiffness, through calibration using thermal vibrations (thermal noise[77]), by the method of added particle masses, or by combining measurements of the resonant frequency with the cantilever physical dimensions and material properties.
Soft cantilevers are susceptible to thermal fluctuations, and the AFM can be used to measure and analyze the movements. The thermal noise spectrum is a plot of the cantilever fluctuations as a function of frequency.[93]

## 5.3 Force distance Measurements

As already mentioned, besides the imaging possibilities of AFM, quantitative force measurements of tip and sample interactions can be determined. In an AFM force experiment, the AFM-chip is moved vertically at a constant z-piezo velocity to the sample surface until contact. In order to measure the deflection of the cantilever a force (F) - distance (cantilever bending $\Delta Z$) curve can be generated. A typical force curve is depicted in Figure 21. The force-distance curve starts with point a. From a-b the AFM tip goes downwards. At point b the tip is very close to the sample surface and at some point the tip jumps to contact the substrate, due to capillary forces (b-c). The next segment (c-d) in the force-distance curve is the slope in the contact region which is a function of the elastic modulus and geometries of the tip and the sample.[94] The opposite movement of c-d is d-e, where the tip is withdrawn. The further course

of the curve (e-f) shows the sample retraction and the adhesion force (f-g), where the cantilever overcomes the adhesion forces and pulls off sharply.

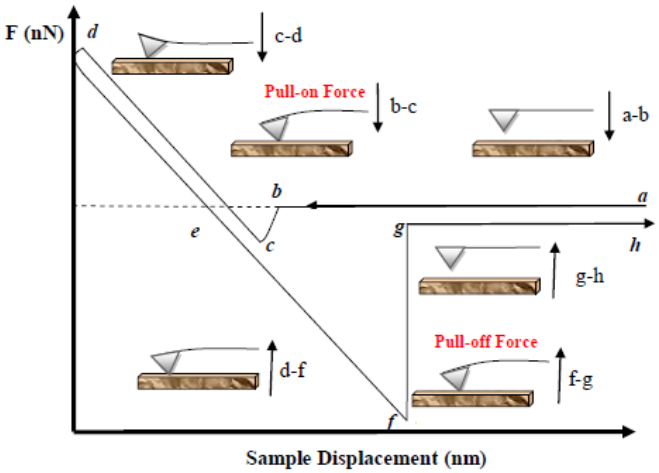


***Figure 21: Force curve with approach (a-d) and retraction (d-h)[95]***

## 5.4 Single-molecule force microscopy

Through the development of new experimental tools in the last 20 years the measurement of forces in the pN range became possible, which allows mechanical experiments with single molecules. Nowadays several techniques differing in force- and dynamic ranges are available. The most prominent techniques are magnetic beads,[96] optical tweezers,[97-99] glass microneedles,[100] the biomembrane force probe (BFP)[101] and AFM.

Single-molecule force microscopy (SMFM)[102] is a way of measuring the nano-mechanical behavior of single molecules adhering to specific substrates. In addition to that, SMFM employs functionalized cantilevers and substrates to detect individual adhesion or unfolding events, for example antibody-antigen recognition[103] or the unfolding of domains on globular proteins such as titin[102]. When the functionalized tip approaches to the substrate, interaction starts to occur at some point. Afterwards the cantilever starts to slowly move upwards. If everything works well, the sample starts to adhere to the surface. As a consequence, the cantilever starts to bend. If the cantilever's spring constant is known, the appropriate force can easily be calculated. Nevertheless, at some point the acting force is too large and the adhesion motif is torn apart from the surface. The process will be monitored in form of force-distance diagrams and the adhesion force can be calculated.

# Objective

In consequence of, the increasing life expectancy, larger numbers of injuries and diseases will occur. Due to the rising demand of fixation and adhesion between tissues, implants or scaffolds, adhesive materials need to be developed and optimized.
Up to now adhesives based on cyanoacrylates, polyurethanes, epoxy resins or poly(methlymethacrylates) still bear several drawbacks ranging from possible allergic response, lack of mechanical strength to toxic side products. Therefore, new biomimetic glues for bonding of tissue-tissue and tissue-implant interfaces will urgently be needed.

The problem in measuring the adhesion properties of bone glue is to distinguish between cohesive and adhesive behavior and the little information at the molecular level. A new approach will be, to measure the adhesion via single molecule force spectroscopy (SMFS) referring to Messersmith *et al.*[104]. In particular, a procedure based on this approach has to be established to graft a single molecule on the tip of an AFM cantilever. In SMFS experiments the AFM tip works as sensor, which is able to measure forces in pN range (see Figure 22).

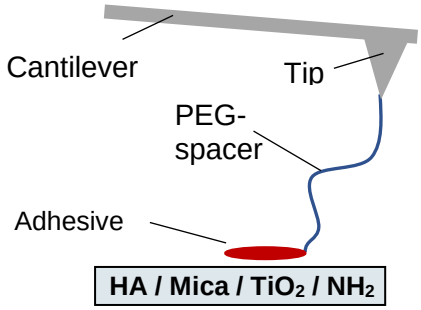


***Figure 22: Schematic model of the single-molecule AFM pulling experiment***

In particular, the aim of this work is to functionalize AFM tips in order to investigate the adhesion of the amino acid sequences D(pS)(pS)EEK and DSSEEK, of a dopamine compound and of adhesive block copolymers, synthesized via RAFT polymerization on various substrates. These should be mica with well-known chemical and physical properties, hydroxyapatite (HA) to replicate the mineral part of the bone, $TiO_2$ to mimic implants and a coated $NH_2$ surface to mimic amino end groups as found in bone proteins.

# General Part

## 1 State of the Art

Strength and toughness of healthy bone are traditionally correlated to bone mineral density, i.e. the density of calcium phosphate in form of hydroxyapatite (HA). However, it is currently acknowledged that the organic components of bone, for example fibrils of collagen type I and non-collagenous proteins (NCPs), are also important determinants of the mechanical competence of bone.[105] That NCPs impact mechanical properties seems obvious from their role in determining ultrastructural assembly of bone by controlling HA crystal nucleation, shape, and size, as well as attachment between collagen and HA crystals. So far, the specific motifs within NCPs responsible for ultrastructure organization are still largely unknown. The NCPs are the nanoscale engineers of bone tissue providing specific attachment to collagen type I fibrils and HA crystals (see Figure 23).[106-109]

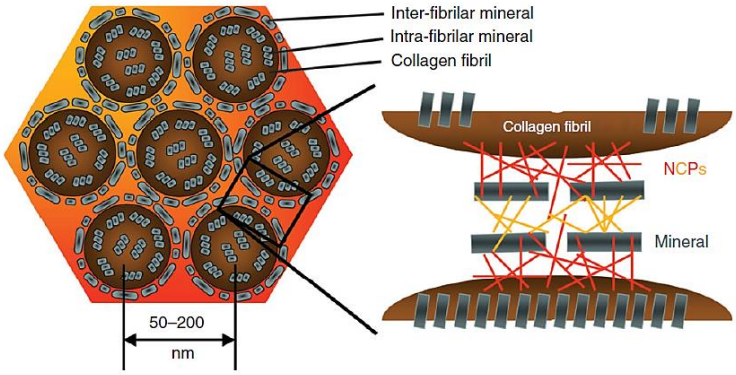


***Figure 23: Nanoscale model of bone***

Whereas a collagen-binding domain has been found in bone sialoprotein (BSP), especially there is known very little about the specific motifs facilitating attachment of NCPs to HA. However, Stayton *et al.*[110] have found a strategy for determining the statherin structure on hydroxyapatite and they have achieved results about the N-terminal domain. The N15-domain of statherin was characterized at six labeled positions ranging from the N-terminus to near the C-terminus. On the one hand, the peptide is strongly bound at the acidic N-terminus which contains a helical domain (**sequence D(pS)(pS)EE**). But on the other hand, the peptide is mobile and dynamic at the middle and C-terminal

regions. This achievements gained from the structural and dynamic studies of N15 peptides led to the development of new bioactive peptide coatings for biomaterials[111]. Further studies about these peptide sequences of the full-length statherin were reported by Long *et al.*[112]

The N15 domain of statherin recognizes hydroxyapatite through the N-terminal acidic pentapeptide sequence that contains two phosphorylated serines and three carboxylate-containing side-chains. Long *et al.*[112] showed a molecular model consistent with the current structural and dynamic studies (Figure 24). They suggested that especially the negatively charged phosphorylated serines (pS), and the carboxylate containing glutamic acids (E) and aspartic acid (D) could be key features responsible for the change in conformation and putative attachment.

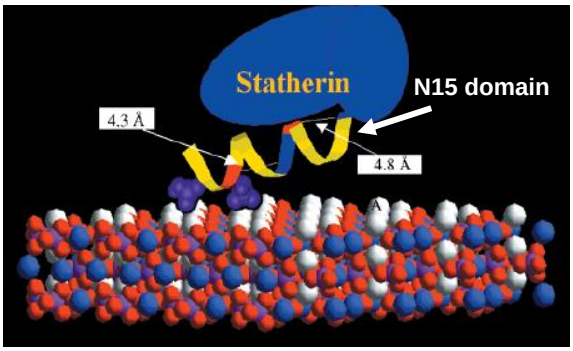


***Figure 24: Schematic model showing statherin interaction with the 001 face of hydroxyapatite[112]; calcium = white spheres, oxygen = red spheres, phosphorus = blue spheres, phosphor serines = purple spheres***

Beyond their role of determining ultrastructure some NCPs, such as osteopontin (OPN) and dentin matrix protein I (DMP I), have also been suggested to directly contribute to the mechanical properties of bone. The intrinsic mechanical properties of OPN networks, were recently elucidated. They are able to repeatedly dissipate and store large amounts of energy and have evidently very high cohesive strength. These properties are thought to be achieved through weak ionic bonds formed between negatively charged sites on the proteins, e.g. phosphorylated serine and $Ca^{2+}$-ions. Similarly, to bone proteins strong adhesion through polyelectrolyte proteins has also been described in other natural systems such as the glue produced by the sandcastle worm Phragmatopoma Californica. Although, in this case the glue protein is rich in both anionic (glu, asp, DOPA) and cationic (lys, arg) residues, suggesting that the cohesive strength derives, in part, from direct ionic

interactions between side-chain residues, as well as interactions between anionic residues and metal cations. Adhesives mimicking this glue protein have been synthesized, but did not include specific end motifs for adhesion.

Another main class of tissue adhesives inspired by naturally occurring **adhesive proteins** which were investigated are the protein glues produced by mussels. Furthermore, many living creatures rely on physical adhesion to objects for essential activities, such as self-defense, protection and movement[113-115]. Generally speaking, there are two different types of bioadhesion: temporary and permanent. An example of temporary bioadhesion is given by the foot hairs used by geckos for climbing sheer surfaces[113]. A typical example of permanent bioadhesion is illustrated by mussels, which secrete is essential for stability within the marine environment[116]. Mussels strongly adhere to several organic or inorganic substrates and they are mechanically robust and operate under saline conditions. The adhesive apparatus of the mussel contains a series of byssal threads that tether the organism to different substrates (see Figure 25a). At least five specialized adhesive protein subtypes are known to contain 3,4-dihydroxy-L-phenylalanine (L-DOPA) (see one protein subtype in Figure 25b). The role of L-DOPA in mussel adhesive proteins is not fully understood, although there is general agreement that oxidized L-DOPA residues play important roles in cross-linking reactions leading to solidification of the secreted liquid protein adhesive[117-120].

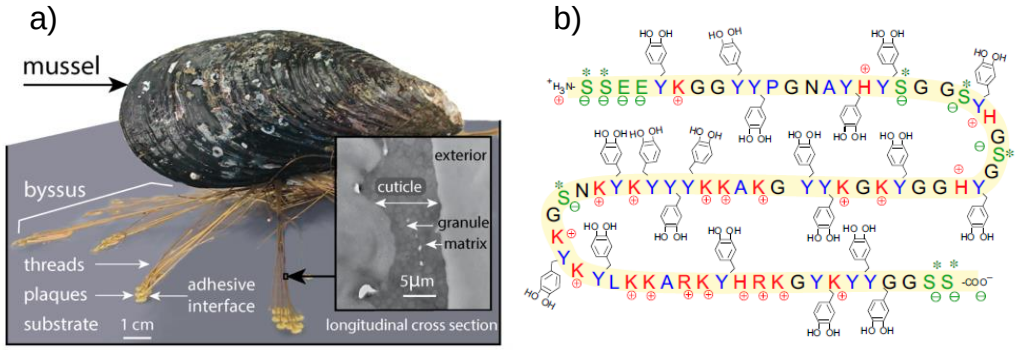


***Figure 25: a) Thread-plaque pairs forming the adhesive byssus that adheres to the surface[121]; b) Dopa-containing adhesive proteins in plaques[122]***

However, it is already demonstrated that oxidation of DOPA by metal ions or enzymes which leads to quinone formation is necessary to adhere to surfaces[123-126]. Spectroscopic analysis showed that addition of $Fe^{3+}$ makes the

mussel protein cross-link, which is created between $Fe^{3+}$ and three DOPA-containing protein strands[127]. This chelate binding proposes how L-DOPA binds to bone or to $TiO_2$, where the metal ion is calcium or titanium instead of iron. The binding mechanism of L-DOPA on $TiO_2$ varies at different pH values[122] (see Figure 26).

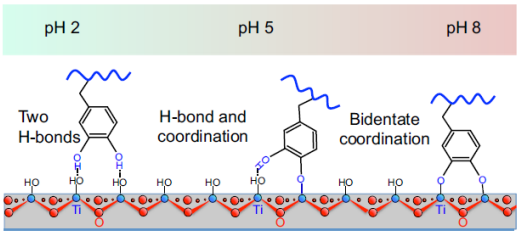


***Figure 26: Catechol bonding to $TiO_2$ changes from H-bonds at acidic pH to bidentate coordination at seawater pH***

Recently, Messersmith *et al.*[104] reported that the catechol form of L-DOPA binds to titanium oxide surfaces with high dissociation energies, providing support in adhesion. Thereby, L-DOPA was tethered to a linker system on an AFM-tip with unreactive PEG chains and the adhesion of L-DOPA on $TiO_2$ was measured. This interaction was very strong (about 800 pN) and is the strongest reversible binding interaction involving a small biological molecule.[104]

Besides, the binding properties of L-DOPA Mehdizadeh *et al.*[128] synthesized new promising injectable citrate-based inspired bio adhesives (iCMBAs). Thereby citric acid, poly(ethylene glycol) (PEG) and dopamine were reacted in a one-step polycondensation reaction (see Figure 27).

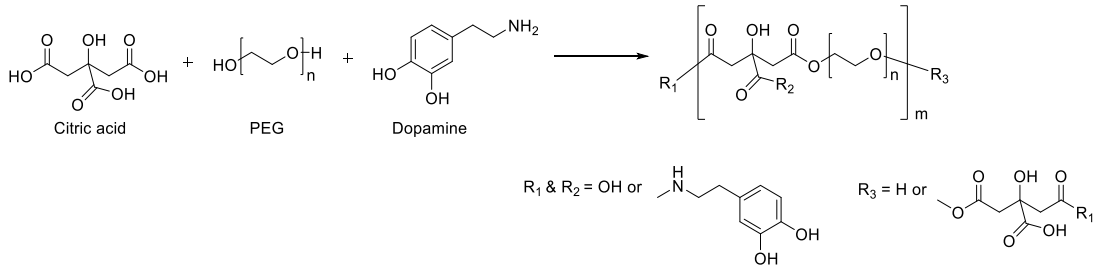


***Figure 27: Synthesis of the injectable citrate-based inspired bio adhesives pre-polymers***

This strategy allows the synthesis of new adhesives with great wet adhesion strength, controllable degradability, biocompatibility and reduced manufacturing costs[129]. The citric acid, a non-toxic metabolic product of the body, was used to form degradable polyesters with PEG and to provide reactive carboxyl groups to conjugate dopamine. In order to cross-link the iCMBAs for medical applications, the adhesive was applied in a dual syringe

System with the prepolymer dissolved in PBS buffer in one syringe and a sodium periodate (initiator) solution in the other (see *Figure 28*a). After mixing the two solutions different cross-linking reactions via the catechol groups occur. *Figure 28*b shows the wound closure and in *Figure 28*c the different possibilities of iCMBAs adhesion to tissues are depicted.

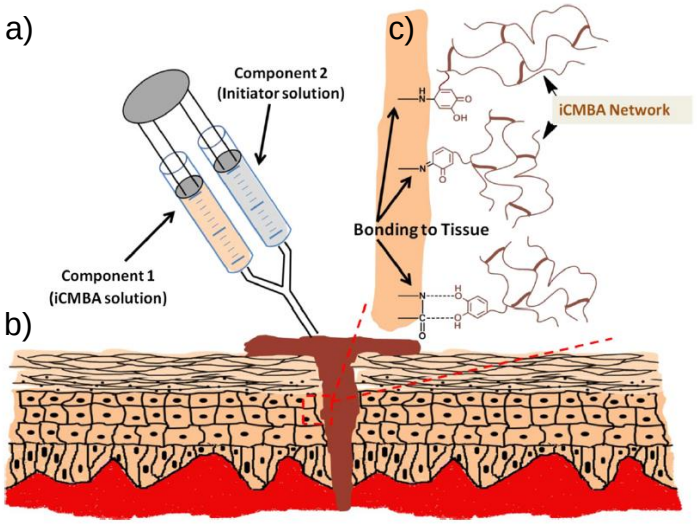


**Figure 28: Wound closure with injectable citrate-based inspired bio adhesives (iCMBA) adhesive application. a) 2-component adhesive with iCMBA solution and initiator solution. b) iCMBA utilized for sutureless wound closure. c) Proposed mechanism of iCMBAs adhesion to tissues[128]**

The cross-linking times varied from 18 s to 5 min, depending on the pre-polymer, the amount of initiator and the amount of dopamine. In vivo studies in rats showed only minor inflammation and the bleeding wounds were closed within 2 min.[128-129]

In the past years, **phosphorus containing monomers and polymers** have been the subject of enormous research.[130-133] The growing interest has led to phosphorus-containing organic materials for applications in the field of tissue engineering[134] and adhesion promoters, because of their properties. In many cases these phosphorus containing monomers were polymerized via methacrylate moieties.[135] Methacrylates are fast to polymerize and cross-link in combination with high mechanical properties and low cost make them attractive as adhesives. Indeed, their biocompatibility has been questioned. A study of alkylene bis(dilactoyl)methacrylate (see Figure 29) showed good biocompatibility[136] but the long term stability studies showed no biocompatibility at all.[137]

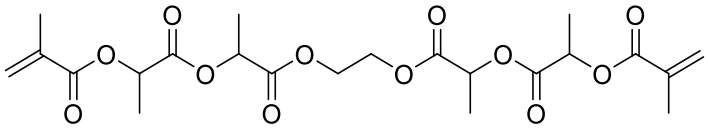

***Figure 29: Structure of alkylene bis(dilactoyl)methacrylate***

After a period of six months there was a deleterious tissue reaction in the former osteotomy gap of the polymer group. The areas were the glue was used presented huge aseptic inflammation.

However, (meth)acrylate-based monomers, such as 2-(methacryloyloxy)alkyl phosphonates, propyl N,N-tetramethylbis(phosphonate)-2-hydroxylbismethyl-eneamine methyl methacrylate (MAC3NP2) and 2-[2,2-bis(diisopropoxy-phosphoryl)ethoxy]methyl methacrylate (MAC3P2) (see Figure 30), were polymerized through RAFT polymerization to achieve low molecular weight polymers.

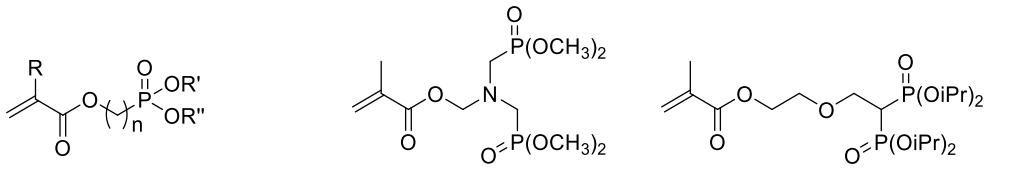

2-(methacryloyloxy)alkyl phosphonates

MAC3NP2

MAC3P2

n = 2; R = H; R' = $CH_3$; R'' = $CH_3$
n = 2; R = H; R' = $CH_3$; R'' = H
n = 2; R = H; R' = H; R'' = H

n = 2; R = $CH_3$; R' = $CH_3$; R'' = $CH_3$
n = 2; R = $CH_3$; R' = $CH_3$; R'' = H
n = 2; R = $CH_3$; R' = H; R'' = H

n = 1; R = $CH_3$; R' = $CH_3$; R'' = $CH_3$
n = 1; R = $CH_3$; R' = $CH_3$; R'' = H

***Figure 30: Phosphorus-based (meth)acrylate monomers used for adhesion properties***

The last few years, new phosphorus-containing monomers for example metha-cryloyloxyethyl phosphorylcholine) MPC and derivatives (see Figure 31) were synthesized for biomedical purposes. The biomimetic structure of MPC with its phospholipid group shows very good blood compatibility and protein adsorption.

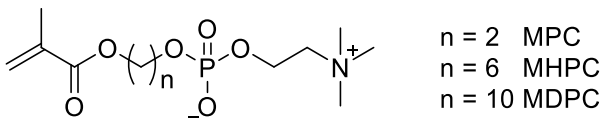

n = 2 MPC
n = 6 MHPC
n = 10 MDPC

***Figure 31: Structure of 2-methacryloyloxyethyl phosphorylcholine (MPC) and derivatives***

Due to the promising current developments new adhesives have to be synthesized based on these peptide-adhesives and the adhesion properties have to be analyzed.

# 2 Adhesion motifs and synthesis thereof

In order to distinguish between cohesive and adhesive behavior and get more information at the molecular level of adhesives, a new strategy was developed to functionalize AFM tips according to Gruber.[138] Thereby, a special linker system was used (see Figure 32). This maleimide-polyethylene glycol-N-hydroxysuccinimide (Mal-PEG-NHS) linker was connected to the AFM tip via the NHS group (see Figure 32, left end-group) and the adhesive was attached via the maleimide group (see Figure 32, right end-group). The easiest way is Michael typ thiole-ene click chemistry. Consequently, the adhesive sample must have a thiol end group.

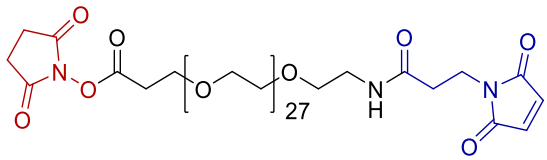


***Figure 32: Maleimide-PEG-NHS linker system***

However, the new strategy has to be implemented and proven. Thus, two similar amino acid sequences were selected and they were tethered to the AFM tip. The amino acid sequence D(pS)(pS)EEK was chosen because of the binding properties on hydroxyapatite in statherin and on $TiO_2$, as it was described in the chapter before (see State of the Art, chapter 1).[110, 112] Due to the phosphorylated serines (pS), there is high interaction to $Ca^{2+}$ in hydroxyapatite. In order to compare this fact, the amino acid sequence DSSEEK with no phosphorylated serines was chosen. This means, the phosphorylated amino acid sequence should show higher adhesion on hydroxyapatite and $TiO_2$ than the non-phosphorylated one. As mentioned above, all samples must have thiol end groups and therefore amino acid sequences with cysteine end groups were ordered (see Figure 33). The N-terminus was protected with an acetyl group.

However, it is necessary to compare adhesion values with literature to confirm the working functionalization method. In literature[104] dopamine is tethered to the AFM tip with a different linker system, but the values should be in the same range. As a consequence, a dopamine thiol (see Figure 33) compound was synthesized. In addition to that, these compounds can be very promising

adhesives based on the marine mussel, as it was described in the chapter before (see State of the Art, chapter 1). [122, 124]

In the same chapter, the usage of phosphorus-based methacrylates was mentioned. [139] Therefore, block copolymers based on phosphorus-containing methacrylates were synthesized via RAFT polymerization. Due to the promising properties of 2-hydroxyethylmethacrylate (HEMA)[140] and dimethyl (2-methacryloyloxyethylphosphonate) (DMMEP)[133, 135], this two monomers were chosen for the synthesis of block copolymers. HEMA shows very good biocompatibility, swellability and can act as viscosity regulator. In addition to that, it is easy to modify, stabilizes collagen and immobilizes proteins or cells.[140] pDMMEP tends to self-aggregation[141] and is hydrolysis stable, because of the $C_2$ spacer and the strong P-C bond.[141] Moreover, it shows strong adhesion on titanium and hydroxyapatite surfaces, concerning the interaction between phosphorus ester groups and metal ions. Nevertheless, biocompatibility stands in contrast with an antibacterial effect.[142-144] This means, the higher the biocompatibility, the lower will be the antibacterial effect. Indeed, these properties also may undergo a radical change if they are assembled in the block copolymer.

The blocks in the polymers were designed in the way that once HEMA was the starting block and one time DMMEP was the starting block (see Figure 33). In particular, there can be differences in reaction behavior at RAFT polymerization and in adhesion force because one end will be attached to the AFM tip and the other end is free. Furthermore, the length of DMMEP was varied, because the more phosphorus ester groups, the higher should be the adhesion force. In the end, the RAFT end group was removed to obtain a thiol end group.

The synthesis of the samples (see Figure 33) were shown in this chapter.

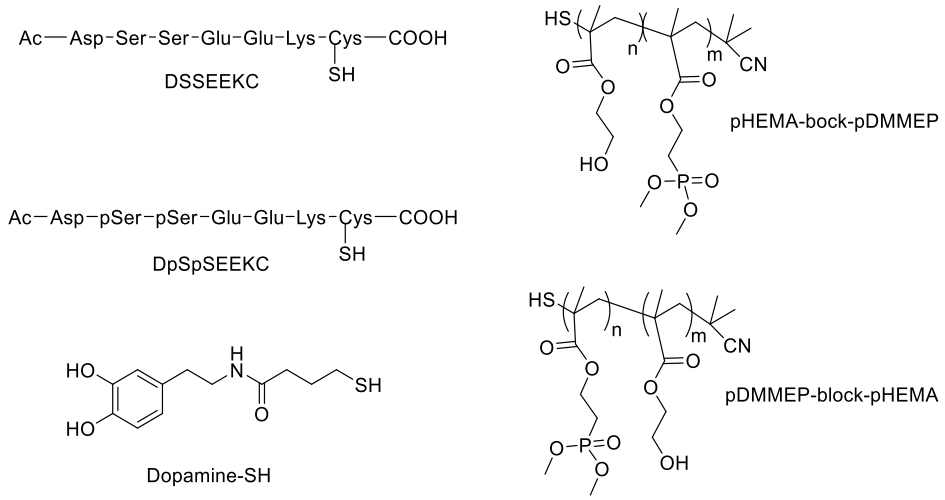


***Figure 33: Samples which were attached to the AFM-tip***

## 2.1 Synthesis of the monomer

Literature provides for the synthesis of dimethyl (2-methacryloyloxyethyl-phosphonate) (DMMEP), different pathways to obtain a phosphonate methacrylate structure. These pathways are summarized and described in the article by Senhaji *et al.*[130] Following reactions are described: Arbuzov reaction[145-146] using a trialkylphosphite, radical addition onto vinyl methacrylate,[147] Michael addition to vinyl phosphonate and methacrylation using a hydroxyphosphonate precursor under Schotten-Baumann conditions.[148] For the preparation of DMMEP it is important to choose a reaction, which is not carried out at high temperatures to avoid unwanted polymerization during the synthesis.

Referring to Rajalakshmi *et al.*[149] the synthesis of methacrylic phosphonates can be carried out using the Michaelis-Becker or Arbuzov reaction. The Michaelis-Becker reaction is usually favored due to the mild reaction conditions and it involves fast nucleophilic substitution of H-phosphite with a methacrylate moiety at room temperature.[132]

In a first attempt to synthesize DMMEP in two steps, 2-hydroxyethyl methacrylate (HEMA) was added slowly to 1.3 eq. of thionyl chloride to obtain 2-hydroxyethyl chloride (CEMA) in 48% yieldafter destillation. In the second step CEMA was mixed together with 1.2 eq. of diethyl phosphite and 1 eq. of potassium t-butoxide in THF at room temperature.

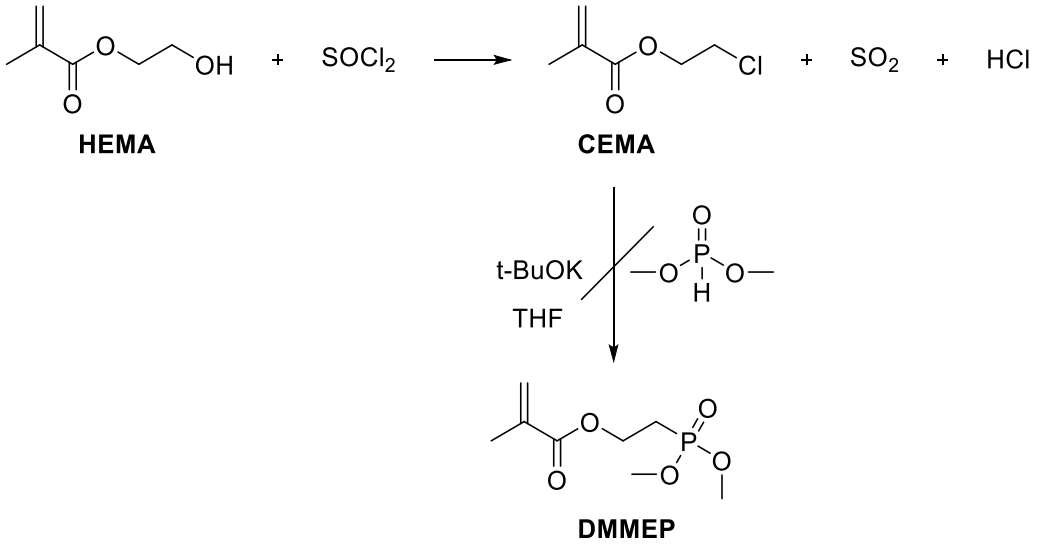


This pathway did not work as it was described in literature.[149] There was an addition reaction to double bound of the methacrylate and according to MS measurements cyclization or dimerization products were found. Moreover, the $^{31}$P-NMR spectrum showed four more phosphorus peaks which are the by-products besides the assumed product peak at 29.69 ppm.

The second synthesis strategy of DMMEP was carried out in accordance to Jeanmaire *et al.*[150] in a different pathway.

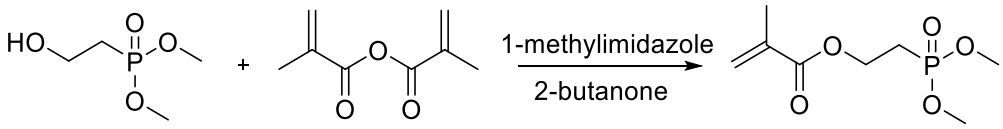


Therefore, 1 eq. dimethyl (2-hydroxyethyl) phosphonate was reacted with 1 eq. methacrylic anhydride in presence of the basic catalyst 1-methylimidazole in dry butan-2-one at 60 °C. The esterification with methacrylic anhydride generates methacrylic acid as side product, which was difficult to remove due to similar solubility of DMMEP, even after alkaline extraction. The crude product was purified via column chromatography to give DMMEP in a yield of 32% as colourless liquid with 10% impurities left (determined by NMR). It is very important to mention that rotary evaporation below 100 mbar leads to polymerization of the product, despite the addition of aerobe and anaerobic inhibitors.

The third synthesis-pathway of DMMEP was based on the procedure according to Avci and Albayrak.[131]

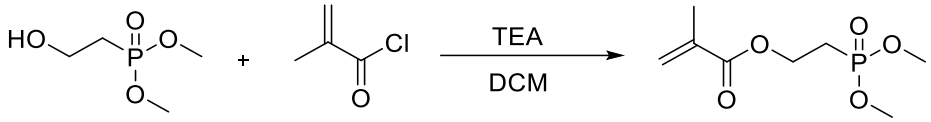


Dimethyl (2-hydroxyethyl) phosphonate was reacted in a Schotten-Baumann reaction with 1 eq. methacryloyl chloride in the presence of 1 eq. triethylamine in dry methylene chloride (DCM) at 0°C. During this acylation reaction the formed hydrogen chloride was scavenged by the addition of trimethylamine (TEA). As a consequence, white ammonium chloride salt precipitates. After the work-up procedure by filtration and extraction, the evaporation of methylene chloride gave the crude product as yellow, viscous liquid in a yield of 75% and a purity of about 98%. Further purification via distillation as reported in literature[151] was not possible. Despite the addition of aerobic and anaerobic inhibitor, the high temperature lead to polymerization and lower vacuum could not be realized. This strategy worked out in the most satisfying way of all three.

## 2.2 Synthesis of RAFT agents

For the synthesis of suitable block copolymers via RAFT polymerization, compatible RAFT-agents (CTAs) have to be synthesized. Therefore the suitable RAFT-agents (CTAs) which are compatible to the used monomers have to be selected. Mitsukami *et al.*[152] and Monge[133] reported that dithiobenzoates give the best results.

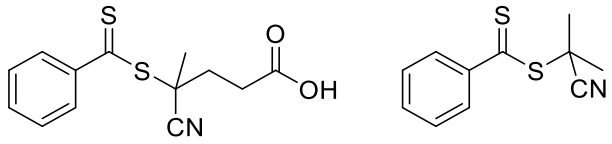


CPADP CPDB

***Figure 34: Selected RAFT agents***

It has been reported that 4-cyanopentanoic acid dithiobenzoate (CPADB) and 2-cyanoprop-2-yldithiobenzoate (CPDB) are very useful in polymerizing styrenes, methacrylates and methacrylamides.[152-153] These two RAFT agents provide good control over molecular weight and yield polymers with low polydispersity. CPADB has the ability to be employed in aqueous conditions as well. The two RAFT agents were synthesized in a multi-step synthesis out of di(thiobenzoyl) disulfide (DTBDS) as reported in literature.[152]

### 2.2.1 Synthesis of the intermediate di(thiobenzoyl) disulfide

In literature several ways to obtain dithiobenzoic acid are described. For example the reaction of trichlorophenylmethane with potassium hydrogen sulfide and potassium hydroxide,[154] the Grignard reaction of phenylmagnesium bromide with carbon disulfide followed by acidification,[153] the reaction of trichlorophenylmethane with sodium sulfide[155] or the reaction of benzyl chloride, elemental sulfur and sodium methoxide.[156] Mitsukami[152] has summarized and reported the best results of the reaction with benzylchloride. Therefore, the synthesis of sodium dithiobenzoate (DTBA) was carried out in accordance to Mitsukami's modification of the method published by Becke and Hagen.[156]

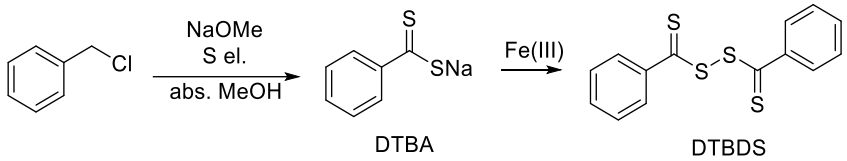


For the synthesis of DTBA, 1 eq. benzyl chloride was placed in dry methanol together with 2 eq. sodium methoxide (30% solution in methanol) and 2 eq. elemental sulfur under argon atmosphere. In consequence of the oxidative instability[157] of sodium dithiobenzoate during the purification process, the aqueous solution of DTBA was used immediately in the next step (one-pot synthesis).

Aamer *et.al.*[158] originally reported using $KI/I_2$ as the oxidizing agent for the synthesis of di(thiobenzoyl) disulfide (DTBS) out of DTBA. However, Mitsukami[152] obtained significantly better yields using potassium ferri-cyanide(III) as oxidizing species. The resulting DTBDS has to be recrystallized from ethanol according to Mitsukami, but Unger[159] described a decomposition of the product. For that reason the purification was quitted in this step and done after the last step.

### 2.2.2 Synthesis of 4-cyanopentanoic acid dithiobenzoate

4-Cyanopentanoic acid dithiobenzoate (CPADB) was prepared according to the procedure of Thang *et.al.*[160]

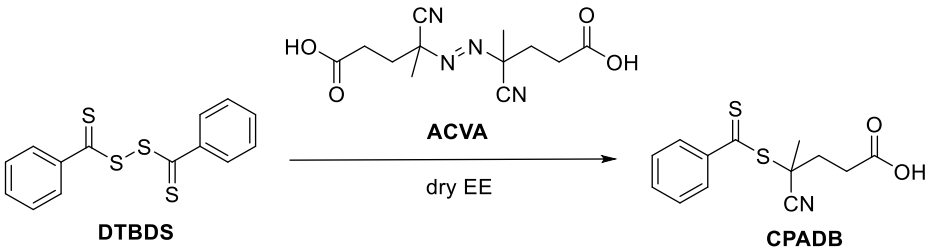


Without any purification DTBA was added to an excess at 1.5 eq. 4,4'-azo-bis(cyanovaleric acid) (ACVA) in dry ethyl acetate under argon atmosphere. The reaction was refluxed over a period of 19 h. The crude product was purified via column chromatography and recrystallized from toluene to give CPADB in a yield of 82% as pink crystals.

### 2.2.3 2-Cyanopropyl-2-dithiobenzoate (CPDB)

2-Cyanoprop-2-yldithiobenzoate was also prepared according to the procedure of Thang.[160]

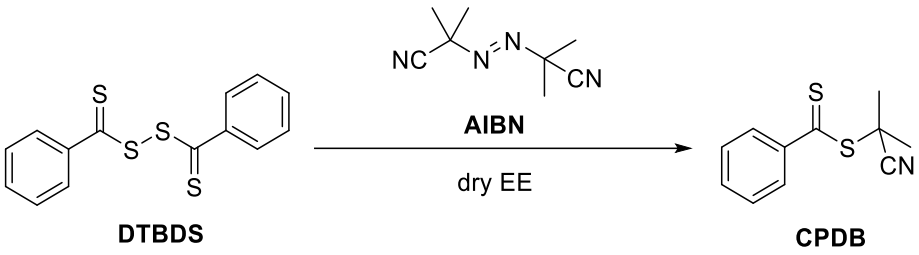


DTBA was added to azobis(isobutyronitrile) (AIBN) in dry ethyl acetate under argon atmosphere. The reaction was refluxed over a period of 20 h. The crude product was purified via column chromatography to give CPDB in a yield of 52% as red viscous liquid. It was not possible to recrystallize it from toluene.

## 2.3 Synthesis of the adhesive block copolymers

The procedure was similar for all synthesized block copolymers. First, the monomer, the related CTA respectively macro-CTA (for block copolymers), the initiator and the internal standard (naphthalene) were dissolved in DMF and

dioxane. The internal standard was used to monitor the monomer conversion. The polymerization in these organic solvents was performed with AIBN as initiator. These polymerizations were done as solution polymerization with a monomer concentration of 1.5 mol $L^{-1}$.

After degassing the solution with argon, the content in the penicillin vial was stirred at 70°C for 500 min. The homopolymer was synthesized with two RAFT agents (CPADB and CPDB) in different solvents and the reaction kinetics were compared.

As soon as the maximum of monomer conversion was attained, the product was precipitated. If the reaction was done in DMF, the precipitated polymers were very sticky and highly viscous. Therefore, they were re-dissolved in methanol and precipitated in hexane or diethylether.

### 2.3.1 Homopolymerization of HEMA

The homopolymerization of HEMA was carried out in accordance to Vega-Rios.[161] In contrast to literature two different RAFT agents CPADB and CPDB in different solvents at constant temperature of 70°C were used.

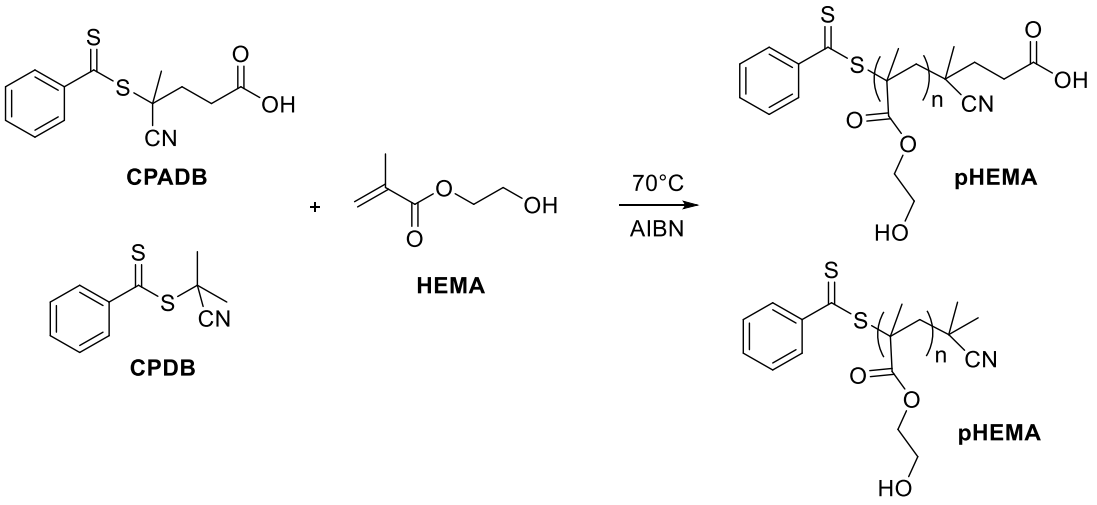


A theoretical molecular weight of 14 kDa for the HEMA homopolymer was calculated using the following idealized Equation 2.

$$M_{n,theo} = \left(\frac{[M]_0}{[CTA]_0} \times M_M \times c_t\right) + M_{CTA}$$

***Equation 2: Theoretical molecular weight calculation for homopolymers***

| | |
|---|---|
| $M_{n,theo}$ | Theoretical molecular weight at $c_x$ [g mol$^{-1}$] |
| $[M]_0$ | Monomer concentration at t = 0 [mol] |
| $[CTA]_0$ | CTA concentration at t = 0 [mol] |
| $M_M$ | Molecular weight of the monomer [g mol$^{-1}$] |
| $M_{CTA}$ | Molecular weight of the CTA [g mol$^{-1}$] |
| $C_t$ | Monomer conversion at t |

The polymerization kinetics were monitored by drawing samples over the whole course of reaction. Therefore, samples (200 µL) were taken by syringe in noted time intervals and quenched by ice cooling to stop the reaction until they were analyzed by $^1$H nuclear magnetic resonance spectroscopy (NMR). In the NMR-spectra the reaction course was investigated.

The conversion can be determined out of the percental decrease of the methacrylate integrals with respect to the internal standard. In the following Figure 35 an overlay of the spectra of the homopolymerization of HEMA at t = 0 min (Figure 35a) and t = 500 min (Figure 35b) is depicted, to show the difference of the methacrylate groups in the spectra after 500 min of polymerization time.

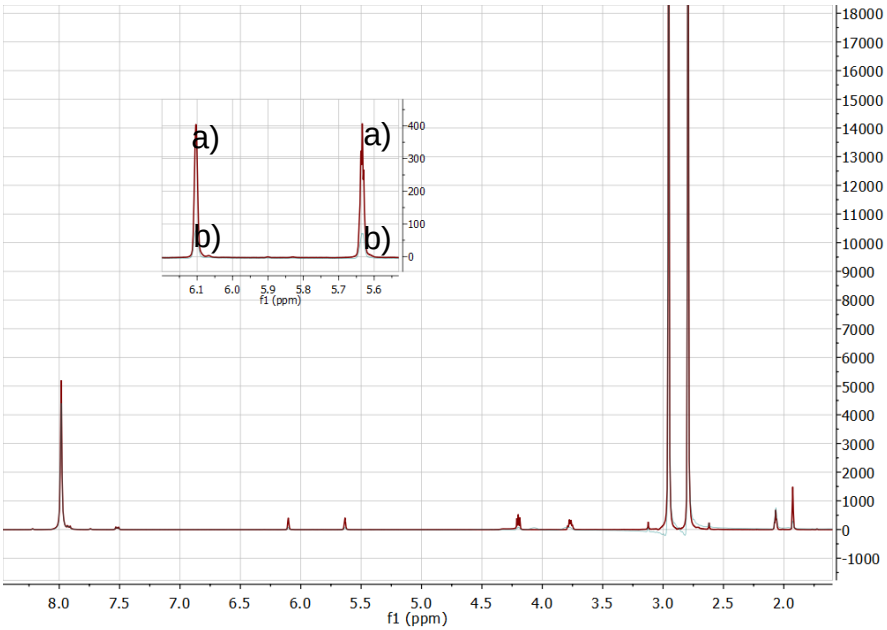


***Figure 35: $^1$H-NMR spectra of the homopolymerization of HEMA after a) t = 0 and b) t = 500***

In the NMR-spectrum the peaks of the internal standard naphthalene stay at 7.51 and 7.91 ppm respectively, while the integral of the methacrylate peak signals of the monomer decreases.

The monomer conversion was determined according to Equation 3.

$$C_t = \left(1 - \frac{Int_t}{Int_0}\right)$$

***Equation 3: Calculation of the monomer conversion***

$C_t$ Monomer conversion at t

$Int_t$ Signal of the methacrylate group at t

$Int_0$ Signal of the methacrylate group at t = 0

Many different CTA : initiator ratios for the homopolymerization of HEMA were tried out, the most promising ones can be seen in Table 3. The best CTA to initiator ratio for pHEMA was 1:0.02 and therefore the kinetic studies were done with this ratio.

***Table 3: Homopolymerization of HEMA with different solvents***

| HEMA | Solvent | CTA | M[a]:CTA:I | $C_m$[b] [%] | $M_{n,Theo}$ [kDa] | $M_{n,NMR}$ [kDa] | Yield [mg] |
|---|---|---|---|---|---|---|---|
| 01 | DMF | CPADB | 234:1:0.02 | 45 | 14 | 14 | 567 |
| 02 | Dioxane | CPADB | 351:1:0.02 | 30 | 14 | 12 | 521 |
| 03 | DMF | CPDB | 230:1:0.02 | 46 | 14 | 14 | 500 |
| 04 | Dioxane | CPDB | 441:1:0.02 | 24 | 14 | 13 | 489 |

[a]Monomer concentration 1.5 M

[b]$C_m$…monomer conversion

The RAFT polymerization of HEMA is very different to the well-known RAFT-polymerization of methylmethacrylate (MMA). Although both monomers are methacrylates, they have a quite different polymerization behavior and different solvation (HEMA is hydrophilic, MMA hydrophobic). The kinetic constant of propagation of HEMA is 3280 L $mol^{-1}$ $s^{-1}$,[162] which is four times higher than that of MMA. Furthermore, this means, that the transfer ability to the CTA is not very efficient for HEMA. As a consequence, it is necessary to increase the CTA to initiator ratio to values between 25 and 50 (10 times higher as for MMA) for controlling the molecular weight and polydispersity.[161, 163] More CTA means higher transfer rate to the CTA and lower polymerization rate.

The controlled radical polymerization of HEMA is only achieved at low polymerization yield, while at higher yields the polydispersity grows to reach values close to non-controlled radical polymerization. This means that side reactions and possibly polymer chain termination through polymer to polymer addition widens the PDI. Additionally, solubility problems with high molecular weight HEMA were reported.[163]

In the following Figure 36 the monomer conversion of HEMA (14 kDa) with CPADB in different solvents was plotted against the reaction time (monomer conversion plot). In Figure 37 the trend of a polymerization with living character can be seen.

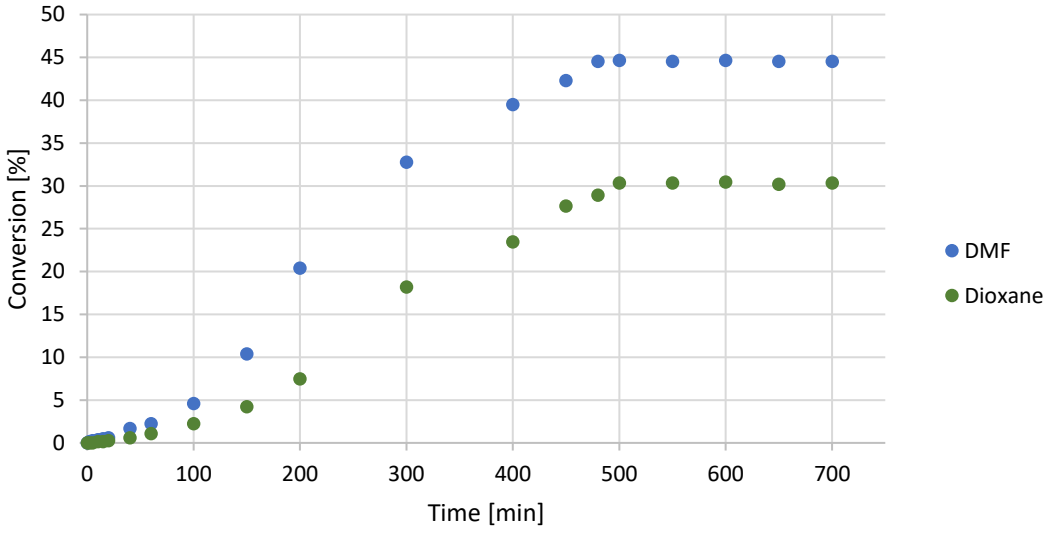


***Figure 36: Polymerization kinetics (monomer conversion plot) of HEMA 14 kDa with CPADB at 70°C***

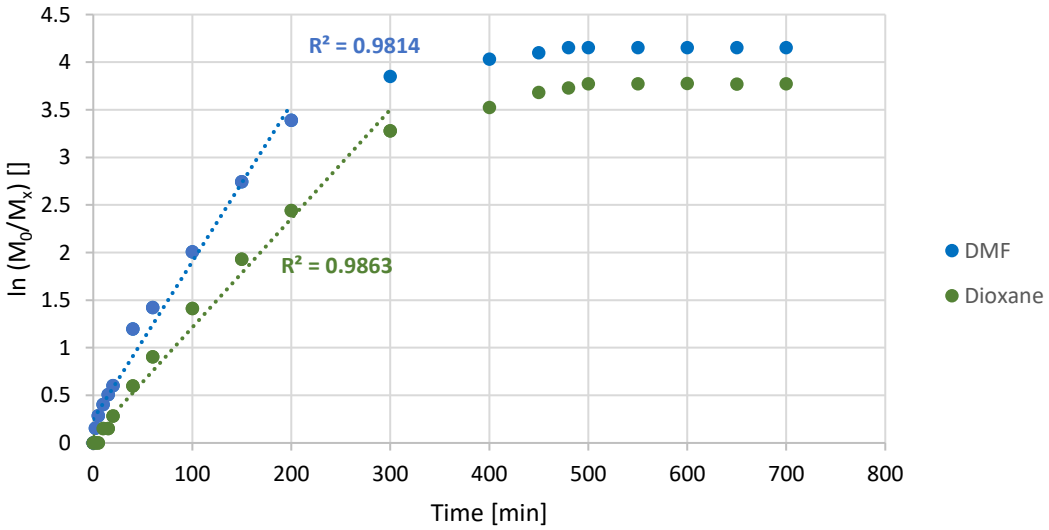


***Figure 37: Pseudo-first order kinetic plot of HEMA 14 kDa with CPADB at 70°C***

In the first 60 minutes of polymerization time in DMF and dioxane the monomer conversion was quite low. Reasons for that could be the degradation of AIBN, which does not occur completely at once, but continuously over a period of time. Furthermore, it was not possible to heat the formulation in the penicillin flask in one second at constant temperature. Further on, inhibition might occur in RAFT polymerization processes, if re-initiation is not sufficiently fast. If there was no significant change in monomer conversion, the polymerization end time was reached.

As mentioned above the controlled radical polymerization of HEMA is only possible with low monomer conversion. This polymerization shows a higher monomer conversion (45%) than in literature (30%).[161]

The living character can be determined by the reaction order. Because first order reaction is one of the requirements for controlled radical polymerization. For this purpose the natural logarithm of the quotient of starting monomer concentration and monomer concentration at a certain point of time is plotted against the time. If the graph shows linear behavior, the reaction is first order. Figure 37 shows linear behavior nearly until the end of the polymerization. At a certain point of time the whole monomer is almost converted and the curve flattens. The following pseudo-first order kinetic plots of the synthesized polymers were shown in the Appendix because all polymers showed a first order behavior in reaction kinetics.

In Figure 38 the monomer conversion of HEMA (14 kDa) with CPDB in DMF and dioxane was plotted against the reaction time.

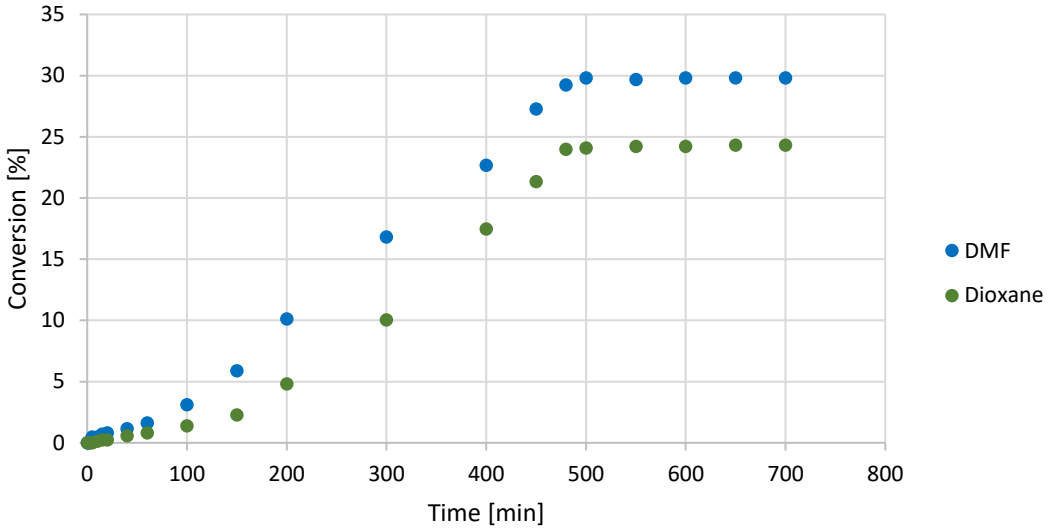


***Figure 38: Monomer conversion plot of HEMA 14 kDa with CPDB at 70°C***

In Figure 38 the monomer conversion of the RAFT polymerization of HEMA with CPDB in DMF and dioxane increases very slowly. But after 100 min the reaction went on faster. The conversion is higher when the reaction takes place in DMF. In Figure 38 the same trend can be seen as in Figure 37. The graph shows linear behavior nearly until the end of the polymerization. At a certain point of time the whole monomer is almost converted and the curve flattens. The pseudo-first order kinetic plot is shown in Figure 82 in the Appendix.

A comparison of the homopolymers synthesized with different RAFT agents in DMF is shown in Figure 39.

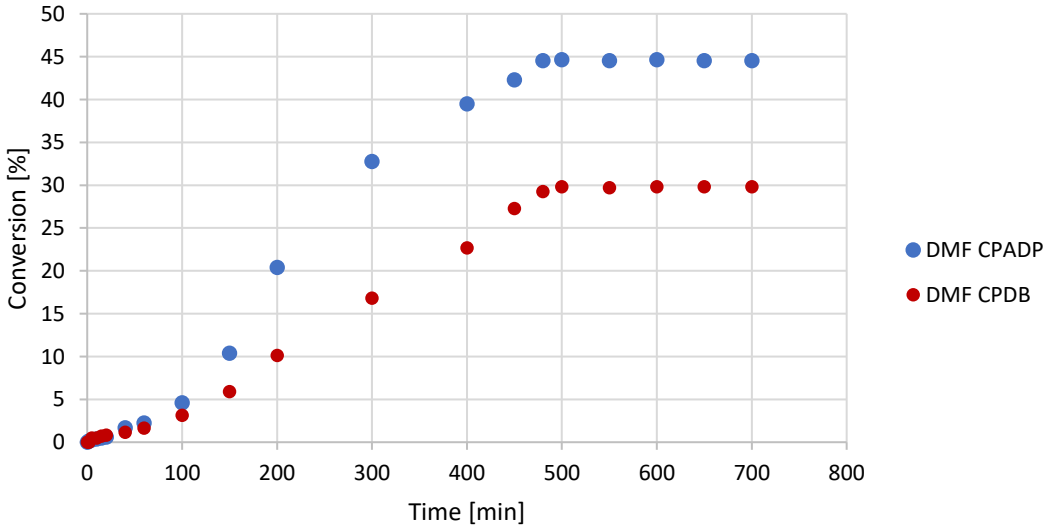


***Figure 39: Monomer conversion plot of HEMA 14 kDa with CPADB compared to CPDB at 70°C***

The comparison of the two RAFT agents shows that the end of the polymerization is the same, but with CPADB higher monomer conversion can be obtained. The slowly rising molecular weight is the result of the lower reaction rate with CPDB.

### 2.3.2 Homopolymerization of DMMEP

In literature, some results are published on the polymerization of a similar phosphonate monomer, called dimethyl(methacryloyloxy)methyl phosphonate (MAPC).[139, 164] Furthermore, reverse iodine transfer polymerization (RITP) in acetonitrile showed that RAFT polymerization of this monomer was sensitive to very low level of oxygen (limiting the conversion and causing the degradation of the dithioester moiety).[164] The addition rate constant is relatively low and a competitive reaction with traces of oxygen in the medium is expected, producing hydroperoxides and thus leading to RAFT degradation. This side reaction possibility increases by the low reactivity of MAPC.[139] It could give also indication of the difficult preparation of high molecular weight dimethyl(methacryloyloxy)ethyl phosphonate (DMMEP).

The homopolymerization of DMMEP was done in DMF and dioxane with the two synthesized RAFT agents CPADB and CPDB.

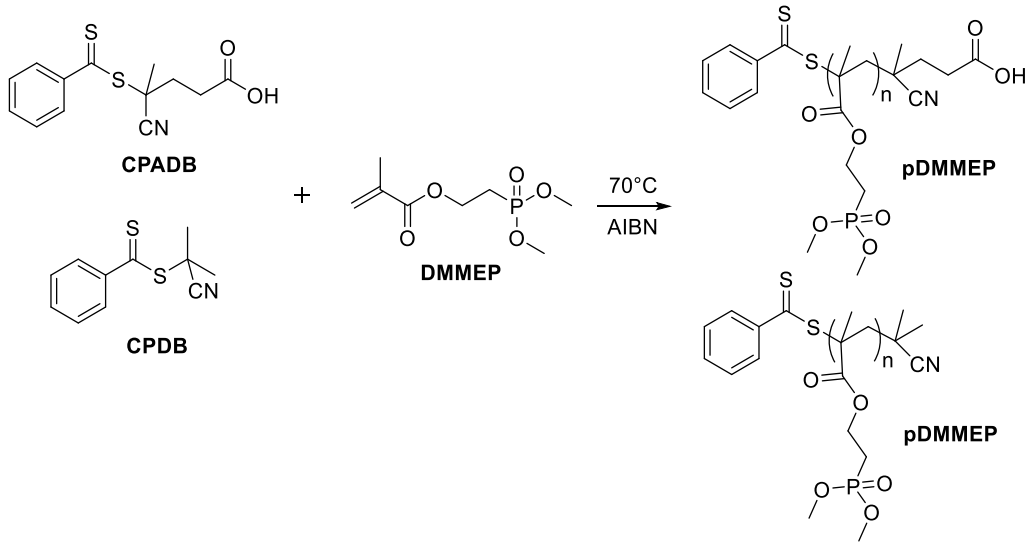


Different ratios of CTA : initiator with an amount of naphthalene as internal standard were dissolved in 1,4-dioxane and in DMF (see Table 2). The best CTA : initiator ratio for DMMEP was 3:1 and therefore the kinetic studies were done with this ratio to have better control over the molecular weight. The

polymerization time was 500 min and the temperature 70 °C. Theoretical molecular weights of 14 kDa and 28 kDa for the homopolymer were calculated. The monomer conversion was again monitored by $^{1}$H-NMR. Subsequently, every time interval of the taken $^{1}$H-NMR spectra was evaluated and the monomer conversion of the samples was calculated by Equation 3.

Referring to Jeanmaire *et al.*[150] polarity of the solvent had an influence on the rate and the control of the polymerization. A lower rate of polymerization was obtained in the less polar solvent. In water the reaction was very fast but transfer reactions occurred. This means, that the best choice of solvent will be a polar solvent, but polarity must not have to be too high to keep the control. In order to check the “living” character of DMMEP in different solvents, some kinetic studies were performed.

***Table 4: Homopolymerization of DMMEP with different solvents***

| DMMEP | solvent | CTA | M[a]:CTA:I | $C_m$[b] [%] | $M_{n,theo}$ [kDa] | $M_{n,NMR}$ [kDa] | Yield [mg] |
|---|---|---|---|---|---|---|---|
| 01 | DMF | CPADB | 65:1:0.33 | 95 | 14 | 14 | 421 |
| 02 | DMF | CPADB | 117:1:0.33 | 95 | 25 | 25 | 412 |
| 03 | Dioxane | CPADB | 69:1:0.33 | 89 | 14 | 13 | 413 |
| 04 | Dioxane | CPADB | 128:1:0.33 | 87 | 25 | 23 | 408 |
| 05 | DMF | CPDB | 65:1:0.33 | 96 | 14 | 14 | 426 |
| 06 | DMF | CPDB | 127:1:0.33 | 88 | 25 | 23 | 421 |
| 07 | Dioxane | CPDB | 70:1:0.33 | 89 | 14 | 13 | 413 |
| 08 | Dioxane | CPDB | 134:1:0.33 | 83 | 25 | 22 | 409 |

[a]Monomer concentration 1.5 M

[b]$C_m$…monomer conversion

In the following Figure 40 the monomer conversion of DMMEP (14 kDa) with CPADB in different solvents was plotted against the reaction time. The determination, if the reaction is really a polymerization with living character, was verified in Figure 83 in the Appendix.

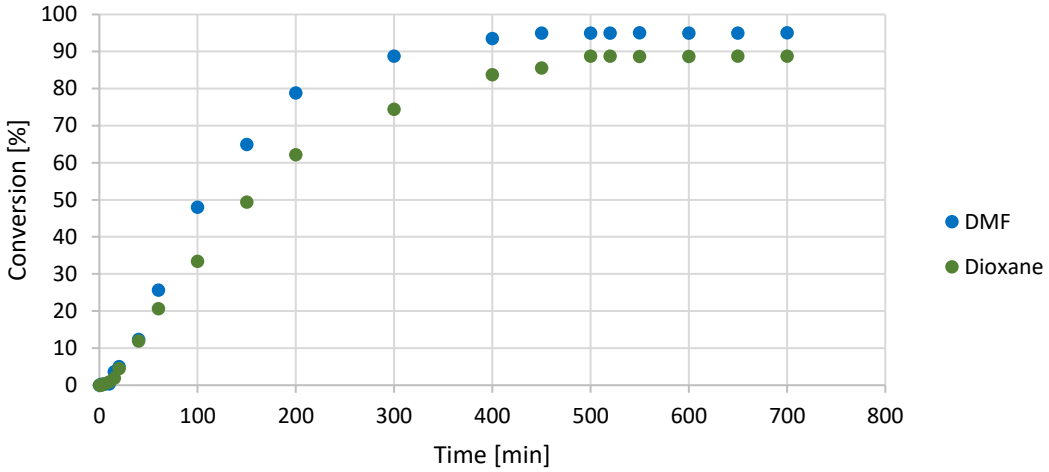


***Figure 40: Polymerization kinetics (monomer conversion plot) of DMMEP 14 kDa with CPADB at 70°C***

The monomer conversion of these two solvents increases steadily and the highest value was reached in DMF. The pseudo-first order kinetic plot of DMMEP (Figure 83) shows a linear behavior in DMF and in dioxane. Through the low monomer concentration at the end of polymerization the curve flattens. In Figure 41 the monomer conversion of DMMEP (25 kDa) with CPADB in different solvents was plotted against the reaction time. The natural logarithm of the quotient of starting monomer concentration and monomer concentration at a certain point of time plotted against the time was shown in the Appendix.

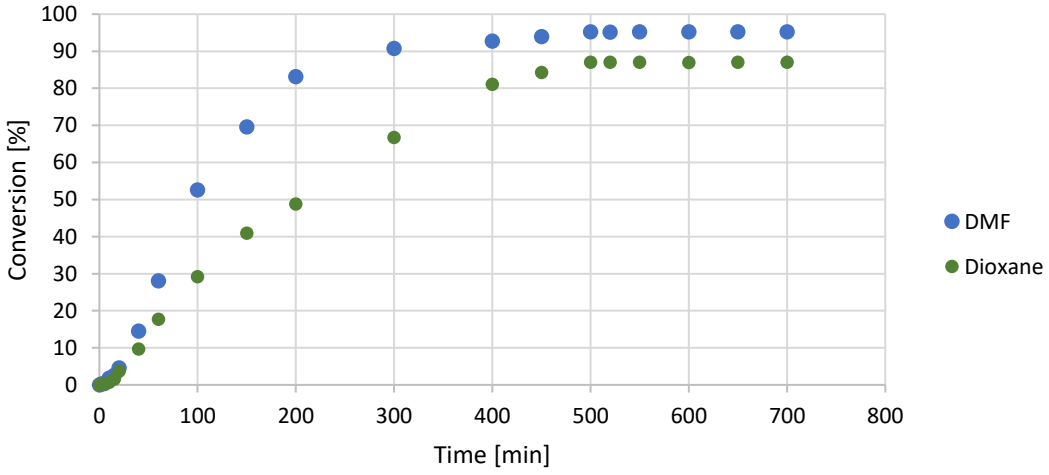


***Figure 41: Monomer conversion plot of DMMEP 25 kDa with CPADB at 70°C***

The monomer conversion of the solvents increases steadily and between DMF and dioxane there was hardly any difference. The pseudo-first order kinetic plot of DMMEP (see Figure 84 Appendix) shows a linear behavior in water until

20 minutes and in DMF and dioxane until 60 minutes. Through the low monomer concentration at the end of polymerization the curve flattens.

In Figure 42 the monomer conversion of DMMEP (14 kDa) with CPDB in DMF and dioxane was plotted against the reaction time. The RAFT agent was not soluble in water.

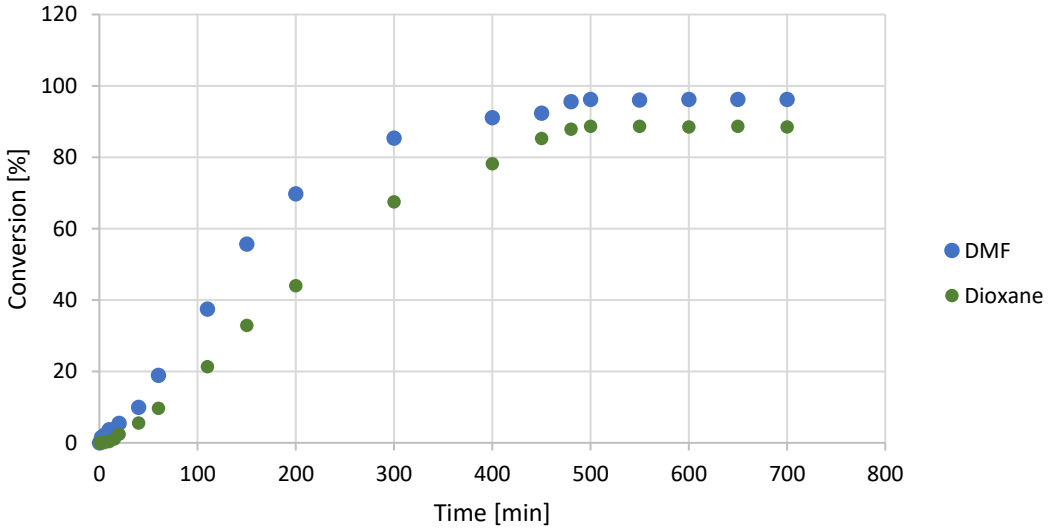


***Figure 42: Monomer conversion plot of DMMEP 14 kDa with CPDB at 70°C***

In Figure 42 the monomer conversion of the RAFT polymerization of DMMEP with CPDB in DMF and dioxane increases very slowly until 60 minutes. Henceforth, the reaction went on faster. The conversion was slightly higher when the reaction took place in DMF. The pseudo-first order kinetic plot is shown in Figure 85 in the Appendix.

In Figure 43 the monomer conversion of DMMEP (14 kDa) with CPDB in DMF and dioxane was plotted against the reaction time.

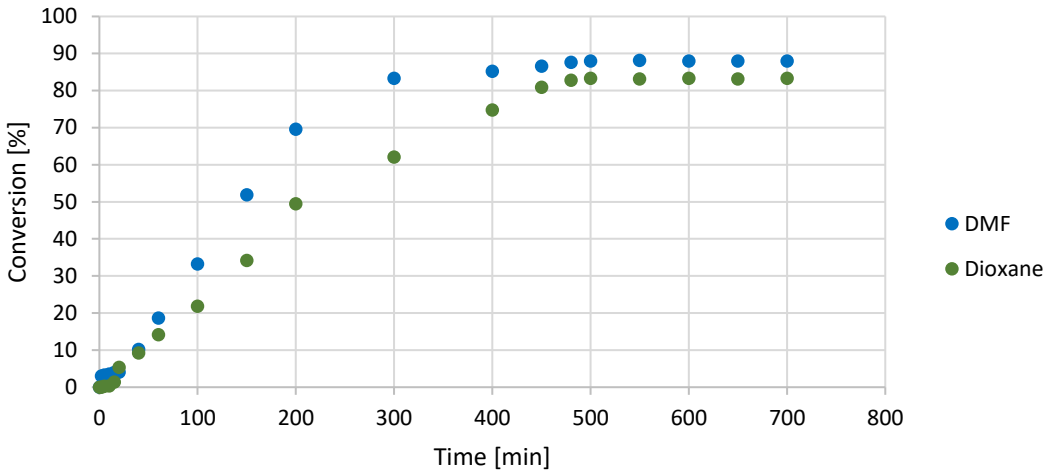


***Figure 43: Monomer conversion plot of DMMEP 25 kDa with CPDB at 70°C***

In Figure 43 the same trends can be seen as in Figure 42. The only difference in this polymerization is the higher molecular weight. Until a polymerization time of 40 minutes there can be seen linear behavior of the graphs. At a certain point of time the whole monomer is almost converted and the curve flattens. The pseudo-first order kinetic plot is shown in Figure 86 in the Appendix.
A comparison of the different RAFT agents and different molecular weights of DMMEP in DMF is shown in Figure 44.

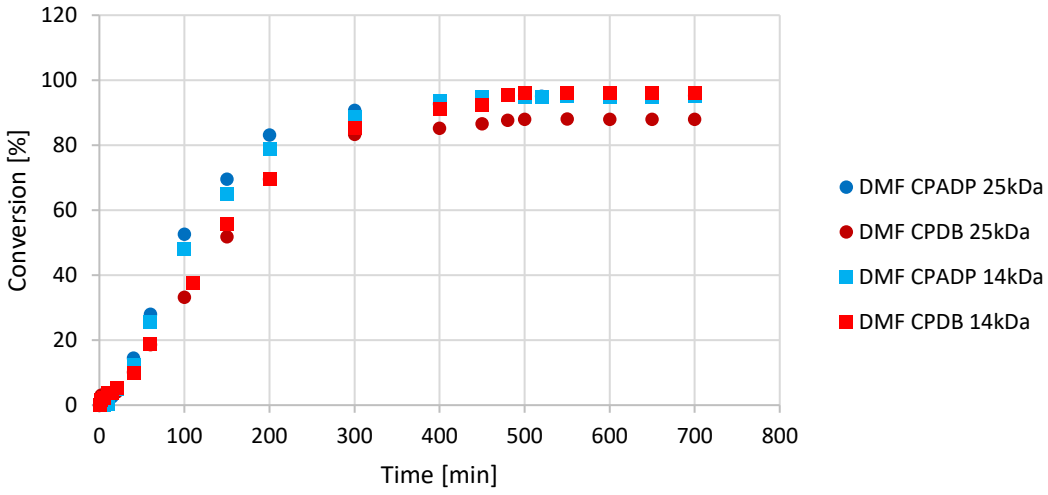


***Figure 44: Monomer conversion plot of DMMEP 14 and 25 kDa with CPADB compared to CPDB at 70°C***

The overlay of four kinetic studies shows RAFT polymerizations with higher monomer concentration obtain higher monomer conversion. In this formulations the RAFT-agent concentration is lower because the monomer concentration is higher and this means that the RAFT equilibrium favored re-initiation.

The curve of the RAFT polymerization with a calculated molecular weight of 25 kDa with CPDB in DMF flattens faster than the other curves. The monomer conversion stopped at 88%.

### 2.3.3 Summary of the homopolymerizations

It was possible to synthesize pHEMA and pDMMEP with two different RAFT agents and in DMF and dioxane via RAFT polymerization. The theoretical molecular weight compared to the analyzed molecular weight by $^{1}$H-NMR shows good conformance (see Table 3 and Table 4).
The transfer ability to the CTA is not very efficient for HEMA. Therefore, it is necessary to increase the CTA to initiator ratio to 50:1 to control the molecular weight and polydispersity. As a consequence, the polymerization rate is lower. In contrast, the homopolymerization of DMMEP was done with a CTA to initiator ratio of 3:1 with a monomer conversion of 95%.
For both homopolymerizations in DMF, a higher monomer conversion and a narrower PDI was obtained. The polymerization time was 500 minutes.

### 2.3.4 Block copolymerization pHEMA-block-pDMMEP

The block copoylmerization of HEMA with DMMEP was done the same way and the same procedure as in the homopolymerization of DMMEP. Instead of the RAFT-agents CPADB or CPDB the macro-RAFT agent pHEMA (14 kDa), AIBN, the internal standard naphthalene and the monomer DMMEP were dissolved in DMF. Due to the high monomer conversion and the absence of side products the block copolymerizations were done in DMF

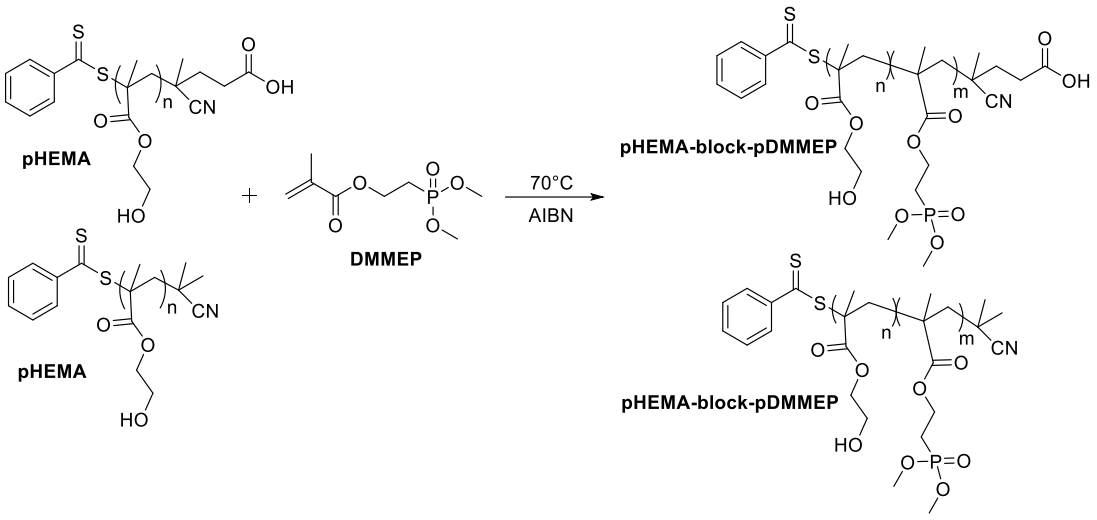


For the block copolymerization the whole conversion considering the molar parts of the monomers can be calculated with Equation 4.

$$C_{all} = \frac{[M_1]_0 \times c_{M_{1,x}} + [M_2]_0 \times c_{M_{2,x}}}{[M_1]_0 + [M_2]_0}$$

***Equation 4: Monomer conversion at copolymerization***

| | |
|---|---|
| $C_{all}$ | Over all conversion at t = x |
| $C_{M\ y,t}$ | Conversion of monomer y at t |
| $[M_y]_0$ | Concentration of monomer y at t = 0 [mol] |

The theoretical molecular weight can be determined according to Equation 5.

$$M_{n,theo} = \frac{[M_1]_0 \times M_{M_1} \times c_{M_1} + [M_2]_0 \times M_{M_2} \times c_{M_2}}{[CTA]_0} + M_{CTA}$$

***Equation 5: Theoretical molecular weight calculation for block copolymers***

| | |
|---|---|
| $M_{n,theo}$ | Theoretical molecular weight at $c_x$ [g mol$^{-1}$] |
| $[M_y]_0$ | Concentration of monomer y at t = 0 [mol] |
| $[CTA]_0$ | CTA concentration at t = 0 [mol] |
| $M_{My}$ | Molecular weight of monomer y [g mol$^{-1}$] |
| $M_{CTA}$ | Molecular weight of the CTA [g mol$^{-1}$] |
| $Cy,_t$ | Conversion of monomer y at t |

Four different block copolymers were synthesized with the two different macro RAFT agents in DMF (see Table 5).

***Table 5: pHEMA-block-pDMMEP copolymers with different end groups in DMF***

| pHEMA-block-pDMMEP | Macro CTA | M[a]:CTA:I | $C_m$[b] [%] | $M_{n,theo}$ [kDa] | $M_{n,NMR}$ [kDa] | Yield [mg] |
|---|---|---|---|---|---|---|
| 01 | CPADB | 68:1:0.33 | 92 | 28 | 28 | 223 |
| 02 | CPADB | 124:1:0.33 | 90 | 39 | 39 | 215 |
| 03 | CPDB | 68:1:0.33 | 92 | 28 | 28 | 229 |
| 04 | CPDB | 124:1:0.33 | 90 | 39 | 39 | 210 |

[a]Monomer concentration 1.5 M

[b]$C_m$…monomer conversion

Table 5 shows monomer conversion, molecular weight and PDI of the pHEMA-block-pDMMEP block copolymer. The essential point is that the use of two different macro-RAFT agents makes no difference in all parameters. Therefore, Figure 45 shows only the reaction kinetics of the block copolymers with CPDB.

Two block copolymers (28 kDa) contain pHEMA with a molecular weight of 14 kDa as the first block, followed by the second block pDMMEP with 14 kDa. These two polymers differ in their end group, which was located on the macro-RAFT agent. The other two block copolymers (39 kDa) contain a pHEMA (14 kDa) block and a pDMMEP (25 kDA) block.

The two different end groups of the block copolymers did not make a difference in the kinetic studies. Therefore, only block copolymers with the same end-group are shown in the next figures.
In Figure 45 the monomer conversion of pHEMA-block-pDMMEP with 28 kDa is compared to the same copolymer with 39 kDa.

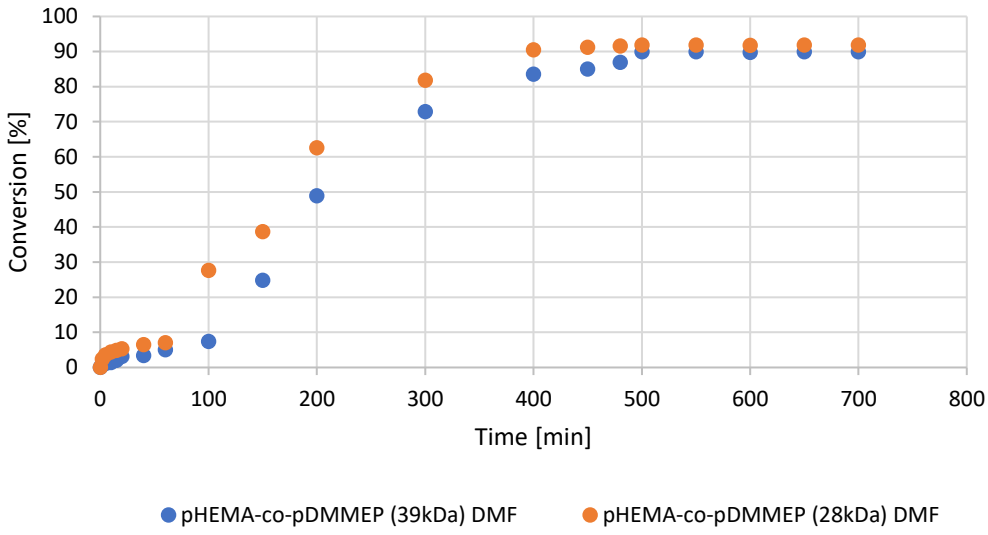


***Figure 45: Monomer conversion plot of pHEMA-block-pDMMEP 28 kDa and 39 kDa with CPDB at 70°C***

Figure 45 shows the same trend as in Figure 44 at the homopolymerization of pDMMEP. During the polymerization the monomer conversion of pHEMA-block-pDMMEP (39 kDa) is higher than the low-molecular-weight copolymer. The monomer conversion increases very slowly in the beginning and from 80 minutes on it increases faster. The polymerization time (500 min) is the same as for the homopolymerization. Both RAFT-polymerizations show a “living behavior” in their pseudo-first order kinetic plot.

### 2.3.5 Block copolymerization pDMMEP-block-pHEMA

The block copolymerization of DMMEP with HEMA was done the same way and the same procedure as in the homopolymerization of HEMA. Instead of the RAFT-agents CPADB or CPDB the macro-RAFT agent pDMMEP (14 and 25 kDa), AIBN, the internal standard naphthalene and the monomer HEMA were dissolved in DMF.

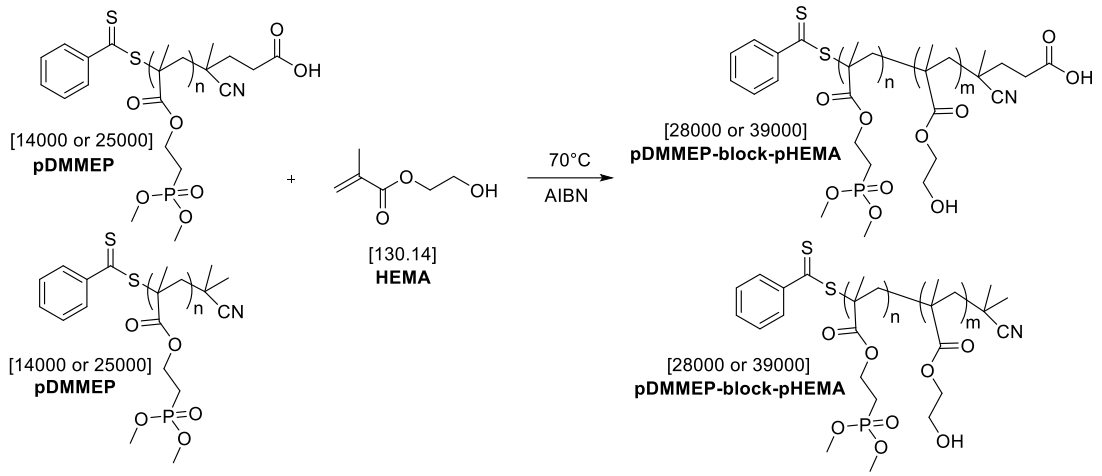


Again four different block copolymers were synthesized, but starting with a HEMA block and ending with DMMEP (see Table 6).

***Table 6: pDMMEP-block-pHEMA Copolymers with different end groups in DMF***

| pDMMEP-block-pHEMA | Macro CTA | M[a]:CTA:I | $C_m$[b] [%] | $M_{n,theo}$ [kDa] | $M_{n,NMR}$ [kDa] | Yield [mg] |
|---|---|---|---|---|---|---|
| 01 | CPADB | 301:1:0.02 | 35 | 28 | 28 | 178 |
| 02 | CPADB | 301:1:0.02 | 35 | 39 | 39 | 174 |
| 03 | CPDB | 303:1:0.02 | 35 | 28 | 28 | 182 |
| 04 | CPDB | 303:1:0.02 | 35 | 39 | 39 | 174 |

[a]Monomer concentration 1.5 M

[b]$C_m$…monomer conversion

Table 6 shows monomer conversion, molecular weight and PDI of the pDMMEP-block-pHEMA block copolymer. The same essential point as in 2.3.4 is that the use of two different macro-RAFT agents makes no difference in all parameters. Therefore, Figure 46 shows only the reaction kinetics of the block copolymers with CPDB.

Two block copolymers (28 kDa) contain pDMMEP with a molecular weight of 14 kDa as the first block, followed by the second block pHEMA with 14 kDa. These two polymers differ in their end group, which was located on the macro-RAFT agent. The other two block copolymers (39 kDa) contain a pDMMEP (25 kDa) block and a pHEMA (14 kDA) block.

The two different end groups of the block copolymers did not make a difference in the kinetic studies. Therefore, only block copolymers with the same end-group are shown in the next figures.

In Figure 46 the monomer conversion of pDMMEP-block-pHEMA with 28 kDa is compared to the same copolymer with 39 kDa.

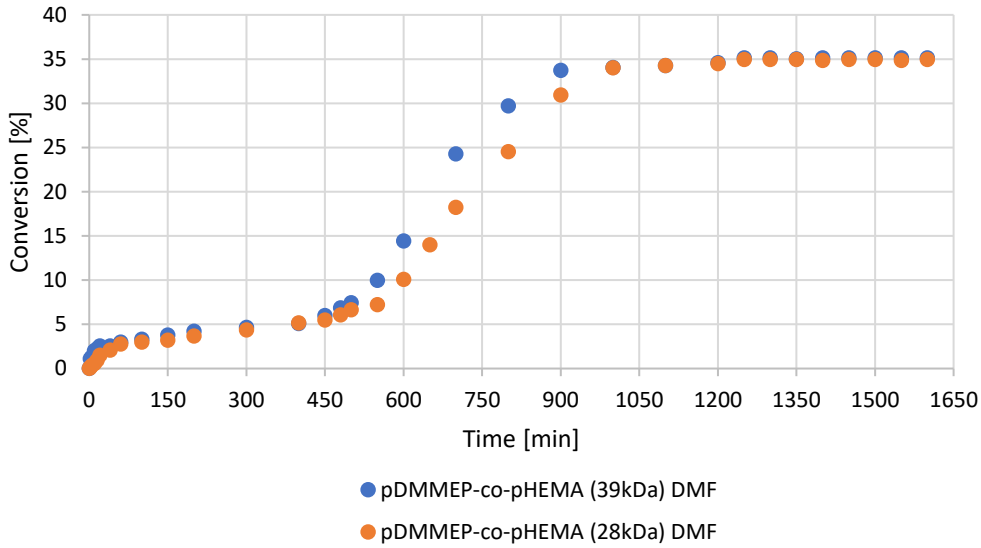


***Figure 46: Polymerization kinetics of pDMMEP-block-pHEMA 28 kDa and 39 kDa with CPDB at 70°C***

Figure 46 is different to the homopolymerization of pHEMA in Figure 39. Because the polymerization time is more than twice as high as the polymerization time of pHEMA. The monomer conversion increases very slowly in the beginning. Not until 450 minutes the monomer conversion gets higher values and the polymerization rate becomes faster. During the polymerization the monomer conversion of pDMMEP-block-pHEMA (39 kDa) is slightly higher than the low-molecular-weight copolymer. Both RAFT-polymerizations show a “living behavior” in their pseudo-first order kinetic plot.

### 2.3.6 Summary of block copolymerization

It was possible to synthesize two pHEMA-block-pDMMEP block copolymers with calculated molecular weights of 28 kDa and 39 kDA with two different end groups. Moreover, two block copolymers starting with a pDMMEP block (pDMMEP-block-pHEMA) with 28 kDa and 39 kDa were synthesized. The theoretical molecular weight compared to the analyzed molecular weight by $^{1}$H-NMR shows good conformance (see Table 5 and Table 6). The polymerization was done in DMF, because it was the best solvent for the homopolymerizations as well.

The essential point is that the use of two different macro-RAFT agents makes no difference in all parameters. Therefore, Figure 47 shows only the reaction kinetics of the block copolymers with CPDB.

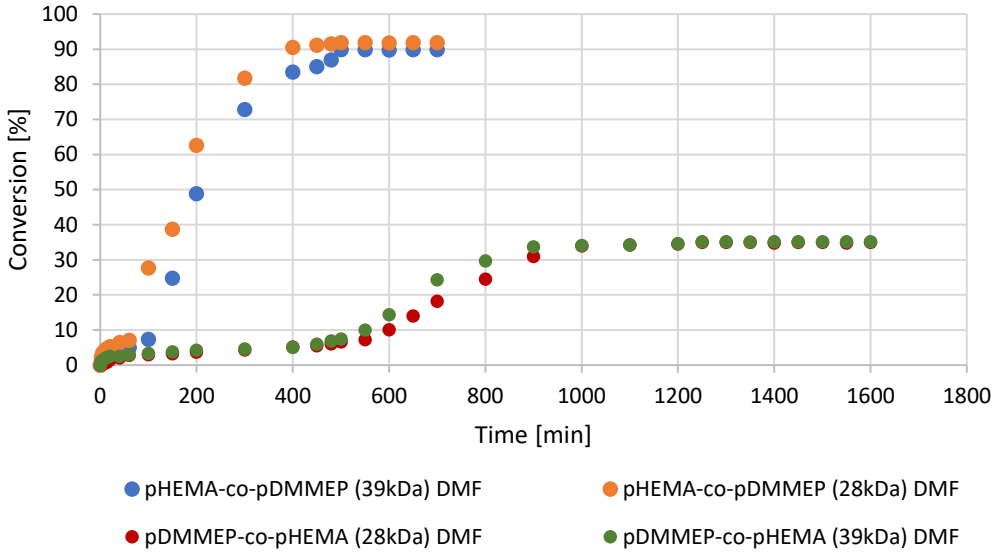


***Figure 47: Block copolymers with different molecular weight and different starting blocks***

Figure 47 shows that it is better to start the block copolymer with pHEMA and end with pDMMEP with a polymerization time of 500 minutes. Because the polymerization time of the reverse strategy is about 1250 minutes and in some cases a gel product was formed.

### 2.3.7 End-group removal via aminolysis

After successful RAFT polymerization of block copolymers with two different molecular weights, the next step for functionalizing the AFM tips with the polymer could be planned. Sometimes it is desirable to transform the thiocarbonylthio group to achieve a preferred functionality or for use in subsequent processes of post-polymerization. There are also examples where simple removal of the thiocarbonylthio group is desirable. The presence of this group means that the polymers may be coloured.[165] Furthermore, decomposition of the polymers can cause bad smell due to the sulphur.[166]

The block copolymers with the acid end group were unsuitable for the adhesion measurements at first instance. For further reactions and attachments the acid group would be more appreciated. But for the attempt to

attach the AFM tips with a polymer and to do adhesion measurements with the above mentioned set-up the free acid group could falsify the results.

There are several ways to modify the end group[167-168] of a RAFT polymer. Figure 48 shows a broad variety of reactions which can be used for the modification or removal of the RAFT end group.[167]

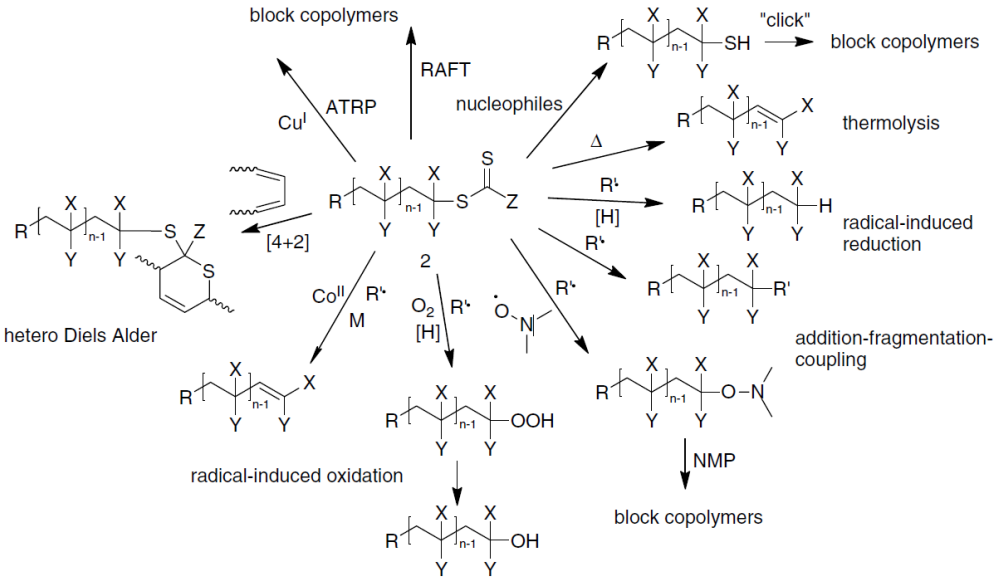


***Figure 48: Overview of RAFT end group modification/removal[167]***

The best strategy was an aminolysis reaction of the dithiocarbonyl moiety with amines. Caused by this the dithiocarbonyl group at the end of the polymer will be attacked nucleophilic by the lone electron pair of the amine (see Figure 49).[169]

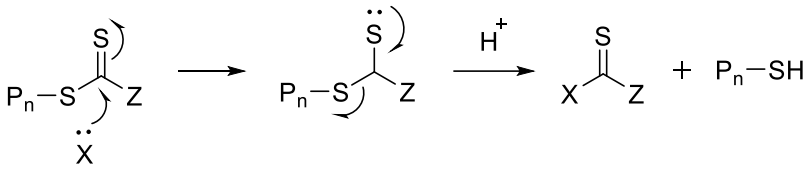

***Figure 49: End-group removal with nucleophiles***

Studies deal with an aminolysis reaction with hexylamine,[170-171] but purification is very often a problem and effortful, because in many cases dialyses have to be done. According to Patton *et al.*[172] aminolysis works pretty good with propylamine and the purification is much easier than with hexylamine. Disulfide formation can be reduced during the reaction with the reducing agent tris(2-carboxyethyl)phosphine (TCEP).[173]

The used linker system for AFM tip functionalization ends with a maleimide group. So it is obvious to do maleimide-click chemistry.[174] In order to obtain free thiol groups for the implementation of this coupling reaction, end-group removal via aminolysis was applied first.

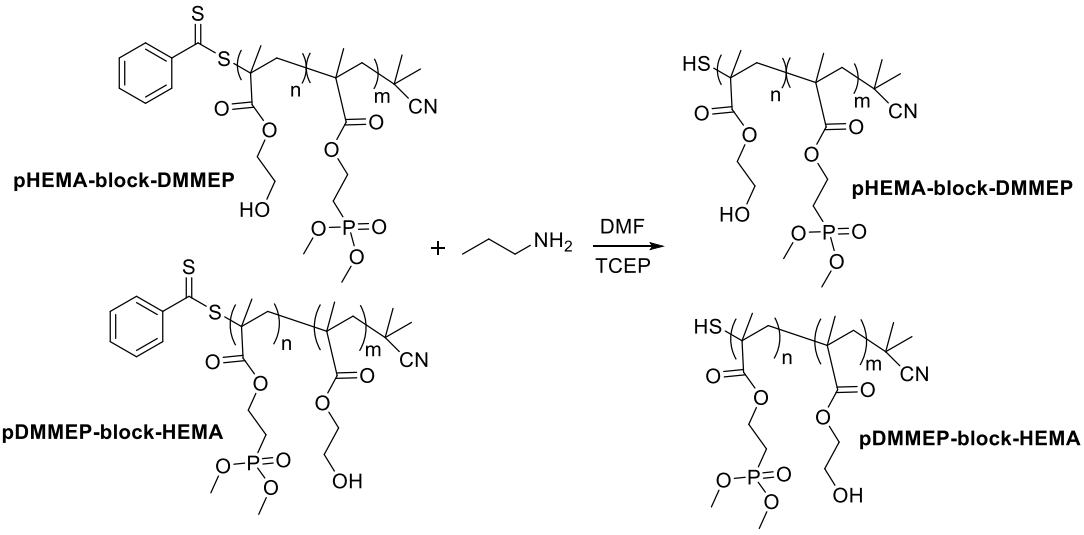


For these reactions 0.2 eq. of the block copolymer (pHEMA-block-pDMMEP 28 kDa, 39 kDa; pDMMEP-block-pHEMA 28 kDa, 39 kDa) and 0.2 eq. of TCEP were dissolved in DMF and degassed with argon. After 30 minutes 1 eq. propylamine was added dropwise and the reaction was stirred for 4.5 h at room temperature. Subsequently, the polymer was precipitated in diethylether, resolved in methanol, again precipitated in diethylether and dried under vacuum.

The reaction process could be confirmed via color change from pink to white (see Figure 50).

***Figure 50: Colour change after end-group removal***

NMR spectroscopy cannot be used to suggest the quantitative reduction of the dithioester end group because the signal attributed to the aromatic end group is very low. Therefore, UV-Vis spectroscopy was used as simple procedure for the characterization of the resulting polymers. The dithioester moiety has a strong absorption band at 300-310 nm in DMF.[168] After aminolysis the

absorption due to the dithioester is absent, which indicates the reduction of the dithioester terminus. Figure 51 shows the UV-Vis absorption spectra of pHEMA-block-pDMMEP and pDMMEP-block-pHEMA synthesized by RAFT polymerization before (-) and after (…) reaction with propylamine.

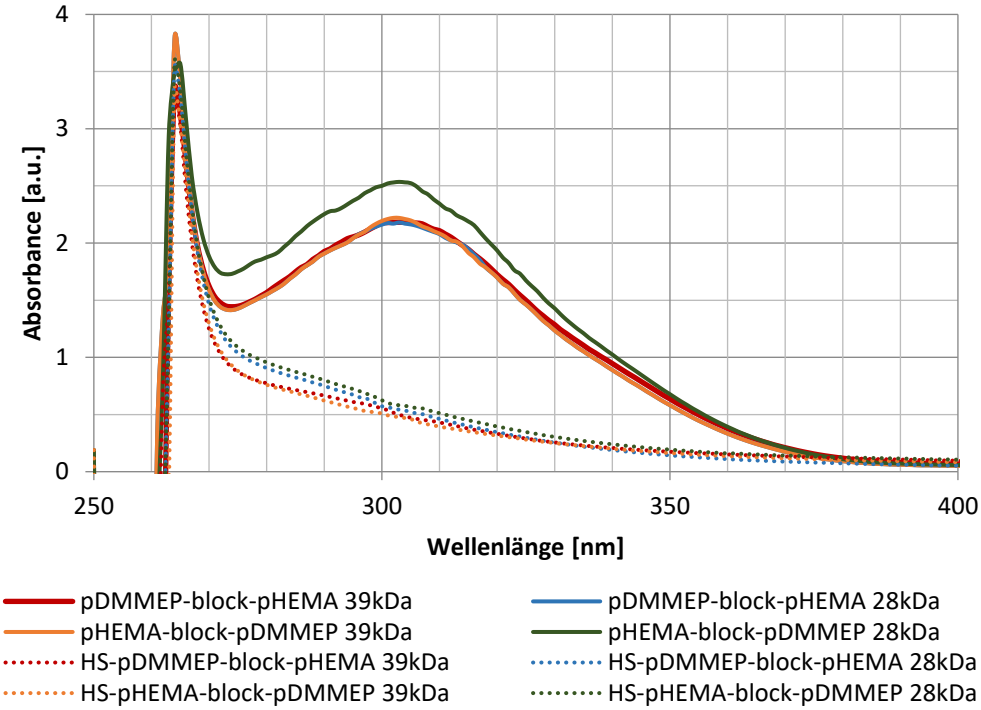


***Figure 51: UV-Vis absorption spectra of pHEMA-block-pDMMEP and pDMMEP-block-pHEMA in DMF***

## 2.4 Dopamine-SH

Due to the very promising adhesion properties[122] and adhesion forces of L-DOPA on different substrates, dopamine was modified with a thiol group. The structure is very similar to 3,4-dihydroxyphenyl-L-alanine (DOPA), a catecholic amino acid. As it was mentioned in the General Part (see State of the Art, chapter 1), DOPA shows very good adhesive properties on nearly all organic and inorganic surfaces in aqueous environments.[122]

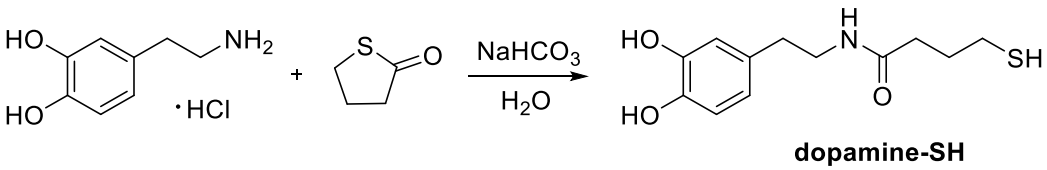


**dopamine-SH**

In order to assemble dopamine hydrochloride with a thiol moiety, a very elegant way will be thiolation according to Espeel and Du Prez.[175] Many synthetic strategies to introduce thiols always imply the use of cyclic precursor

molecules. Thiolactones are very well suited as cyclic precursors. The most important property of these cyclic thioesters related to their reactivity is the possibility of nucleophilic attack to the carbonylic center, leading to the opening of the ring (Figure 52).

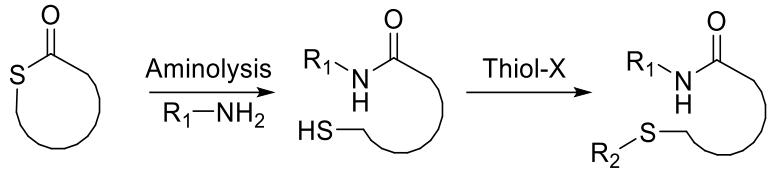


***Figure 52: Ring opening of the cyclic thiolactone through aminolysis***

Several nucleophiles can be considered for the ring opening. According to Olofsson *et al.*[176] 1 eq. dopamine hydrochloride reacts with 1 eq. γ-thiobutyrolactone to N-(3,4-dihydroxyphenetyl)-4-mercapto-butanamide (dopamine-SH) in water. Extraction with THF and solvent evaporation gave the thiol component and the disulfide as yellow, viscous liquid in a yield of 97%. Further purification via silica column chromatography to separate the thiol from the disulfide component was not possible, because the compound was retarded on the column. But the dopamine-SH will be treated in further reactions with TCEP to reduce the disulfide, so further purification is not necessary.

## 2.5 Model reactions

In order to verify if thiol-ene click chemistry with the synthesized samples works under the same conditions as in the last step of the tip functionalization, model reactions were carried out.[177] The pH have to be chosen carefully, otherwise side reactions will occur. In case of too high pH values (above 8) maleimides will favor a reaction with primary amines (e.g. lysine) over thiols. Therefore, the reaction should be carried out in buffered solutions to guarantee a pH between 6.5 and 7.5. Moreover, a reducing agent is necessary because cysteine is susceptible to get oxidized and forms disulfides.

For the synthesis a thiol compound was dissolved in deionized water. To this solution ethylenediaminetetraacetic acid (EDTA) a complexation agent, 4-(2-hydroxyethyl)-1-piperazineethanesulfonic acid (HEPES), a buffer solution and TCEP (see Experimental Part, chapter 2.5) were pipetted together in the same chronological order. Since the thiol compound was dissolved in water,

maleimide was added. EDTA is necessary to prevent re-oxidation during the coupling procedure on a time scale of few hours. For longer reaction times it is advantageous to do the reactions under argon atmosphere.

### 2.5.1 Cysteine

In the first model experiment the amino acid cysteine (thiol compound) and maleimide were selected to yield S-(2,5-dioxopyrrolidin-3-yl)cysteine. This experiment should mimic the used amino acid sequences.

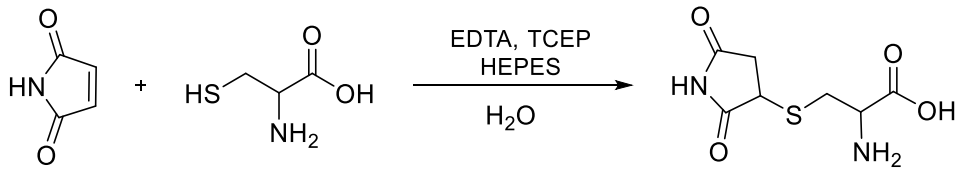


[97.07] [121.15] [218.23]

$^1$H-NMR-experiments showed, that the thiol-ene click chemistry worked under the suggested conditions. In a blank experiment B, where only maleimide, but no cysteine was added, no conversion of the maleimide was found (Figure 53).

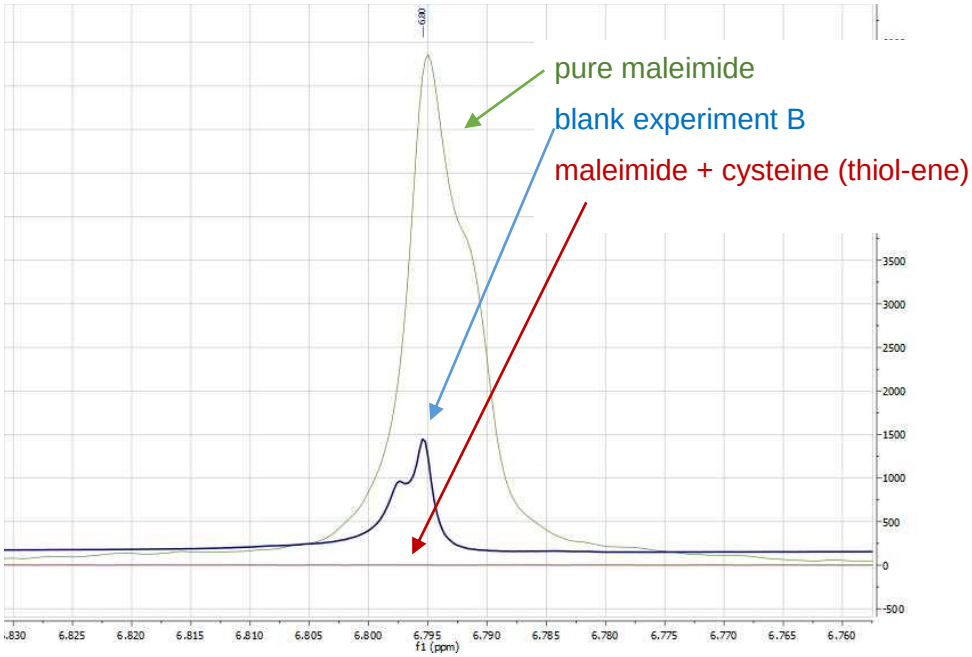


***Figure 53: Verification of the model experiment with cysteine via $^1$H-NMR-experiments***

### 2.5.2 Dopamine-thiol

In the second model experiment dopamine-thiol was dissolved in water and EDTA, HEPES 1, TCEP and HEPES 2 were added. After complete dissolution of dopamine-thiol, the appropriate amount of maleimide was added.

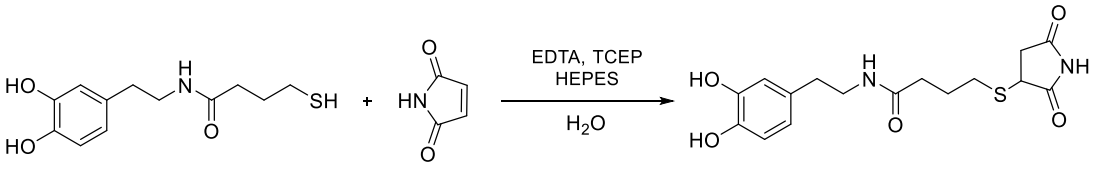


[255.33] [97.07] [352.41]

Again the $^{1}$H-NMR-experiments showed, that the thiol-ene click chemistry worked under the recommended conditions. In a blank experiment B, where only maleimide, but no dopamine-thiol was added, no conversion of the maleimide was found (Figure 54).

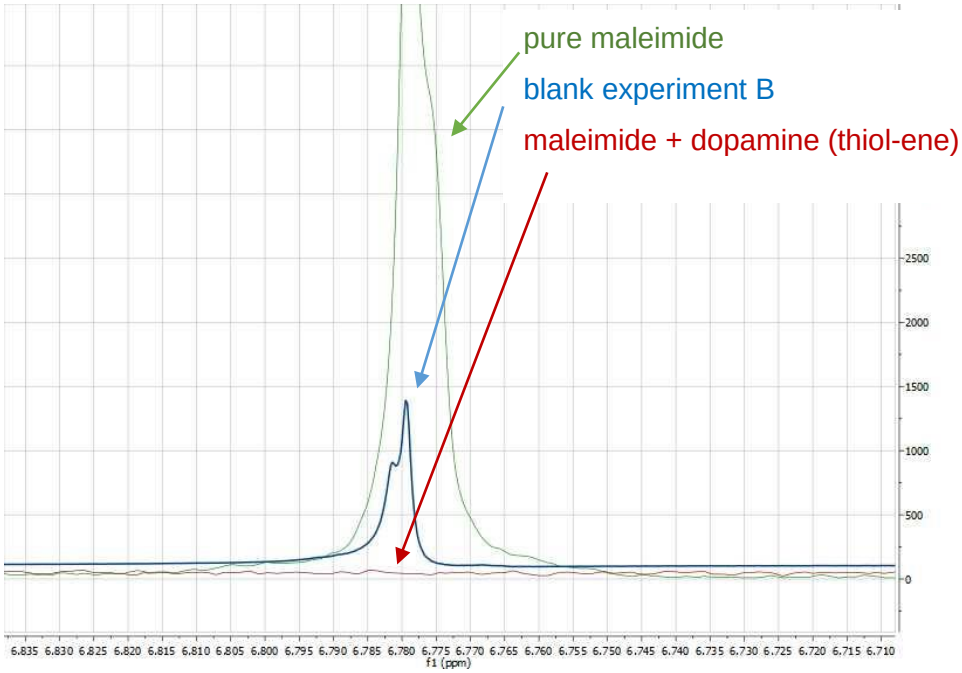


***Figure 54: Verification of the model experiment with dopamine-thiol via $^{1}$H-NMR-experiments***

### 2.5.3 Block copolymer-thiol

In order to test, if the block copolymers work properly for thiol-ene click chemistry or not, the last model experiment was performed with one of the block copolymers. Therefore, HS-pHEMA-co-pDMMEP (39 kDa) was dissolved in water and EDTA, HEPES 1, TCEP and HEPES 2 were added. After complete dissolution of dopamine-thiol, the appropriate amount of maleimide was added.

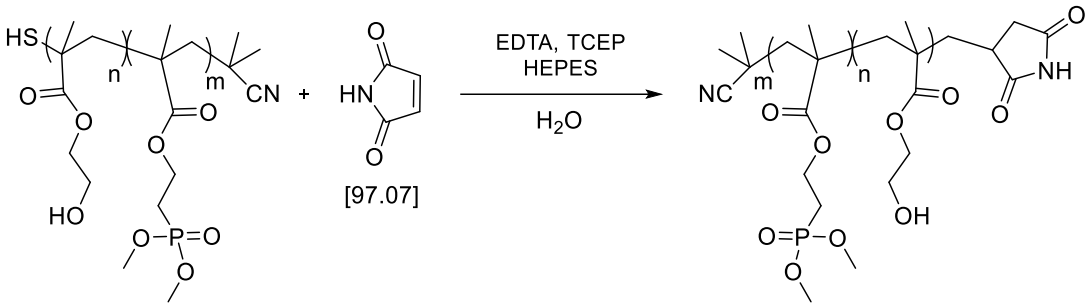


Again the $^{1}$H-NMR-experiments showed, that the thiol-ene click chemistry worked under the recommended conditions. In a blank experiment B, where only maleimide, but no dopamine-thiol was added, no conversion of the maleimide was found (Figure 55).

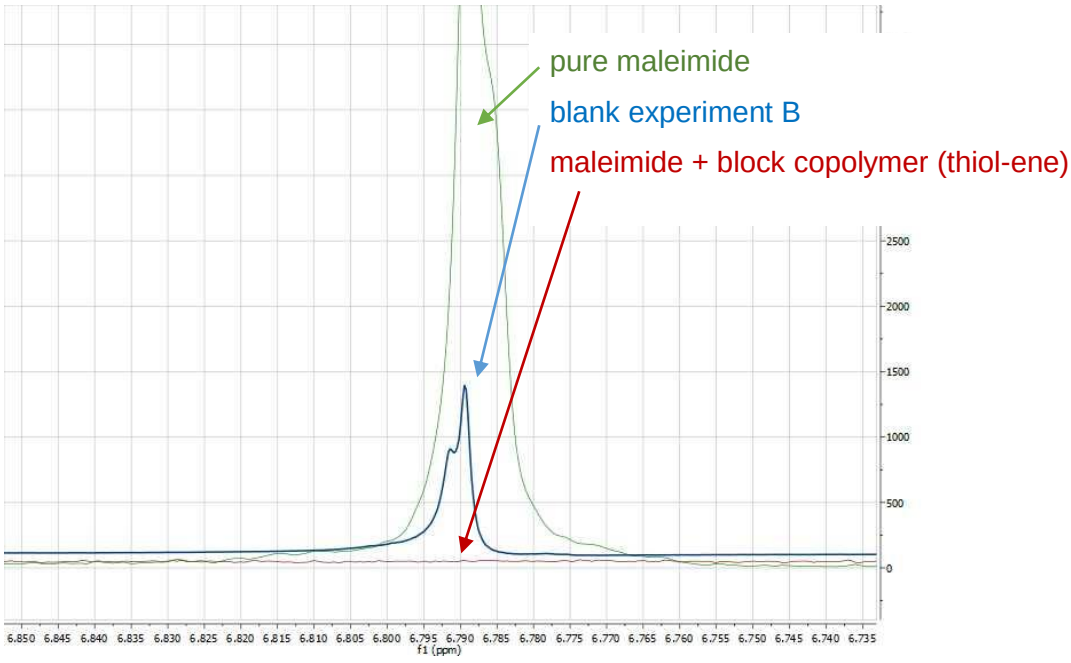


***Figure 55: Verification of the model experiment with one block copolymer without end-group via $^{1}$H-NMR-experiments***

# 3 Single Molecule Force Microscopy (SMFM)

In order to measure adhesion forces via single molecule force spectroscopy (SMFS), it was necessary to develop a strategy for functionalizing AFM chips. Due to the promising adhesion properties of the above-mentioned materials two amino acid sequences (DSSEEKC and DpSpSEEKC), dopamine-thiol and four different block copolymers out of 2-hydroxyethylmethacrylate (HEMA) and dimethyl(2-methacryloyloxyethylphosphonate) (DMMEP) were measured on different substrates. All about the synthesis of the samples can be seen in chapter before.

## 3.1 Substrate preparation

The adhesion measurements of the synthesized samples were performed on mica (muscovite) with well-known chemical and physical properties, hydroxyapatite (HA) to replicate the mineral part of the bone, a silicon wafer functionalized with $TiO_2$ nanoparticles to mimic implants and a silicon wafer coated with amino groups to mimic bone proteins.

The HA pellet was polished, washed with dest. $H_2O$ and sonicated. The top layer of mica was removed with an adhesive tape. Afterwards the HA pellet and the mica disc were glued on a glass slide (see Figure 56a). In Figure 56b a $TiO_2$ coated silicon wafer (Si-$TiO_2$) and a functionalized silicon wafer with amino groups (Si-$NH_2$) were glued on the glass slide. Subsequently, to be able to do AFM measurements in PBS-buffer, a Teflon-ring was sticked around the substrates on the glass slide (Figure 56). This ring was sealed with picodent twinsil®, an addition-curing duplicating silicone (1:1 mixture).

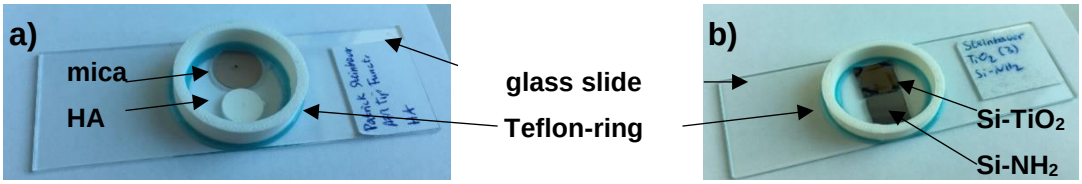


***Figure 56: Substrate preparation on glass slides***

Before coating and functionalizing, these two silicon wafers were cut in a square of 0.5 x 0.5 cm and then they have to be cleaned. Therefore, a cleaning protocol was used (see Experimental part 3.1) to remove all organic and inorganic substances. Right before the coating, the two silicon wafers were cleaned by a UV cleaner.

After implementation of a cleaning protocol, the production of the silicon wafer coated with $TiO_2$ (see Figure 57) was done by the Institute of Materials Chemistry (Dr. Alexey Cherevan).

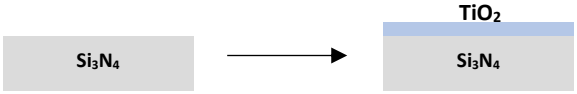


***Figure 57: Silicon nitride wafer coated with $TiO_2$ nanoparticles***

The silicon wafer was spin-coated with $TiO_2$ nanoparticles[178] and afterwards calcinated. The determination of the layer thickness was done by ellipsometry (next chapter).

The amino-functionalization of the other silicon wafer, was done according to Pasternack *et al.*[179] in two functionalization steps (Figure 58).

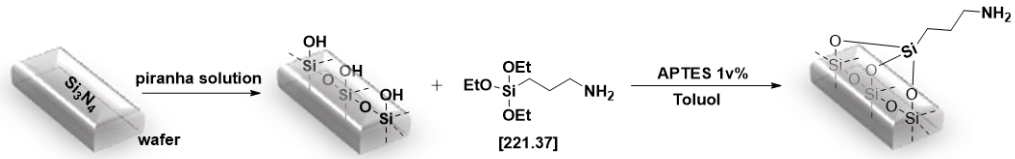


***Figure 58: Silicon nitride wafer oxidation and functionalization with 3-aminopropyltriethoxysilane (APTES)***

The cleaned silicon wafer was activated in piranha solution ($H_2SO_4$ : $H_2O_2$ (30%) = 3:1) at 80°C for about 1 h. Thereafter, the wafer was dried with argon and washed with $H_2O$ by sonification. Subsequently, the activated silicon wafer was amino-functionalized with a solution of 3-aminopropyltriethoxysilane (APTES) in toluene (1 vol%) for about 20 h at room temperature. The determination of the layer thickness was done by ellipsometry (next chapter).

### 3.1.1 Measurement of layer thickness of the silicon wafers by ellipsometry

The layer thicknesses of the coated and functionalized silicon wafers was determined by ellipsometry. Film thicknesses from 0.05 nm – 250 µm can be investigated, depending on the spectral range used and the homogeneity of

the films. Ellipsometry[180] is based on the irradiation of the surface under a certain angle with monochromatic linearly polarized light. The light will be reflected from the upper layer of the surface and the inner layer border from the substrate. This process results in an elliptical signal and will be detected.
Table 7 shows the results of the layer thickness measurement via ellipsometry.

***Table 7: Layer thickness measurement by ellipsometry***

| Sample | Layer thickness [Å] | Confidence$^{95\%}$ [Å] |
|---|---|---|
| Blank: $SiO_2$ | 13.95 | 0.25 |
| $TiO_2$ coated Si | 285.71 | 0.5 |
| Blank: $SiO_2$ | 13.85 | 0.15 |
| $NH_2$ functionalized Si | 232.69 | 0.76 |

The results show an increase of layer thickness after the $TiO_2$ coating and the amino-functionalization method compared to the blank silicon wafers.

## 3.2 Determination of AFM-Cantilever spring constants

Before tip functionalization, the spring constants of the cantilevers (cantilever stiffness) have to be determined. As mentioned in the introduction of AFM the calibration is necessary to define them because manufacturers provide them with large fluctuation margins. The AFM chip is clamped in the probe holder and the spring constant is defined on air with the “Sader”-method using thermal vibrations (thermal noise). The spring constants of each cantilever on the AFM chips can be seen in Table 15 in the Experimental Part (chapter 3.2).
The values of the spring constants do not change if the measurement is in air or in liquid. It is impossible to use the “Sader”-method in liquid.

## 3.3 AFM functionalization

The principle of AFM spectroscopy and different AFM-chip materials were described in the introduction. After determination of the spring constants the AFM chips were functionalized according to Gruber.[138]
In the first step, prior to functionalization, the Bruker MSNL-10 AFM chips were spontaneously oxidized in ambient atmosphere, resulting in a thin layer of silicon dioxide. This generates a thin layer of silanol groups (Si-OH) on the

surface, which are ready for subsequent amino-functionalization on the tip surface.

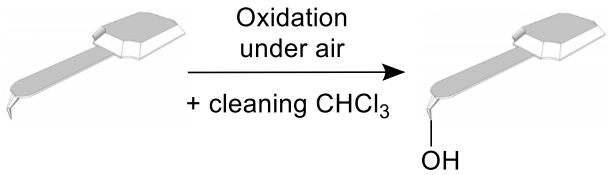


Furthermore, to get rid of organic and non-polar contaminations, the silicon nitride chips were cleaned (see Figure 59) in dry chloroform[181] and then dried with argon.

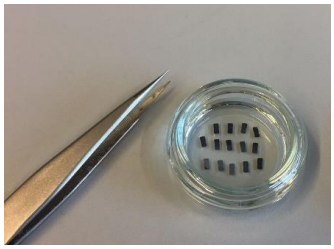

***Figure 59: Silicon nitride AFM chip cleaning procedure in petri dishes***

The second step was the amino-functionalization. Many amino-functionalization protocols (in ethanol or other polar solvents) are inapplicable because long, viscous polymers are formed,[182] which make AFM tips extremely adhesive. This problem can be avoided by applying two alternative methods of amino-functionalization.[183] The amino-functionalization with ethanolamine hydrochloride using DMSO as solvent and the vaporisation of (3-aminopropyl) triethoxysilane (APTES) were the most prevalent methods. They generate a relatively low density of amino groups on the tip surface, which is perfect for performing single molecule force microscopy.

In this thesis, the ethanolamine method was chosen, because it is much simpler and more suited for beginners. As already mentioned it is better to bind as few molecules as possible to the AFM tip. Moreover the ethanolamine pathway needs no special equipment, like deposition chambers, because the modification of APETS only works as a gas phase reaction in a deposition chamber. Nevertheless, according to literature[184] the APTES method produces better AFM results.

The amino-functionalization was accomplished by dissolving ethanolamine hydrochloride in dry DMSO. Moreover, molecular sieve beads were immersed to adsorb produced water and a Teflon-disc was placed in the middle of the

beaker to protect the AFM chips. The solution was heated to 70°C and degassed in a desiccator.

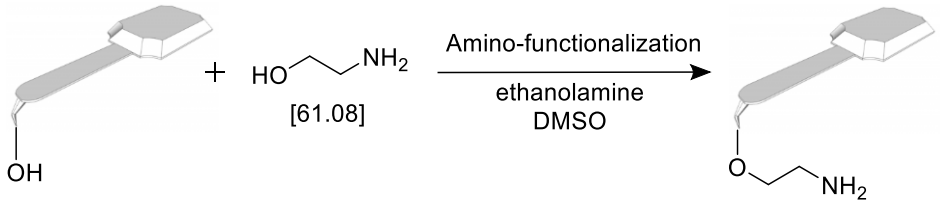


The oxidized AFM-chips were placed on the Teflon-disc, shortly after (Figure 60). After several hours reaction time, the chips were washed with DMSO and ethanol.

***Figure 60: Amino-functionalization method with aminoethanol***

The third step was the attachment of the linker system. Some protocols use physiochemical adsorption[185] while others bind their molecules covalently to the tip. The latter approach is much more advantageous because it guarantees better surface attachment. Covalent bonds are about ten times stronger than typical receptor-ligand bonds.[186]

Introducing a long, thin, flexible polymer chain between the AFM tip and the ligand has many considerable advantages. Firstly, the ligand molecule can flip rapidly, resulting in much higher chances for binding a receptor molecule on the sample surface. Secondly the polymer chain shows higher elasticity than the cantilever. Thirdly, the long chain avoids adhesion between the tip and the sample surface directly. But a too long polymer chain can cause the binding probability to significantly decrease.[187]

For the attachment of the spacer PEG chains with a length of 20 nm and a molecular weight around 1500 g/mol are used.[188-189]

In literature[190] many PEG-NHS-linker systems (Figure 61) were described. Due to the Mal-PEG-NHS linker system site-specific coupling is achieved by linking cysteine to maleimide or binding of $His_6$-tagged proteins to tips carrying tris-NTA functions.[138, 191] The reaction of amino-functionalized AFM tips with Biotin-PEG-NHS results in tips with flexibly linked biotin that has a high affinity

for immobilized avidin or streptavidin.[192] The acetal-PEG-NHS linker system is used for protein coupling, but also for small molecules like ATP to AFM tips. Therefore, the acetal group is converted into an aldehyde group with citric acid. The disadvantage of aldehyde coupling is that one of the many amino groups is randomly chosen for coupling.[193-194] The Azide-PEG-NHS is coupled with the help of a catalyst ($Cu^{2+}$ and ascorbate) to an alkyne-derivatized ligand via click chemistry.[138] The major advantage is that synthetic ligands can easily be equipped with alkyne groups and reacted with the azide-tip, without getting into conflict with the chemical functions of the ligand molecule.

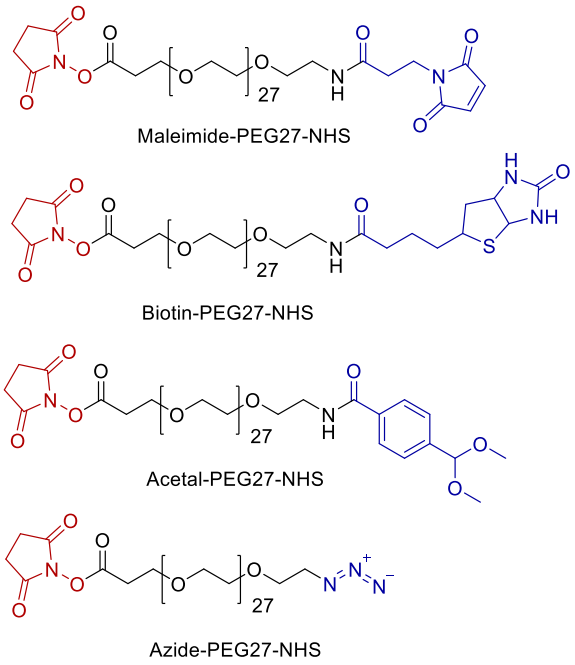


***Figure 61: Different linker-systems reported for AFM tip functionalization***

In this work the maleimide-PEG-NHS linker system was chosen and for that reason all samples were synthesized with a thiol end group to use Michael type maleimide-click chemistry.

Considering that the AFM tip is amino-functionalized, one end of the PEG linker should have an NHS-ester reactive group. Because NHS ester-activated compounds react with primary amines in physiologic to slightly alkaline conditions (pH 7-9) to yield stable amide bonds (see Figure 62). The reaction releases N-hydroxysuccinimide (NHS).

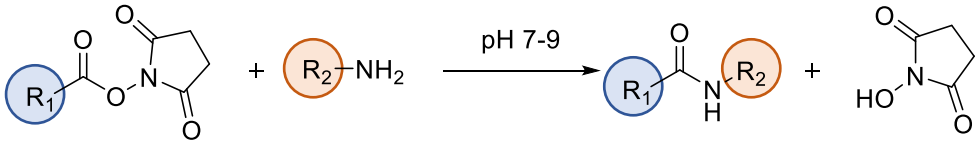


***Figure 62: NHS esterification***

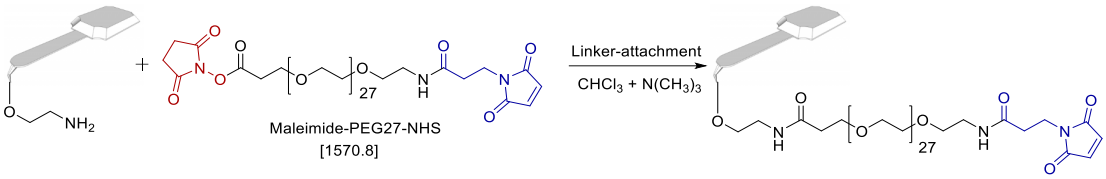


In order to attach the linker system to the amino groups of ethanolamine, it was dissolved in dry chloroform and mixed with dry triethylamine. This solution was injected in four reaction chambers of a Teflon-block (Figure 63) and the AFM chips were immersed. The reaction chambers were closed with a Teflon-disc. After two hours, the chips were washed with dry chloroform, to remove unreacted linker molecules, and dried with nitrogen.

***Figure 63: Teflon-block with reaction chambers***

The last step is the attachment of the sensor molecule. In this step AFM chips (spring constants of all used AFM cantilevers see in Experimental Part chapter 3.2) were functionalized with two different amino acid sequences, with dopamine-thiol and with four different block copolymers synthesized by RAFT polymerization. As mentioned before these samples contain thiol groups and so Michael type thiol-ene click chemistry was done. The coupling of thiols to maleimides has many advantages: (a) in contrast to disulfide coupling,[195] coupling to maleimides is much faster and not reversed by excess of thiol ligand in the solution, (b) it allows site-specific attachment of the peptide (c) low micromolar concentrations of thiol-modified compounds can be coupled,[196] (d) coupling in presence of tris(2-carboxyethyl)phosphine (TCEP) converts disulfides into reactive thiol functions[197] and TCEP does not react with maleimide, in contrast to other reducing agents.

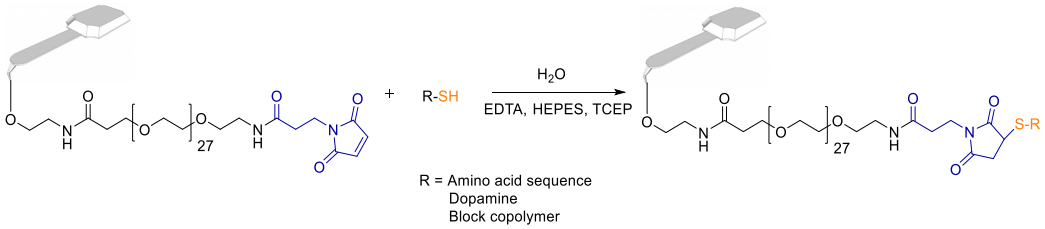


AFM-chips, which were functionalized with the same adhesion motif, were positioned in a circle on a Parafilm. The amino acid sequence, dopamine-thiol

or one of the block copolymers was dissolved in deionized water and mixed with EDTA, HEPES 1, TCEP and HEPES 2 (preparation see Experimental Part 2.5 – stock solutions). This sample solution was pipetted in the center of the AFM chip circle (Figure 64). EDTA is necessary to prevent re-oxidation during the coupling procedure on a time scale of few hours and HEPES as buffering agent. For longer reaction times it is advantageous to do the reactions under argon atmosphere.

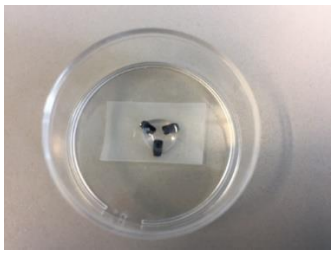

***Figure 64: Circle of AFM chips with droplet of DSSEEKC solution***

In order to check the suitability of the reducing agent and the special reaction conditions (pH) the last step of this tip functionalization method was simulated in model reactions (see in Experimental Part 2.5).

## 3.4 Area density

In order to prove the possibility of tethering one molecule on the apex of the AFM-tip and to perform single molecule atomic force microscopy some calculations concerning the quantification of coupling sites on the used AFM tips were done.
In Riener *et al.*[198] and Ebner *et al.*[183] the quantification of coupling sites is done by a marker enzyme assay. After amino functionalization of silicon nitride chips with ethanolamine, aminophenyl-trimethoxysilane (APhS) or aminopropyl-triethoxysilane (APTES), the attachment of Biotin-PEG-NHS ensues to the typical procedure (Figure 65).

A silicon nitride chip was tethered with a biotin-PEG-NHS linker system according to Gruber (see Figure 65a).[192] In the next step of the marker enzyme assay ExtrAvidin-peroxidase is bound to the biotin groups and the unbound enzyme is washed away (see Figure 65b). Due to the addition of o-phenylene diamine (OPD) and $H_2O_2$ the peroxidase converts the colorless precursors into

brown color (see Figure 65c). Figure 65d is a control experiment with biotin-blocked ExtrAvidin-peroxidase- This control shows the extent of non-specific adsorption to the chip surface.

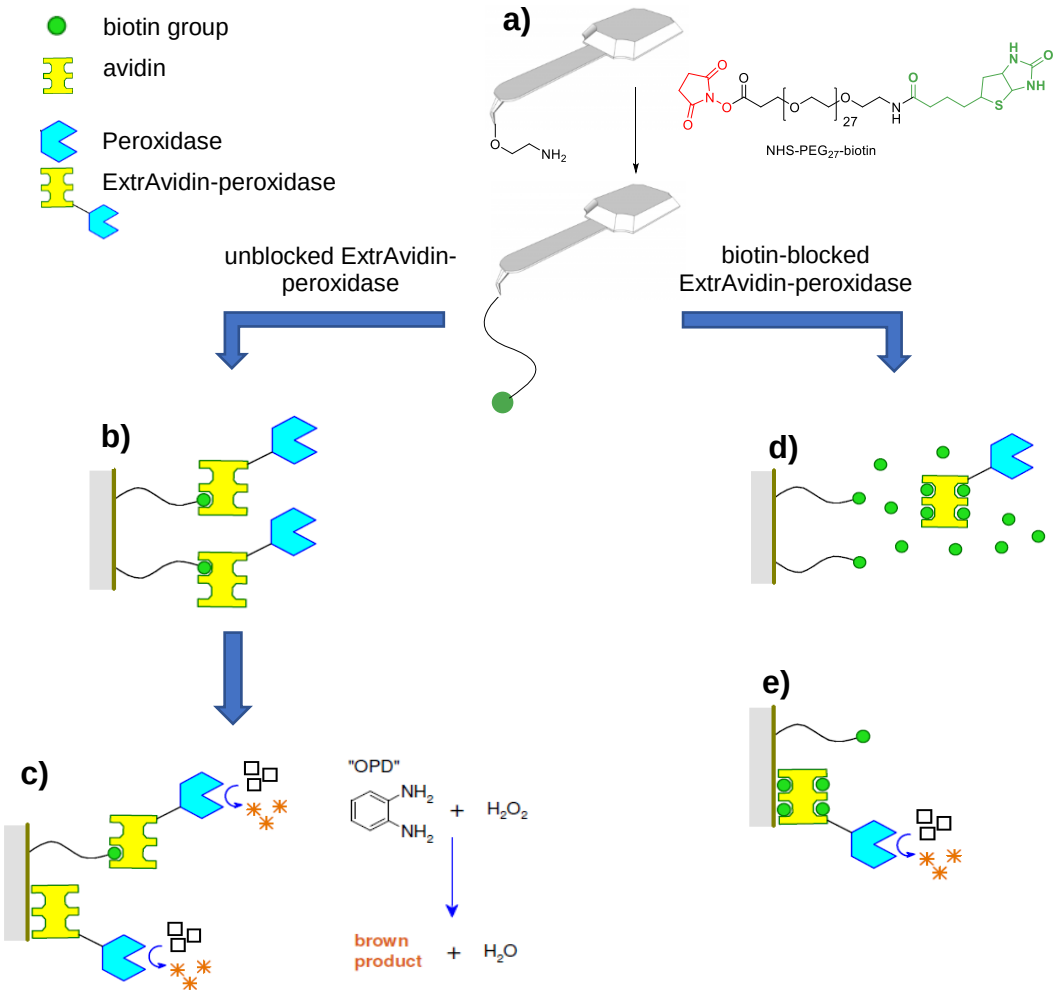


***Figure 65: Enzymatic assay for the density of biotin groups.***

***a) Biotin-PEG-linker system is attached to the AFM b) ExtrAvidin-peroxidase is immobilized by specific binding to surface-linked biotin and by non-specific adsorption to the surface. c) Due to the addition of o-phenylene diamine (OPD) and $H_2O_2$ brown colored product was formed by the peroxidase. d) + e) In presence of free biotin, all biotin-binding sites are blocked and ExtrAvidin-peroxidase is immobilized by non-specific adsorption only.[183]***

The number of specifically bound ExtrAvidin-peroxidase molecules is obtained by subtracting the number of nonspecifically bound molecules from the total number bound molecules quantified via UV-Vis.

Ebner *et al.*[183] reported the afore-remarked three methods of amino functionalization and the resulting area density of reactive sites in molecules per µm$^2$ (see Figure 66 and Table 8).

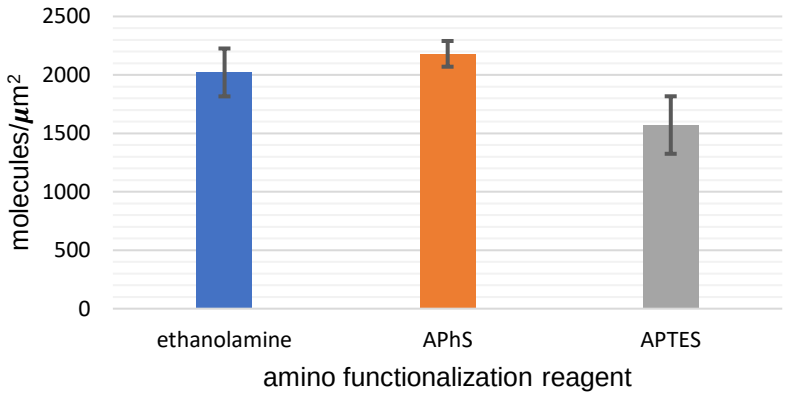


***Figure 66: Quantification of coupling sites by a marker enzyme assay[183]***

***Table 8: Marker enzyme assay area density[181]***

| amino functionalization | area density [molecules/µm²] |
|---|---|
| ethanolamine | 2021 ± 205 |
| APhS | 2180 ± 110 |
| APTES | 1571± 246 |

As mentioned before, in this thesis the amino functionalization was done via the ethanolamine method according to Gruber[182] and Bruker MSNL-10 AFM Chips were used. The resulting area density of reactive sites with ethanolamine is 2021 ± 205 molecules/µm$^2$. The apex of the AFM tip has a nominal radius ($r_{nom}$) of 2 nm and a maximal radius ($r_{max}$) of 12 nm. In calculations below $r_{max}$ and the highest possible area density were chosen.

**Calculation:**

$$A\ (area\ of\ apex) = {r_{max}}^2 * \pi = 452{,}39\ nm^2$$

$$molecules\ tethered\ to\ apex = A * \rho_{area} \cong \mathbf{1\ molecule}$$

By the use of the amino functionalization method and this Bruker AFM chips, only one molecule can maximal be tethered to the apex of the AFM tip. The type of the linker system is irrelevant as long as it is not too bulky or causes in other interactions.

Furthermore, if the molecule chains were tethered to the side of the AFM tip (Figure 67), more retraction signals will be seen in the force distance curve. Because some chains will retract earlier or even later.

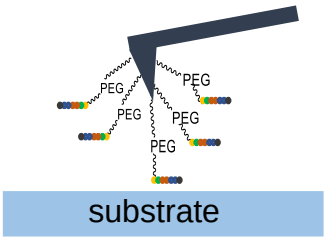


***Figure 67: Attachment of the linker-PEG-chains***

## 3.5 AFM measurement

In order to measure the adhesion forces of the functionalized tips on mica, HA, Si-$NH_2$ and Si-$TiO_2$ the measurements have to be done in PBS-buffer (pH 7.2-7.4, sterile filtered). After every functionalization step, a chip was stored in PBS-buffer. As a consequence, the adhesion forces of the different functionalization steps can be compared. Due to the short lifetime of the tip (tip contamination or damage), the AFM probes have to be measured within one week. In particular, when the sample surface is fragile and contaminated with loosely bound material, the adhesion of the sample may be lost after recording a few force curves. The softest cantilever of the AFM chip was chosen for the AFM measurements.

The deflection of the cantilever is directly proportional to the tip-sample interaction force. It is important to mention that this method does not directly measure the deflection on the end of the cantilever, but rather the slope of the cantilever at the position where the laser is reflected.[199] This means before each experiment, a **calibration** procedure has to be done. Thereby, the photodetector voltage signal with the deflection (sensitivity) of the cantilever is changed. The cantilever is calibrated by approaching to a very hard surface (glas, mica) and assuming the AFM tip not indent into the surface. Since the substrate is much stiffer than the cantilever, the piezo movement is completely translated into cantilever deflection leading to a linear part in the upper curve region. The slope of this linear part is defining the sensitivity (see Figure 68 and Equation 6).

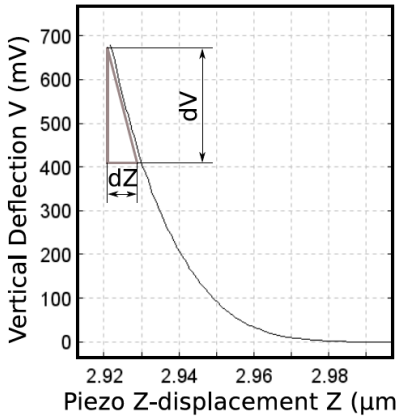


***Figure 68: Definition of the sensitivity***

$$sensitivity\left[nm\,Volts^{-1}\right] = \frac{dZ}{dV}$$

**Equation 6: Calculation of the cantilever sensitivity**

All probes were measured in a force map with 10 x 10 force curves (1 x 1 µm$^2$ area) with 0 s, 2 s, 4 s and 8 s delay time. At every delay time 100 force curves were recorded. The delay time is the time which the piezo remains at the surface. The higher the delay time the higher should be the adhesion force (or pull off force) because the amino acid sequences or polymers have more time to adhere and to align to the surface. The parameters for the AFM measurement were summarized in Table 9

***Table 9: Measurement parameters***

| parameter | adjustment |
|---|---|
| set point | 0.5 nN |
| speed | 2 µm s$^{-1}$ |
| z-length | 1 µm |

An important fact is that the measurements cannot be done with a reflected light camera because in liquid it is hard to see anything. This means that a specific region on hydroxyapatite could not be seen.

## 3.6 AFM data analysis

In a typical experiment, the functionalized tip was lowered at a constant speed of 2 µm $s^{-1}$ onto surface (constant loading rate) and then retracted at the same speed while the force versus distance was recorded (extension and a retraction curve). In case of no adhesion the retraction curve follows closely the extension curve. If the sample shows adhesion to the surface, an increasing attractive (neg.) force is detected. Predominantly, single and double rupture events were observed, but multiple consecutive events occurred very rarely. These events are accompanied by a characteristic nonlinear force signal due to elastic extension of the distensible PEG-linker and the sample, which is sometimes visible in the retract curve (see Figure 69).

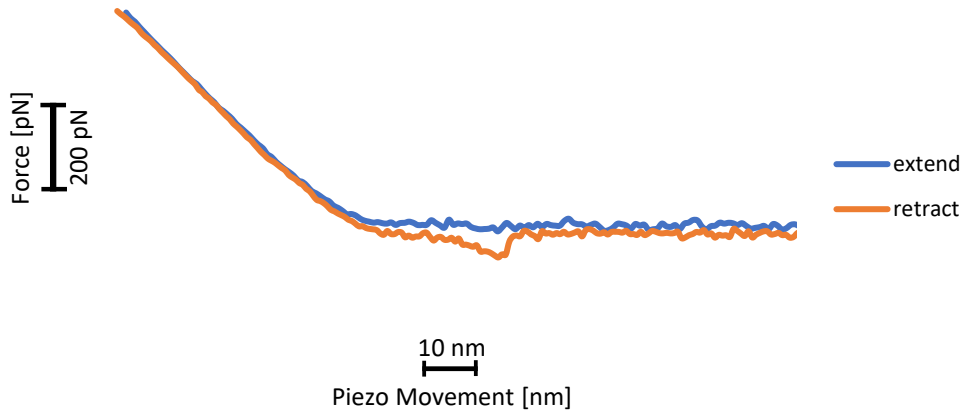


***Figure 69: Typical force distance curve with a single unbinding event caused by the PEG linker***

Prior to analysis, only single rupture events (adhesion events) were taken into account ensuring over 95% probability and the adhesion event was mediated by a single bound.[200] Because careful considerations are required in dealing with multiple rupture events in force distance diagrams. In case the cantilever jumps back to the baseline between each of the consecutive rupture events all events can be regarded as independent (see Figure 70).[201] If the return to the baseline is lacking, it is likely that load is shared between all bonds.[202-204]

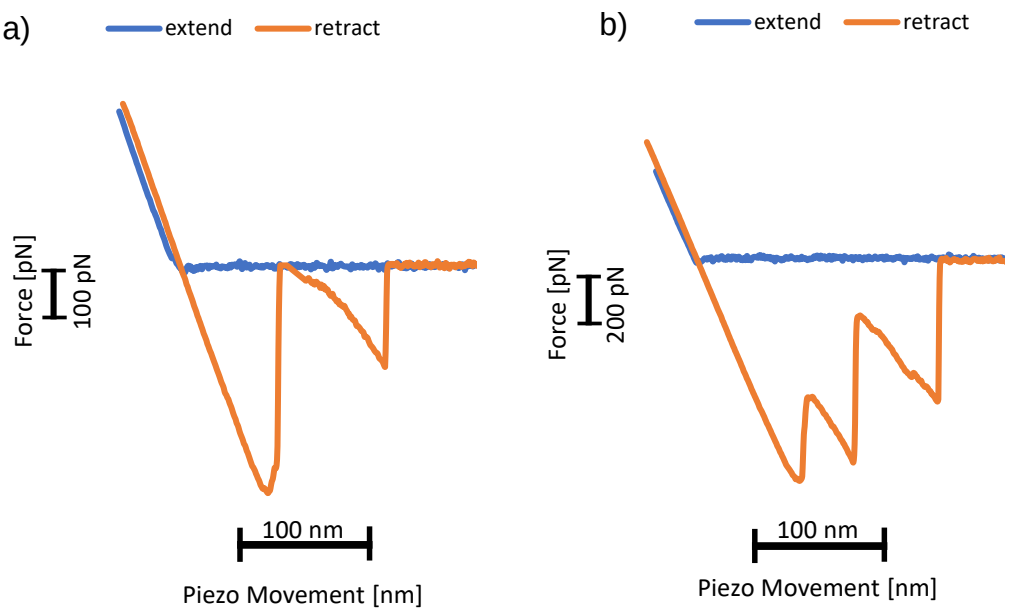


***Figure 70: Typical force distance curves with a) double independent events and with b) multiple rupture events which share their loads between all bonds***

Furthermore, multiple rupture events will occur when other linker molecules are tethered to the side of the tip (see Figure 71). This complex issue can be avoided by looking only at the single rupture events.

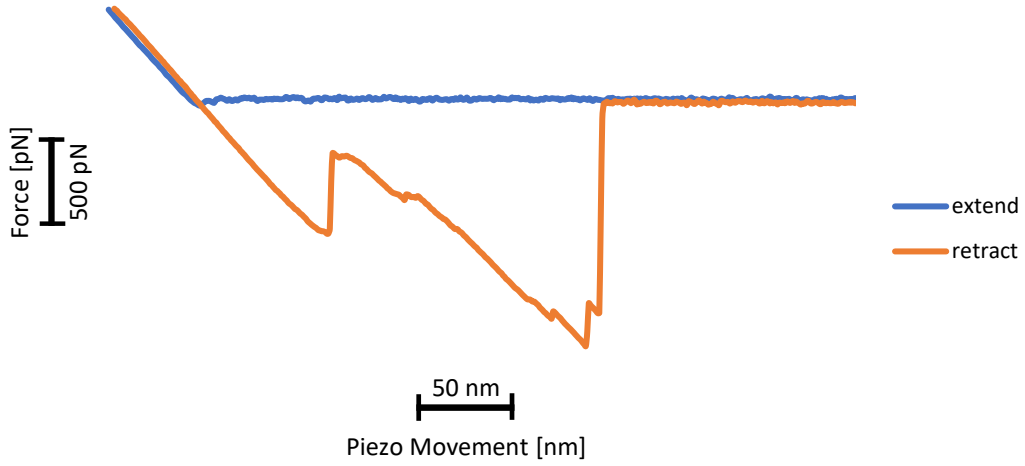


***Figure 71: Typical force distance curve with multiple events caused by the attachment of a linker chain on the side of the AFM tip***

The binding forces are generally a combination of electrostatic, hydrophobic, dipole-dipole interactions, and hydrogen bonding and depend on the conditions such as pH and ionic strength.

In order to control the functionalization steps and the method *per se*, an un-functionalized AFM tip (naked tip), the linker system attached to an AFM tip and the amino acid sequences DSSEEKC and DpSpSEEKC were measured on mica, hydroxyapatite, $TiO_2$ and on $NH_2$ functionalized silicon nitride surfaces. In addition to that, all samples with a delay time of 8 s were chosen for the statistical tests. Figure 72 shows the mean values and standard deviations of the measured adhesion forces at different delay times. They were obtained from a minimum of 50 force distance curves.
The selection of the different statistical tests was discussed in the experimental part. All statistical tests were displayed in the Appendix.
Kolmogorov-Smirnov and Shapiro-Wilk normality tests were performed on each substrate to check the distribution (see Table 19, Table 23, Table 27, Table 31 in the Appendix). The adhesion forces at 8 s delay time were not always normally distributed and therefore a distribution-free test was done. Furthermore, Levene's test was performed on all data of all four substrates (see Table 20 Table 24 Table 28 Table 32 in the Appendix). The assumption of homogeneity of variance has been violated ($F(8, 764) = 19.89$, $p < 0.01$) on mica, ($F(8, 528) = 13.37$, $p < 0.01$) on HA, ($F(8, 797) = 17.950$, $p < 0.01$) on $TiO_2$ and ($F(8, 812) = 27.377$, $p < 0.01$) on $NH_2$, which is shown by the fact that the significance of Levene's test is less than 0.05. Summarizing, these data are not normally distributed and the groups have heterogeneous variances.

In the absence of an attached sample, the naked AFM tips showed essentially no hysteresis between extension and retraction curves in experiments conducted under identical conditions (see Figure 72a-d). In Figure 72a) the naked tip shows a maximum mean force of 274 pN $\pm$ 77 pN at 8 s delay time (force distance curve see Figure 73) on hydroxyapatite, indicating that there are some H-bridge bondings between the oxidized tip (Si-OH) and the substrate.


naked linker DSSEEKC DpSpSEEKC dopamine

**a)**

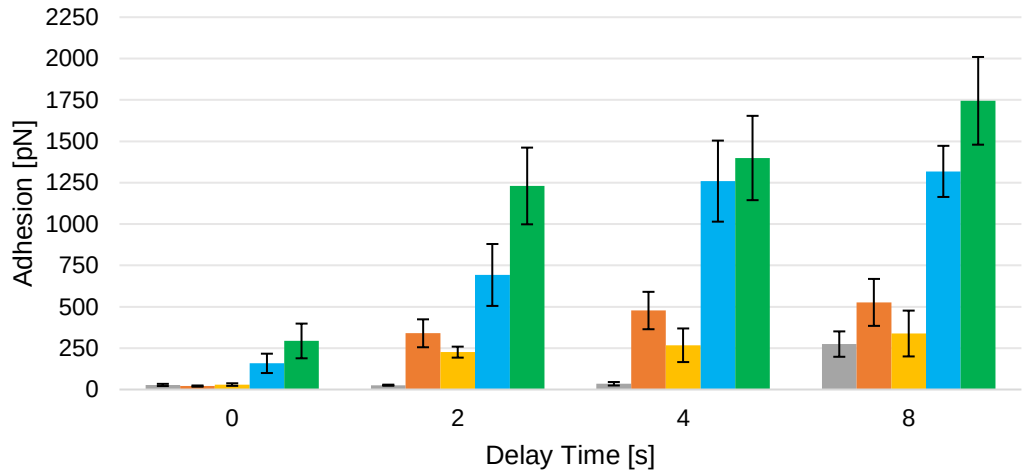


**b)**

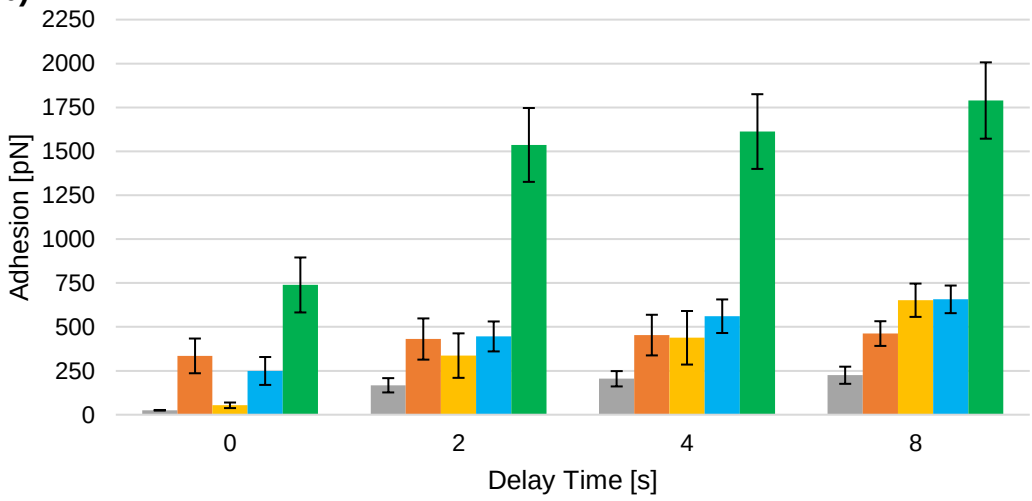

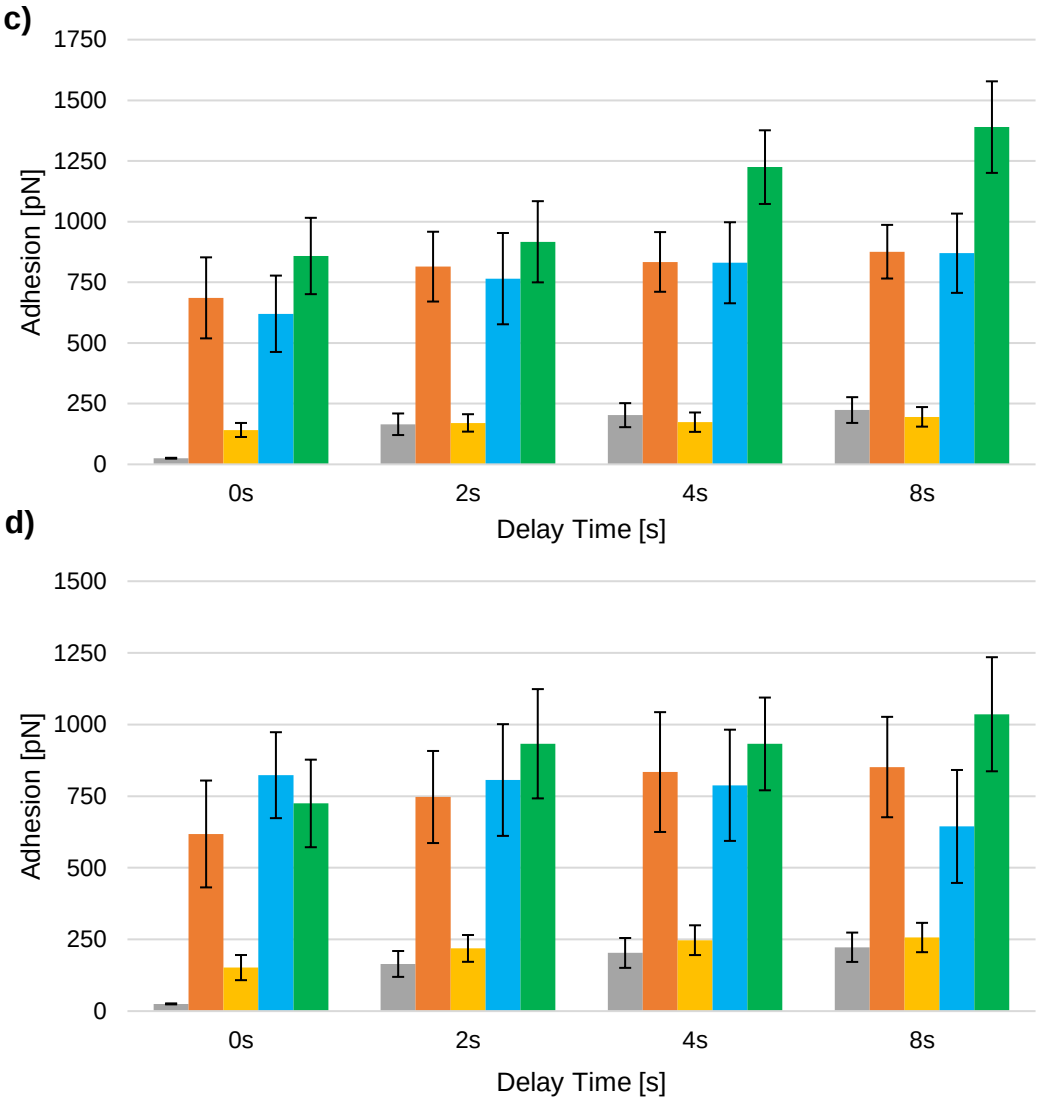


***Figure 72: Mean values of adhesion force of a naked tip, linker tip, DSSEEKC tip, DpSpSEEKC tip and a dopamine tip at different delay times measured on a) hydroxyapatite, b) mica, c) $TiO_2$ and d) on $NH_2$ functionalized silicon nitride.***

In Figure 72c,d the pull-off forces at 8 s delay time of the naked tip are significantly lower than of the linker functionalized tip. In Figure 72a,b the adhesion values of the naked tip and of the linker tip differ significantly, except the values with 8 s delay time. As a consequence, the attachment of the linker system was successful. The high adhesion value of the linker sample on $TiO_2$ can not be explained, maybe there was some contamination. Due to the reaction of the maleimide of the linker system with the amino functionalized surface, higher adhesion values can be seen in Figure 72d.

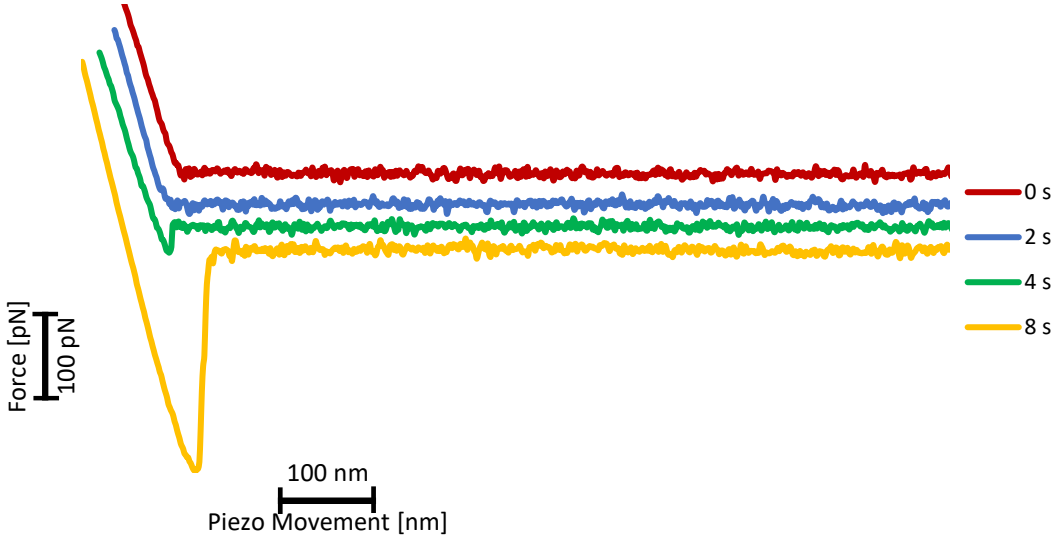


***Figure 73: Force distance curves of the naked AFM tip on hydroxyapatite measured at different delay times***

Furthermore, the Kruskal-Wallis test (H-test) and the Dunn-Bonferroni correctioni showed that the adhesion values of the linker system and of the amino acid sequence DSSEEKC differ significantly except on mica and HA. But on these two substrates the pull-off force of DSSEEKC is very low anyhow. The attachment of the amino acid sequence must be successful due to the significant force values on $TiO_2$ and $NH_2$. In particular, through the addition of DSSEEKC to the linker, the maleimide was blocked and this sequence interacts weakly with the substrates (see Figure 74b).

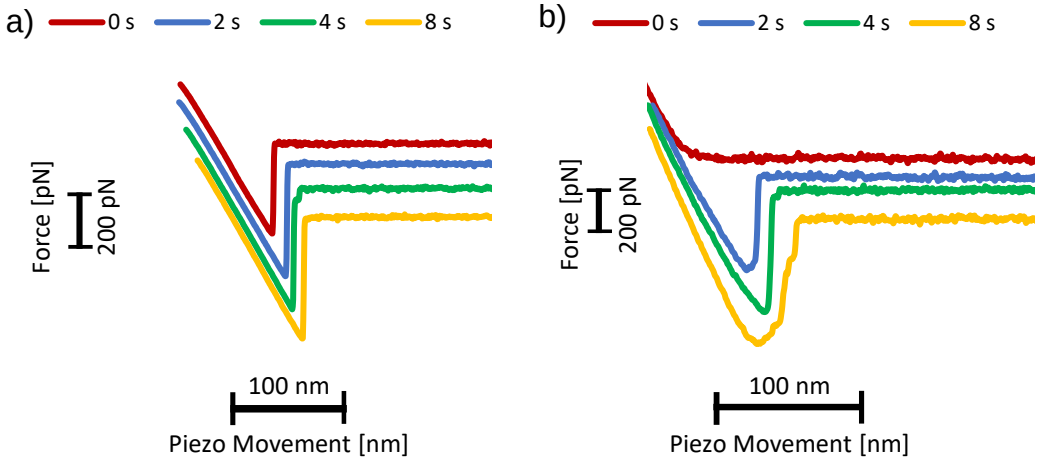


***Figure 74: Force distance curves of the a) linker functionalized AFM tip measured on mica and b) DSSEEKC measured on hydroxyapatite at different delay times***

The mean adhesion force values of DpSpSEEKC on hydroxyapatite, $TiO_2$ and $NH_2$ were significantly higher than the values of DSSEEKC (force distance curves see Figure 75).

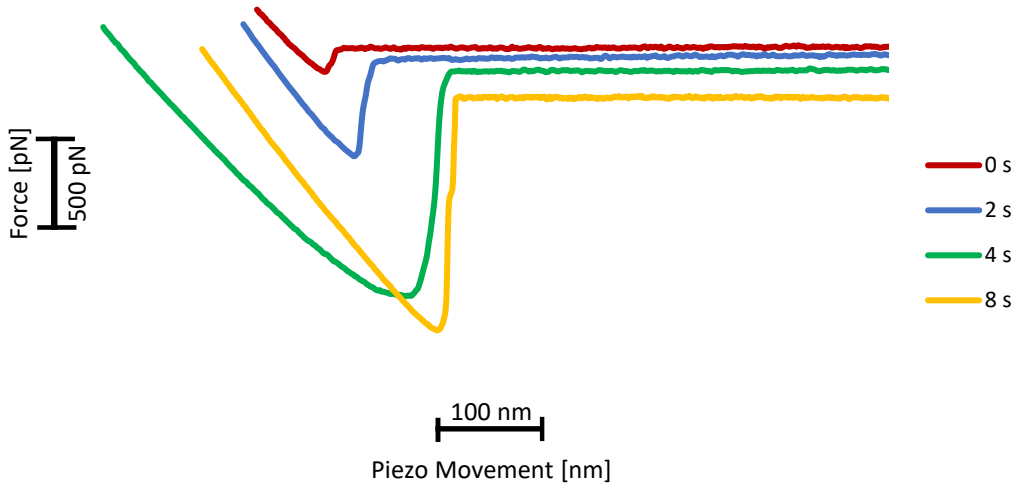


***Figure 75: Force distance curves of the DpSpSEEKC functionalized AFM tip on hydroxyapatite measured at different delay times***

As a result, the phosphorylated serines were responsible for the higher adhesion force on hydroxyapatite as it was described in literature.[110, 112] Additionally, the phosphorylated serines were also the reason for strong adhesion on $TiO_2$. On mica, the phosphorylated serines were not responsible for the higher pull-off forces. Because the mean values of the two amino acid sequences were in the same range and so they differ not significantly (see Figure 72b).

Another important fact is the comparison of the mean adhesion values of dopamine on $TiO_2$ (see Figure 72c) with the values in literature.[104] There, the mean force value was calculated to be 847 pN ± 157 pN (250 ± 62 nN $s^{-1}$ loading rate) on $TiO_2$ with a different linker system. The measured mean force value in Figure 72c) was 859 ± 157 pN (0 s delay time) and with higher delay time the pull-off force gets even higher (see Figure 76).

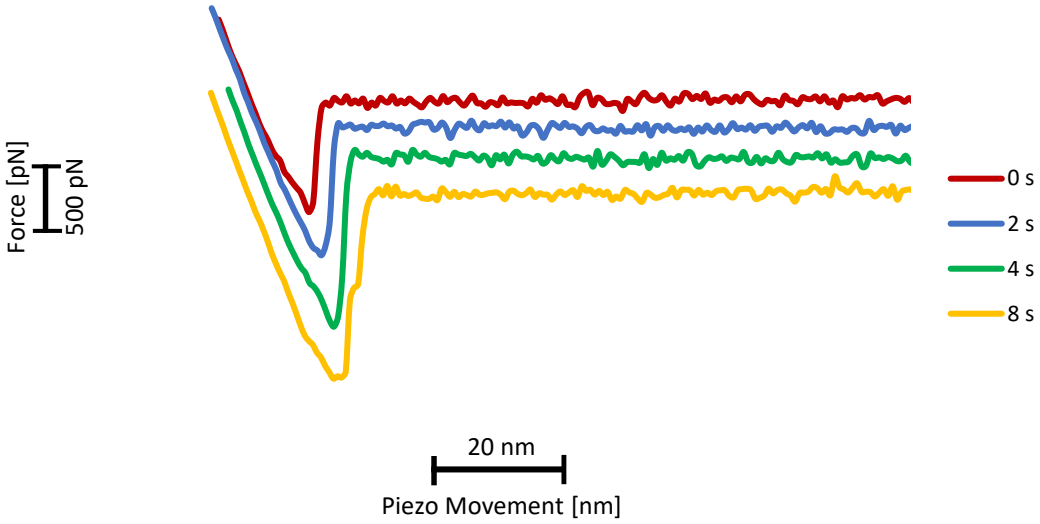


***Figure 76: Force distance curves of the dopamine functionalized AFM tip on $TiO_2$ measured at different delay times***

In order to put this adhesion force value in perspective, Oesterhelt *et al.*[205] have determined that a few nN of force were required to rupture a single covalent bond.

As last point, it is important to mention, that the standard deviations on hydroxyapatite and the $NH_2$ functionalized surface were quite high. The surface of hydroxyapatite was polished, but it was still too rough for AFM measurements and the functionalized surface was not covered with the same number of molecules over the whole area. This problem could be avoided, if the measurements were done on a polished piece of bone with organic and inorganic parts.

In Figure 77a-d) the mean adhesion values of dopamine as a reference and the synthesized block copolymers measured on hydroxyapatite, mica, $TiO_2$ and $NH_2$ were shown.

The block copolymers had significantly higher pull-off forces than dopamine on $TiO_2$ and $NH_2$ (see Figure 77c,d). The pull-off force on mica of the polymers with 39 kDa was significantly higher than of dopamine (see Figure 77b). The mean adhesion values on HA of the polymers with 39 kDa were in the same range as the values of dopamine and the polymers with 28 kDa showed even lower adhesion forces.

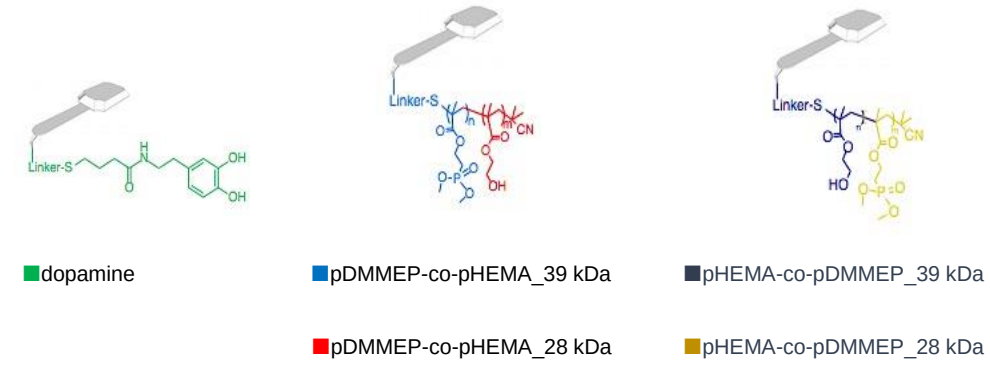
Linker-S
OH
OH
Linker-S
CN
OH
Linker-S
CN
HO

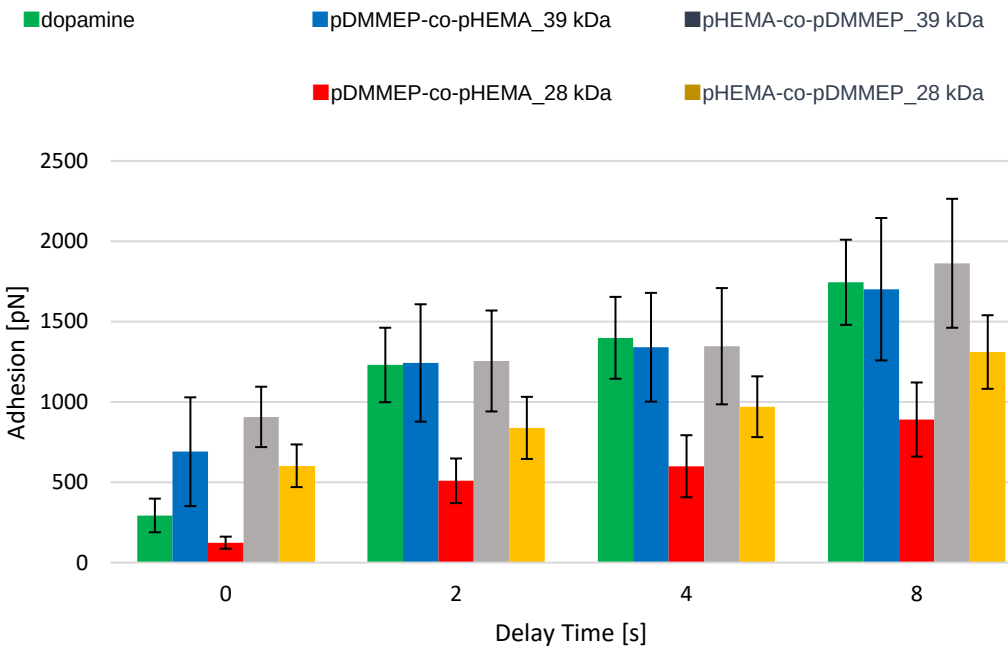
dopamine
pDMMEP-co-pHEMA_39 kDa
pHEMA-co-pDMMEP_39 kDa
pDMMEP-co-pHEMA_28 kDa
pHEMA-co-pDMMEP_28 kDa
2500
2000
1500
1000
500
0
Adhesion [pN]
0
2
4
8
Delay Time [s]

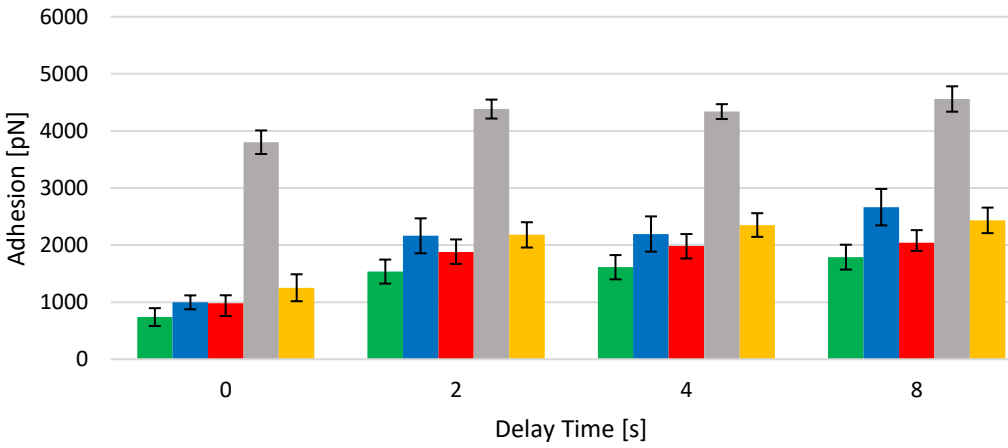
6000
5000
4000
3000
2000
1000
0
Adhesion [pN]
0
2
4
8
Delay Time [s]

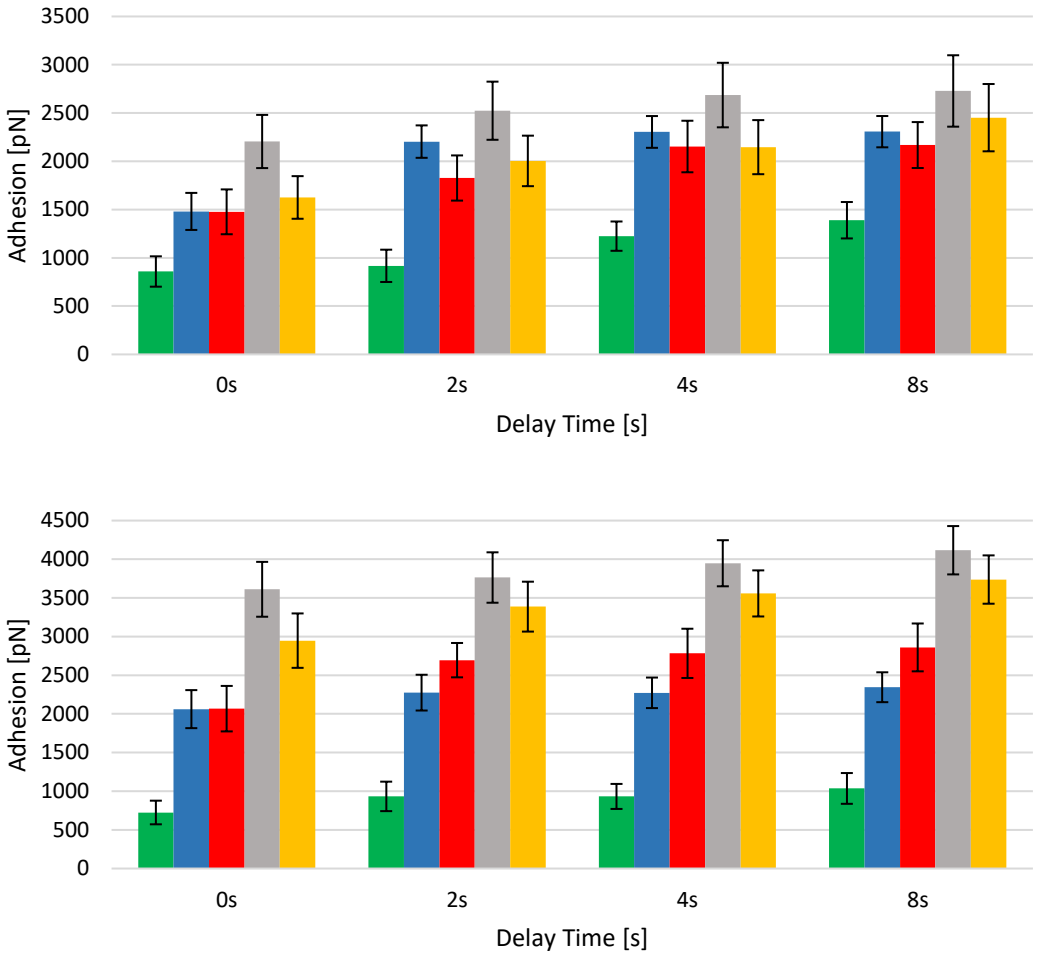


***Figure 77: Mean values of adhesion force of the synthesized block copolymers and dopamine as a reference at different delay times measured on a) hydroxyapatite, b) mica, c) $TiO_2$ and on d) $NH_2$ functionalized silicon nitride.***

In Figure 77 the higher adhesion forces of the polymers with 39 kDa are remarkable, indicating that the block copolymers with 39 kDa contain more DMMEP than the 28 kDa ones. Thereby, the phosphorus ester plays an important role to adhere on these substrates. In particular, the adhesion forces of the block copolymers with 39 kDa on mica were significantly higher than of the block copolymers with 28 kDa.

If the 39 kDa polymers and the 28 kDa polymers were compared among themselves, there can be seen significantly higher adhesion forces of the block copolymers starting with the HEMA block than of the polymers starting with a DMMEP block on mica and $NH_2$. In particular, when the HEMA block is attached to the linker system, the DMMEP block is on the free end of the chain and the interaction of the phosphorus ester groups with the surface is higher.

The mean adhesion forces of the 39 kDa pHEMA-co-pDMMEP block copolymer on all four substrates were very high, especially on mica (see Figure 78a) and $NH_2$ (Figure 78b).

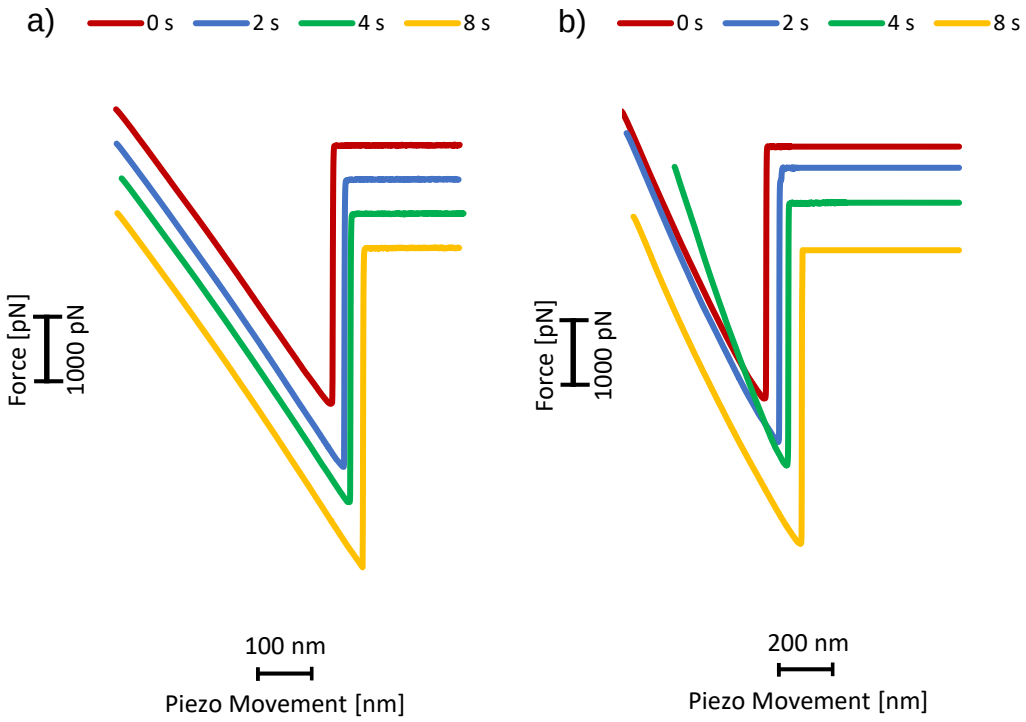


***Figure 78: Force distance curves of the pHEMA-block-pDMMEP (39 kDa) functionalized AFM tip measured on a) mica and on b) the amino functionalized silicon nitride wafer at different delay times***

All mean adhesion force values and standard deviations were summarized in Table 18 in the Experimental Part (chapter 3.6).

# Experimental Part

## 2 Adhesion motifs and synthesis thereof

### 2.1 Synthesis of the Monomer

The synthesis of dimethyl(2-methacryloyloxyethylphosphonate) (DMMEP) was carried out in three different pathways according to literature[131, 149-150].

#### 2.1.1 Synthesis of dimethyl(2-methacryloyloxyethylphosphonate) (DMMEP) (1)

The first step of pathway one was the **synthesis of 2-chloroethylmethacrylate (CEMA)**.

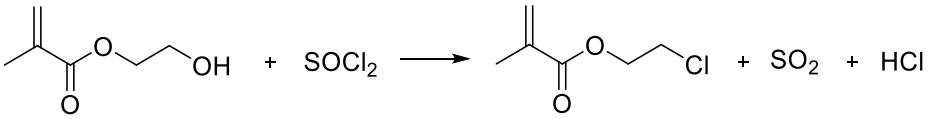


[130.14] **HEMA** [118.96] [148.59] **CEMA**

| reagents | n [mmol] | m [g] | V [mL] |
|---|---|---|---|
| 2--hydroxyethylmethacrylate (HEMA) | 130 | 16.92 | 15.81 |
| thionylchloride | 180 | 21.41 | 13.06 |

**Procedure:**

Thionyl chloride was taken in a three-necked round-bottomed flask fitted with a condenser and a dropping funnel. The apparatus was purged three times with Argon. HEMA was added dropwise over the course of approximately 1.5 h under vigorous stirring. After complete addition, the temperature of the oil bath was gradually raised to 80°C and the solution was stirred for 4h. The excess of thionyl chloride was removed by applying vacuum. After that, 10 mg of phenothiazine were added and 2-chloroethylmethacrylate (CEMA) was distilled under reduced pressure (72°C, 24 mbar).

**Yield:** 9.05 g (47% theoretical yield), colorless liquid

**$R_f$-value** (PE:EE 4:1): 0.68

**RI $n_D^{25°C}$:** 1.452 (Lit.: 1.4515)

**$^1$H-NMR**: (400 MHz, $CDCl_3$) δ (ppm): 6.16 (s, 1H, C<u>H</u>$_2$=C <u>cis</u>), 5.61 (s, 1H, C<u>H</u>$_2$=C <u>trans</u>), 4.39 (dd, 2H, $J_1$ = 6.3 Hz, $J_2$ = 5.2 Hz, O-C<u>H</u>$_2$), 3.72 (dd, 2H, $J_1$ = 6.3 Hz, $J_2$ = 5.2 Hz, C<u>H</u>$_2$-Cl), 1.95 (s, 3H, C<u>H</u>$_3$)

**$^{13}$C-NMR**: (100 MHz, $CDCl_3$) δ (ppm): 166.96 (<u>C</u>=O), 135.81(<u>C</u>H$_2$=C), 126.31 (CH$_2$=<u>C</u>), 64.25 (O-<u>C</u>H$_2$), 41.59 (<u>CH$_2$</u>-Cl), 18.23 (<u>C</u>H$_3$)

**MS** (m/z): calcd. 148.59, found 149.07 [M]

### 2.1.2 Synthesis of dimethyl(2-methacryloyloxyethylphosphonate) (DMMEP) (2)

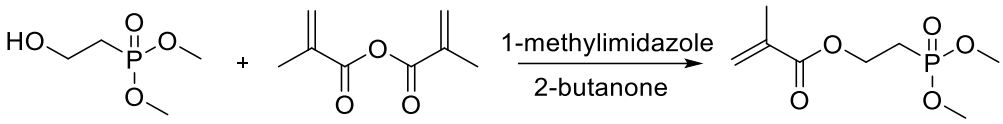


[154.10] [154.17] [222.18]
**DMMEP**

| reagents | n [mmol] | m [g] | V [mL] |
|---|---|---|---|
| dimethyl(2-hydroxyethyl)phosphonate | 50 | 7.71 | |
| methacrylic anhydride | 50 | 7.71 | |
| 1-methylimidazole | 0.25 | 0.01 | |
| 2-butanone | | | 18 |

**Procedure:**

Dimethyl(2-hydroxyethyl)phosphonate and 1-methylimidazole were combined with 10 mL dry butan-2-one in a three-necked round-bottomed flask. The apparatus equipped with a dropping funnel was purged with Argon for three times. Methacrylic anhydride and 7.5 mL dry butan-2-one were transferred into the dropping funnel and the oil bath temperature was brought up to 68°C. Afterwards the solution was added in a dropwise manner. The mixture was then stirred for 6 h. Solvent and residual products were evaporated under vacuum. The crude product was purified via silica column chromatography

(gradient PE:EE 1:1 → EE) to yield a colorless liquid. $^{31}$P-NMR showed still a second peak from an impurity.

**Yield:** 2.92 g (26% theoretical yield), colorless liquid

**$R_f$-value** (EE): 0.21

**$^{1}$H-NMR**: (400 MHz, $CDCl_3$) δ (ppm): 6.10 (s, 1H, C<u>H</u>$_2$=C <u>cis</u>), 5.57 (s, 1H, C<u>H</u>$_2$=C <u>trans</u>), 4.32 (dt, 2H, $J_1$ = 13.4 Hz, $J_2$ = 7.3 Hz, O-C<u>H</u>$_2$), 3.74 (s, 6H, 2x O-C<u>H</u>$_3$), 2.15 (dt, 2H, $J_1$ = 18.8 Hz, $J_2$ = 7.3 Hz, C<u>H</u>$_2$-P), 1.92 (s, 3H, C<u>H</u>$_3$)

**$^{13}$C-NMR**: (100 MHz, $CDCl_3$) δ (ppm): 166.96 (<u>C</u>=O), 135.93 (<u>C</u>=CH$_2$), 125.98 (C=<u>C</u>H$_2$), 58.61 (2x O-<u>C</u>H$_3$), 53.01 (O-<u>C</u>H$_2$), 24.23 (<u>C</u>H$_2$-P), 18.17 (<u>C</u>H$_3$)

**$^{31}$P-NMR**: ($CDCl_3$) δ (ppm): 33.14 (s, impurity), 29.61 (s)

**MS** (m/z): calc. 222.18, found 222.08 [M]

### 2.1.3 Synthesis of dimethyl(2-methacryloyloxyethylphosphonate) (DMMEP) (3)

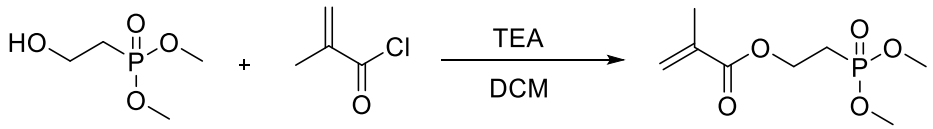


[154.10] [104.53] [222.18]
**DMMEP**

| reagents | n [mmol] | m [g] | V [mL] |
|---|---|---|---|
| Dimethyl(2-hydroxyethyl)phosphonate | 100 | 15.41 | 12.43 |
| methacrylic chloride | 105 | 10.98 | 10.07 |
| triethylamine | 125 | 12.65 | 17.33 |
| dry methylene chloride (DCM) | | | 125 |

**Procedure:**

A 100 mL three-neck round-bottomed flask equipped with a magnetic stir bar, dropping funnel and condenser was dried, filled with Argon, charged with dimethyl (2-hydroxyethyl)phosphonate, dry triethylamine and diluted in 20 mL dry methylene chloride. Methacrylic chloride was added dropwise under cooling and the mixture was stirred at 0°C for 2h. After stirring overnight at

room temperature, the formed precipitate was filtered off and washed with 40 mL diethyl ether. The organic phases were combined and washed with 80 mL of brine. The pH value was adjusted to 1 with 2 N hydrochloric acid. In addition to that, the organic phases were washed with 80 mL of 10 wt% aqueous solution of $NaHCO_3$ and 100 mL of brine. Excess triethylamine and triethylamine/HCl salt were then removed by extraction with deionized water (3 x 20 mL). The organic layer was separated and dried over $CaCl_2$. The evaporation of methylene chloride gave the product as a yellow, viscous liquid.

**Yield:** 18.52 g (83% theoretical yield); colorless, viscous liquid

**$R_f$-value** (EE): 0.20

**$^1$H-NMR**: (400 MHz, $CDCl_3$) δ (ppm): 6.12 (s, 1H, C$\underline{H}_2$=C cis), 5.58 (s, 1H, C$\underline{H}_2$=C trans), 4.39 (dtd, 2H, $J_1$ = 13.4 Hz, $J_2$ = 7.3 Hz, $J_3$ = 1.2 Hz, O-C$\underline{H}_2$), 3.76 (s, 6H, 2x O-C$\underline{H}_3$), 2.19-2.07 (dtd, 2H, $J_1$ = 18.8 Hz, $J_2$ = 7.3 Hz, $J_3$ = 1.1 Hz, C$\underline{H}_2$-P), 1.93 (s, 3H, C$\underline{H}_3$)

**$^{13}$C-NMR**: (100 MHz, $CDCl_3$) δ (ppm): 167.06 ($\underline{C}$=O), 135.97 ($\underline{C}$=$CH_2$), 126.08 (C=$\underline{C}H_2$), 58.68 (2x O-$\underline{C}H_3$), 52.69 (O-$\underline{C}H_2$), 25.66 ($\underline{C}H_2$-P), 18.22 ($\underline{C}H_3$)

**$^{31}$P-NMR**: ($CDCl_3$) δ (ppm): 29.69 (s)

**MS** (m/z): calc. 222.18, found 222.12 [M]

## 2.2 Synthesis of RAFT agents

### 2.2.1 Synthesis of di(thiobenzoyl) disulfide (DTBDS)[152]

For the synthesis of di(thiobenzoyl) disulfide (DTBDS), benzoyl chloride was reacted to **sodium dithiobenzoate (DTBA).**

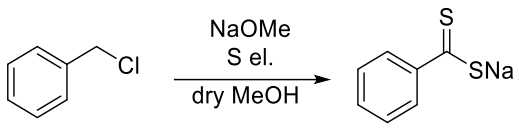


[126.58] [176.23]
**DTBA**

| reagents | n [mmol] | m [g] | V [mL] |
|---|---|---|---|
| benzyl chloride | 250 | 31.65 | |
| sodium methoxide (30 wt% NaOH in MeOH) | 500 | 90.38 | |
| sulfur | 500 | 16.03 | |
| dry methanol | | | 160 |

**Procedure:**

A 500 mL three-neck round-bottomed flask equipped with a magnetic stir bar, dropping funnel and thermometer was dried, filled with Argon, charged with sodium methoxide (30wt% solution in methanol) and diluted in 160 mL dry methanol. Subsequently the appropriate amount of sulfur was added under Argon counter flow. Benzyl chloride was added dropwise over the course of approximately 1.5 h at room temperature. The color of the solution changed from orange to deep red. The reaction mixture was heated in an oil bath at 75°C for 20 h. After this time, the reaction mixture was cooled to 0°C using an ice bath. The precipitated salts were removed by filtration, washed with 50 mL of methanol and then the solvent was evaporated. The residue was dissolved in 250 mL of deionized water and the precipitated salts were removed by filtration again. Hereafter the solution was transferred into a 1 L separatory funnel and washed with diethyl ether (3 x 150 mL). Diethyl ether (150 mL) and 250 mL 1 N HCl were added to the deep red solution. Suddenly a pink precipitate appeared. Then dithiobenzoic acid was extracted into the ethereal layer (purple color). Afterwards 150 mL deionized water and 300 mL 1 N NaOH were added to the ethereal layer. Whereby sodium dithiobenzoate was

extracted to the orange-red aqueous layer. This washing process was repeated two more times to finally yield a 500 mL solution of sodium dithiobenzoate.

The last step was the **synthesis of di(thiobenzoyl) disulfide (DTBDS).**

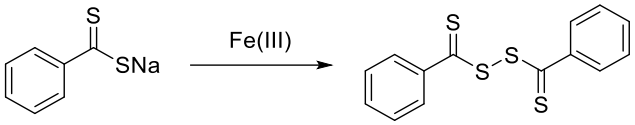


[176.23]
**DTBA**

[306.47]
**DTBDS**

| reagents | n [mmol] | m [g] | V [mL] |
|---|---|---|---|
| aqueous sodium dithiobenzoate solution | | | 500 |
| Potassium ferricyanide (III) | 150 | 90.38 | |

**Procedure:**

For the synthesis of di(thiobenzoyl)disulfide the aqueous sodium dithiobenzoate solution was transferred in an 1 L round-bottomed flask with magnetic stirrer. Besides potassium ferricyanide (III) was dissolved in 300 mL deionized water and then carried-over in a dropping funnel. Afterwards the potassium ferricyanide (III) solution was added dropwise over the course of approximately 2.5 h under vigorous stirring. The red precipitate was filtered and washed with deionized water until the washings became colorless. The red solid was dried in vacuum for 6 h at room temperature.

**Yield:** 16.53 g (22% theoretical yield), red crystals

**$R_f$-value** (PE:EE 20:1): 0.67

**$^1$H-NMR**: (400 MHz, $CDCl_3$) δ (ppm): 7.96 (d, 4H, o-Ar<u>H</u>), 7.63 (m, 2H, p-Ar<u>H</u>), 7.51 (m, 4H, m-Ar<u>H</u>)

**$^{13}$C-NMR**: (100 MHz, $CDCl_3$) δ (ppm): 167.77 (-<u>C</u>=S), 133.33 (-Ar<u>C</u>-C=S), 131.21 (p-Ar<u>C</u>), 129.73 (m-Ar<u>C</u>), 129.04 (o-Ar<u>C</u>)

**IR** (ATR) v ($cm^{-1}$): 1236.2 (C=S), 1041 (C=S)

### 2.2.2 Synthesis of 4-cyanopentanoic acid dithiobenzoate[152]

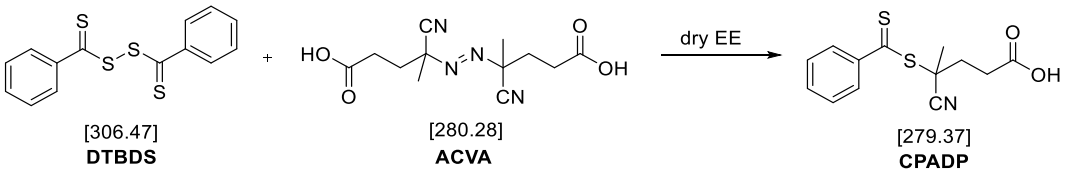


| reagents | n [mmol] | m [g] | V [mL] |
|---|---|---|---|
| di(thiobenzyol)disulfide (DTBDS) | 250 | 4.60 | |
| 4,4'-azobis(4-cyanovaleric acid) (ACVA) | 500 | 6.31 | |
| ethylacetate | | | 87 |

**Procedure:**

Ethyl acetate was pre-dried over $K_2CO_3$ for 12 h, decanted and distilled from 10 g/L $P_2O_5$. A 250 mL round-bottomed flask was purged three times with Argon and charged with di(thiobenzyol)disulfide (synthesis see 2.2.1), 4,4'-azobis(4-cyanovaleric acid) and dry ethyl acetate. The solution was heated at reflux for 19 h. Afterwards the ethyl acetate was removed in vacuum. The crude product was purified by silica column chromatography (gradient PE →PE:EE 1:2 → EE; addition of 0.5 mL acetic acid/liter solvent) to yield a red oily liquid. Thereafter the product was recrystallized from toluene.

**Yield:** 3.43 g (82% theoretical yield), pink crystals

**$R_f$-value** (PE:EE 1:1 + 1 drop acetic acid/2.5 mL solvent): 0.49

**$^1$H-NMR**: (400 MHz, $CDCl_3$) δ (ppm): 7.91 (m, 2H, o-Ar<u>H</u>), 7.56 (m, 1H, p-Ar<u>H</u>), 7.41 (m, 2H, m-Ar<u>H</u>), 2.78-2.51 (m, 2H, -C<u>H</u>$_2$-CH$_2$-COOH), 2.50-2.41 (m, 2H, -CH$_2$-C<u>H</u>$_2$-COOH), 1.95 (s, 3H, -C<u>H</u>$_3$)

**$^{13}$C-NMR**: (100 MHz, $CDCl_3$) δ (ppm): 222.16 (-<u>C</u>=S), 176.17 (-<u>C</u>OOH), 144.52 (-Ar<u>C</u>-C=S), 133.10 (p-Ar<u>C</u>), 128.61 (m-Ar<u>C</u>), 126.70 (o-Ar<u>C</u>), 118.39 (-<u>C</u>N), 45.62 (-<u>C</u>-CH$_3$), 33.07 (-<u>C</u>H$_2$-COOH), 29.36 (-<u>C</u>H$_2$-CH$_2$-COOH), 24.21 (-<u>C</u>H$_3$)

**MS** (m/z): calc. 279.37, found 279 [M]

**IR** (ATR) v (cm$^{-1}$): 3300-2500 (broad band, COO<u>H</u>), 2232 (CN), 1700.8 (C=O), 1227.3 (C=S), 1047.7 (C=S)

### 2.2.3 Synthesis of 2-cyanopropyl-2-dithiobenzoate (CPDB)[152]

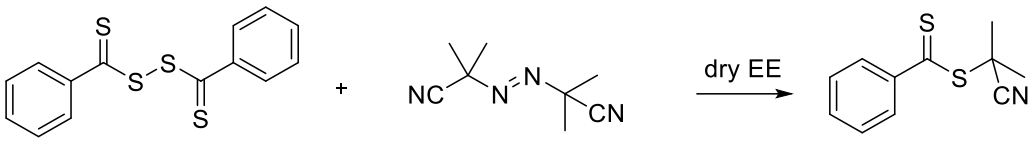


[306.47] **DTBDS** | [192.27] **AIBN** | [221.34] **CPDB**

| reagents | n [mmol] | m [g] | V [mL] |
|---|---|---|---|
| di(thiobenzyol)disulfide (DTBDS) | 15 | 4.69 | |
| 2,2'-azobisisobutyronitrile (AIBN) | 9 | 1.73 | |
| ethylacetate | | | 87 |

**Procedure:**

CPDB was synthesized in a 250 mL round-bottomed flask which was purged three times with Argon and was charged with di(thiobenzoyl)disulfide (synthesis see 2.2.1), 2,2'-azobis(2-methylpropionitrile) and distilled ethyl acetate. The reaction solution was heated at reflux for 20h. Afterwards the ethyl acetate was removed in vacuum. The crude product was purified by column chromatography (PE:EE 20:1) to yield in a red viscous liquid.

**Yield:** 2.43 g (52% theoretical yield), red viscous liquid

**$R_f$-value** (PE:EE 10:1): 0.51

**$^1$H-NMR**: (400 MHz, $CDCl_3$) δ (ppm): 7.91 (m, 2H, o-Ar<u>H</u>), 7.55 (m, 1H, p-Ar<u>H</u>), 7.39 (m, 2H, m-Ar<u>H</u>), 1.94 (s, 3H, C<u>H</u>$_3$)

**$^{13}$C-NMR**: (100 MHz, $CDCl_3$) δ (ppm): 223.15 (-<u>C</u>=S), 144.59 (-Ar<u>C</u>-C=S), 132.91 (p-Ar<u>C</u>), 128.56 (m-Ar<u>C</u>), 126.67 (o-Ar<u>C</u>), 119.98 (-<u>C</u>N), 41.75 (-<u>C</u>-CN), 26.50 (2x -<u>C</u>$H_3$)

**MS** (m/z): calcd. 222.34, found 221 [M]

**IR** (ATR) v ($cm^{-1}$): 2232.7 (CN), 1227.3 (C=S), 1047.7 (C=S)

## 2.3 Synthesis of the adhesive block copolymers

### 2.3.1 Homopolymerization of HEMA[161]

The homopolymerization of HEMA was carried out with two different RAFT agents CPADB and CPDB in DMF and dioxane.

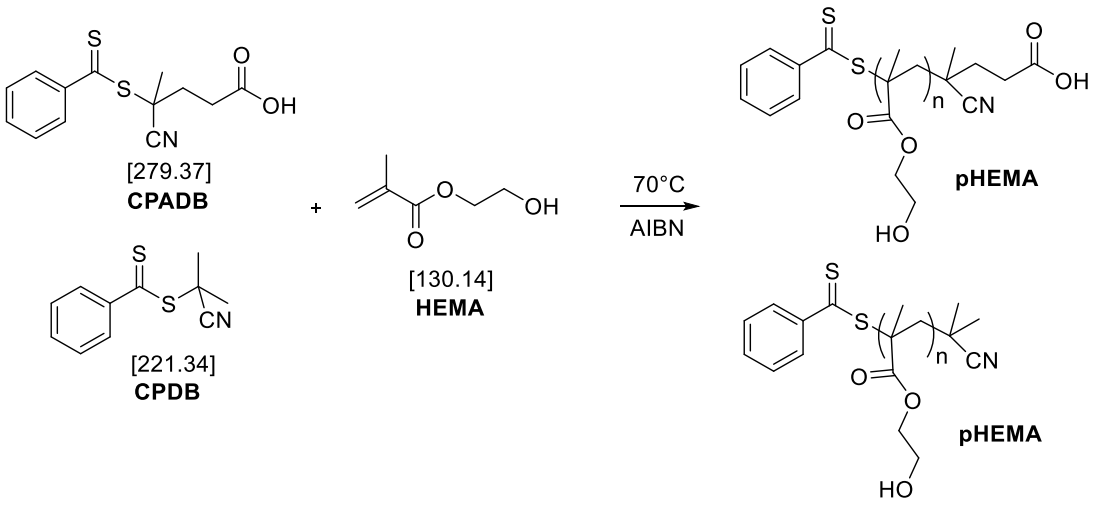


reaction temperature: 70 °C

polymerization time: 500 min (DMF, dioxane)

monomer concentration: 1.5 g $mol^{-1}$

initiator: AIBN (DMF, dioxane)

internal standard: naphthalene (DMF, dioxane)

monomer : standard = 6:1

precipitating agent: diethylether

| HEMA | solvent | monomer [mg] | CTA [mg] | | initiator [mg] | M:CTA:I |
|---|---|---|---|---|---|---|
| 01 | DMF | 3045 | CPADB | 27.95 | 0.38 | 234:1:0.02 |
| 02 | dioxane | 4568 | CPADB | 27.95 | 0.39 | 351:1:0.02 |
| 03 | DMF | 2993 | CPDB | 22.15 | 0.38 | 230:1:0.02 |
| 04 | dioxane | 5739 | CPDB | 22.13 | 0.38 | 441:1:0.02 |

**Procedure:**

In order to perform the RAFT polymerization of HEMA, the monomer, initiator, RAFT-agent (CPADB or CPDB) and the internal standard were dissolved in DMF, dioxane or water. The solution was degassed for about 40 min. Afterwards the penicillin flaks were placed in a pre-heated metal heating block (70 °C). The polymerization kinetics were investigated by drawing samples over the whole course of reaction. Therefor, an amount of about 200 µL of samples were taken by syringe in noted time intervals and quenched by ice cooling to stop the reaction until they were analyzed by $^{1}$H nuclear magnetic resonance spectroscopy (NMR). After complete polymerization time the reaction mixture was quenched by liquid nitrogen and precipitated in cold diethylether. The sticky polymer was re-dissolved in methanol and precipitated in cold diethylether for three more times to yield a pink polymer.

**$^{1}$H-NMR**: (400 MHz, DMSO-$d_6$) δ (ppm): 4.92-4.67 (br, 1H, -OH), 3.90 (s, 2H, -O-C$\underline{H}_2$-), 3.60 (s, 2H, -C$\underline{H}_2$-OH), 2.02-1.68 (br, 2H, -C$\underline{H}_2$-), 0.95 (s, 3H, -C$\underline{H}_3$)

### 2.3.2 Homopolymerization of DMMEP[139]

The homopolymerization of DEMMP was carried out with two different RAFT agents CPADB and CPDB in DMF and dioxane.

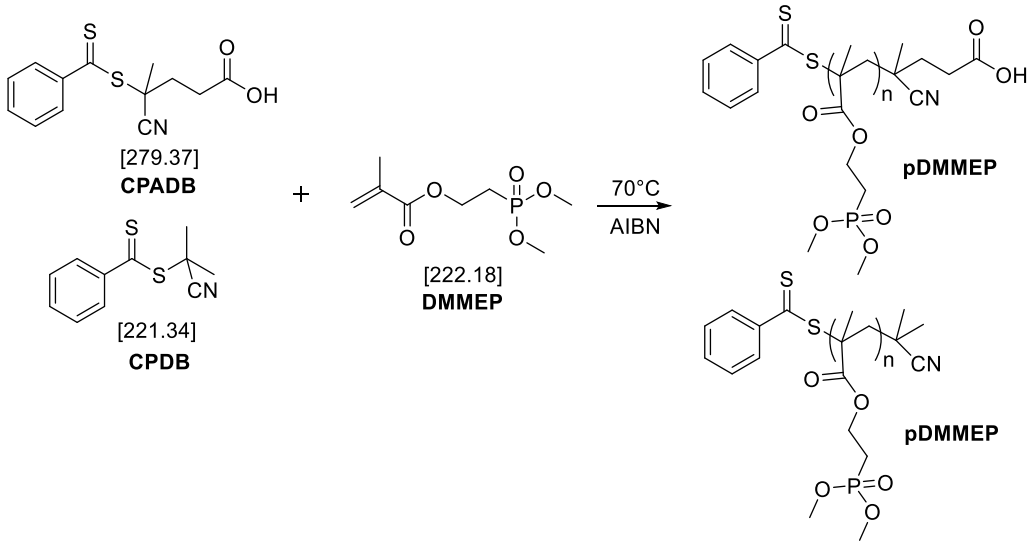

reaction temperature: 70 °C

polymerization time: 500 min (DMF, dioxane)

monomer concentration: 1.5 g $mol^{-1}$

initiator: AIBN (DMF, dioxane)

internal standard: naphthalene (DMF, dioxane)

monomer : standard = 6:1

precipitating agent: hexane

| DMMEP | solvent | monomer [mg] | CTA [mg] | | initiator [mg] | M:CTA:I |
|---|---|---|---|---|---|---|
| 01 | DMF | 1444 | CPADB | 27.95 | 6.35 | 65:1:0.33 |
| 02 | DMF | 2599 | CPADB | 27.95 | 6.35 | 117:1:0.33 |
| 03 | dioxane | 1533 | CPADB | 27.94 | 6.35 | 69:1:0.33 |
| 04 | dioxane | 2844 | CPADB | 27.96 | 6.36 | 128:1:0.33 |
| 05 | DMF | 1444 | CPDB | 22.14 | 6.34 | 65:1:0.33 |
| 06 | DMF | 2822 | CPDB | 22.15 | 6.34 | 127:1:0.33 |
| 07 | dioxane | 1555 | CPDB | 22.13 | 6.33 | 70:1:0.33 |
| 08 | dioxane | 2977 | CPDB | 22.13 | 6.35 | 134:1:0.33 |

**Procedure:**

The RAFT polymerization of DMMEP was also done in penicillin flasks and the monomer, initiator, RAFT-agent (CPADB or CPDB) and the internal standard were dissolved in DMF, dioxane or water. The solution was degassed for about 40 min. Afterwards the penicillin flaks were placed in a pre-heated metal heating block (70 °C). The polymerization kinetics were investigated by drawing samples over the whole course of reaction. Therefor, an amount of about 200 µL of samples were taken by syringe in noted time intervals and quenched by ice cooling to stop the reaction until they were analyzed by $^{1}H$ nuclear magnetic resonance spectroscopy (NMR). After complete polymerization time the reaction mixture was quenched by liquid nitrogen and precipitated in cold hexane. The sticky polymer was re-dissolved in methanol and precipitated in cold hexane for three more times to yield a pink polymer.

**$^{1}$H-NMR**: (400 MHz, DMSO-$d_6$) δ (ppm): 4.17-3.97 (br, 2H, -O-C$\underline{H}_2$-), 3.69 (d, 6H, $J_1$ = 10.4 Hz, 2x -O-C$\underline{H}_3$), 2.29-2.11 (br, 2H, -C$\underline{H}_2$-), 1.13-1.06 (br, 2H, -C$\underline{H}_2$-P), 1.03-0.8 (br, 3H, -C$\underline{H}_3$)

**$^{31}$P-NMR**: (DMSO-$d_6$) δ (ppm): 29.86 (s)

### 2.3.3 Block copolymerization pHEMA-block-pDMMEP

The blockcopoylmerization of HEMA with DMMEP was done the same way and the same procedure as in the homopolymerization of DMMEP.

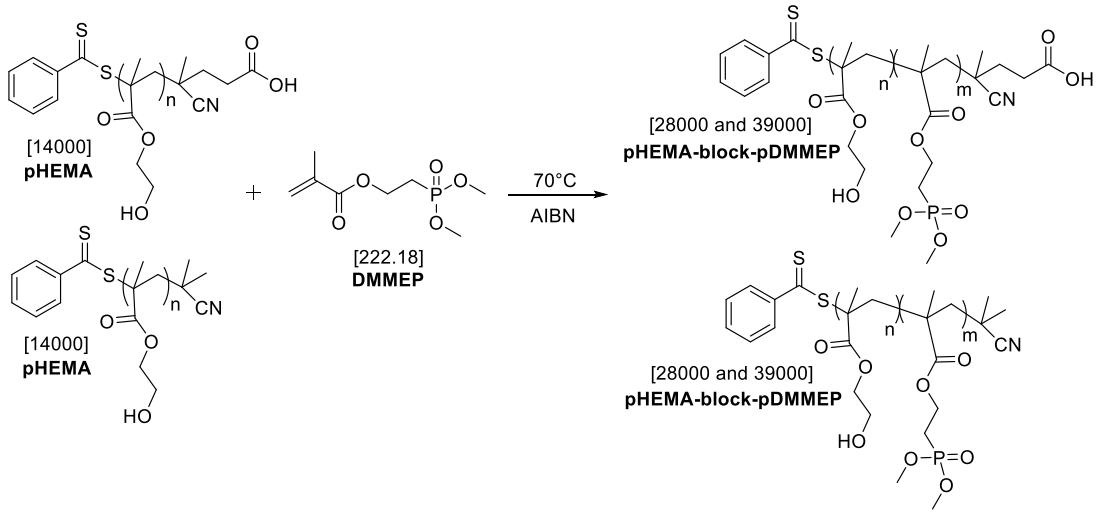


reaction temperature: 70 °C

polymerization time: 500 min

solvent: DMF initiator: AIBN

monomer concentration: 1.5 g mol$^{-1}$

internal standard: naphthalene monomer : standard = 6:1

precipitating agent: hexane

| pHEMA-block-pDMMEP | monomer [mg] | macro-RAFT agent [mg] | initiator [mg] | M:CTA:I |
|---|---|---|---|---|
| 01 | 1511 | 1400 (CPADB) | 6.34 | 68:1:0.33 |
| 02 | 2755 | 1400 (CPADB) | 6.35 | 124:1:0.33 |
| 03 | 1510 | 1400 (CPDB) | 6.35 | 68:1:0.33 |
| 04 | 2755 | 1400 (CPDB) | 6.33 | 124:1:0.33 |

**Procedure:**

In order to perform the block copolymerization of pHEMA-block-pDMMEP via RAFT polymerization, the monomer, AIBN, macro RAFT-agent (CPADB or CPDB) and the internal standard naphthalene were dissolved in DMF. The solution was degassed for about 40 min. Afterwards the penicillin flaks were placed in a pre-heated metal heating block (70 °C). The polymerization kinetics were investigated by drawing samples over the whole course of reaction. Therefor, an amount of about 200 µL of samples were taken by syringe in noted time intervals and quenched by ice cooling to stop the reaction until they were analyzed by $^{1}$H nuclear magnetic resonance spectroscopy (NMR). After complete polymerization time the reaction mixture was quenched by liquid nitrogen and precipitated in cold hexane. The sticky polymer was re-dissolved in methanol and precipitated in cold hexane for three more times to yield a pink polymer.

**$^{1}$H-NMR**: (400 MHz, DMSO-$d_6$) δ (ppm): 4.97-4.62 (br, 1H, -OH), 4.17-3.91 (m, 4H, -O-C$\underline{H}_2$-), 3.94 (s, 2H, -O-C$\underline{H}_2$-), 3.71-3.58 (m, 8H, -C$\underline{H}_2$-OH, 2x -O-C$\underline{H}_3$), 2.29-1.58 (br, 4H, -C$\underline{H}_2$-), 1.13-1.06 (br, 2H, -C$\underline{H}_2$-P), 1.13-0.75 (br, 6H, -C$\underline{H}_3$)

**$^{31}$P-NMR**: (DMSO-$d_6$) δ (ppm): 29.51 (s)

### 2.3.4 Block copolymerization pDMMEP-block-pHEMA

The blockcopoylmerization of DMMEP with HEMA was done the same way and the same procedure as in the homopolymerization of HEMA.

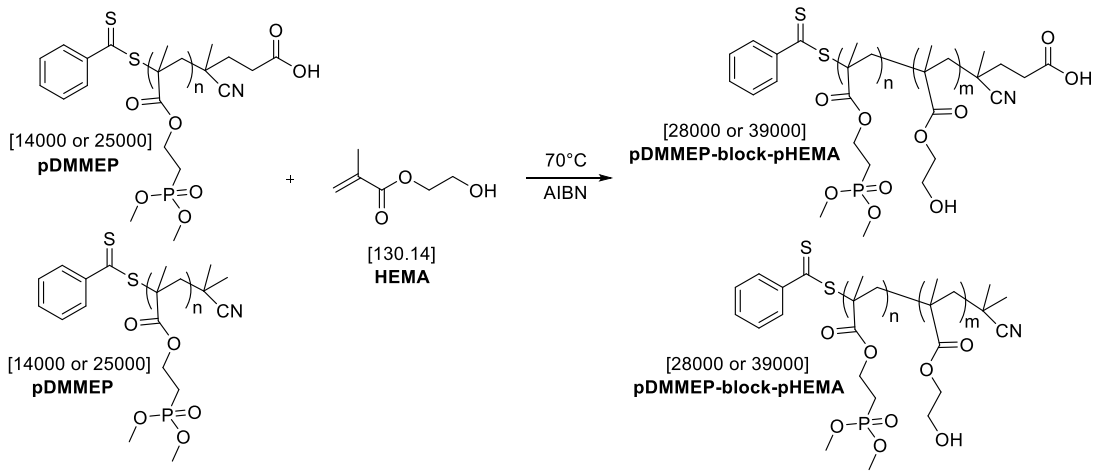

reaction temperature: 70 °C

polymerization time: 1250 min

solvent: DMF initiator: AIBN

monomer concentration: 1.5 g $mol^{-1}$

internal standard: naphthalene monomer : standard = 6:1

precipitating agent: diethylether

| pDMMEP-block-pHEMA | monomer [mg] | macro-RAFT agent [mg] | initiator [mg] | M:CTA:I |
|---|---|---|---|---|
| 01 | 3917 | 1400 (CPADB) | 0.39 | 301:1:0.02 |
| 02 | 3917 | 2500 (CPADB) | 0.38 | 301:1:0.02 |
| 03 | 3943 | 1400 (CPDB) | 0.38 | 303:1:0.02 |
| 04 | 3943 | 2500 (CPDB) | 0.38 | 303:1:0.02 |

**Procedure:**

The block copolymerization of pDMMEP-block-pHEMA via RAFT polymerization was done nearly the same way as pHEMA-block-pDMMEP. Therefor, the monomer, AIBN, macro RAFT-agent (CPADB or CPDB) and the internal standard naphthalene were dissolved in DMF. The solution was degassed for about 40 min. Afterwards the penicillin flaks were placed in a pre-heated metal heating block (70 °C). The polymerization kinetics were investigated by drawing samples over the whole course of reaction. Therefor, an amount of about 200 µL of samples were taken by syringe in noted time intervals and quenched by ice cooling to stop the reaction until they were analyzed by $^{1}$H nuclear magnetic resonance spectroscopy (NMR). After complete polymerization time the reaction mixture was quenched by liquid nitrogen and precipitated in cold diethylether. The sticky polymer was re-dissolved in methanol and precipitated in cold diethylether for three more times to yield a pink polymer.

**$^{1}$H-NMR**: (400 MHz, DMSO-$d_6$) δ (ppm): 4.94-4.58 (br, 1H, -OH), 4.21-3.93 (m, 4H, -O-C$\underline{H}_2$-), 3.92 (s, 2H, -O-C$\underline{H}_2$-), 3.70-3.55 (m, 8H, -C$\underline{H}_2$-OH, 2x -O-C$\underline{H}_3$), 2.29-1.58 (br, 4H, -C$\underline{H}_2$-), 1.13-1.06 (br, 2H, -C$\underline{H}_2$-P), 1.13-0.78 (br, 6H, -C$\underline{H}_3$)

**$^{31}$P-NMR**: (DMSO-$d_6$) δ (ppm): 29.52 (s)

### 2.3.5 End-group removal via aminolysis

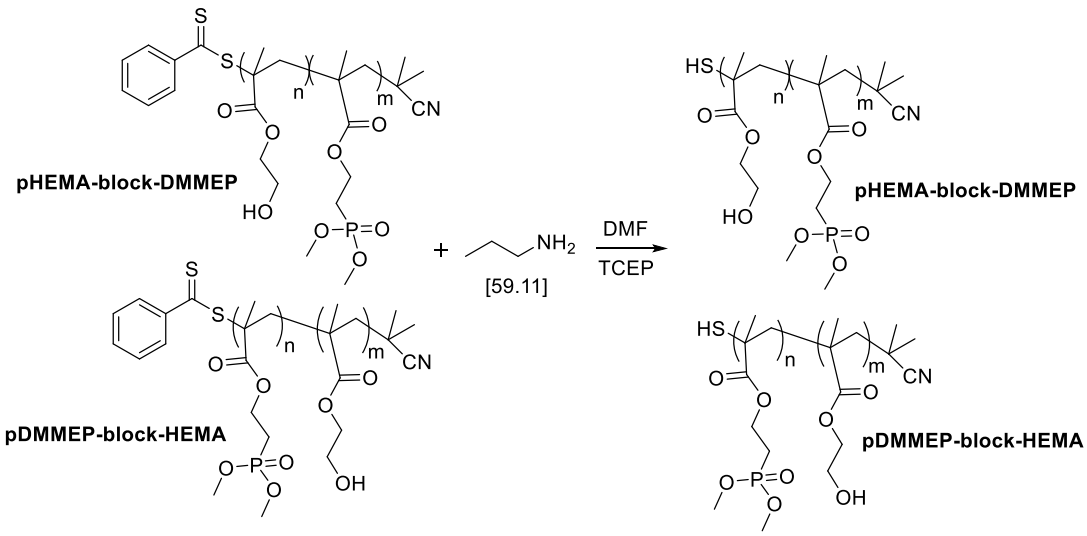


| reagents | n [mmol] | m [mg] | V [mL] |
|---|---|---|---|
| pHEMA-block-pDMMEP_39 kDa | 0.01 | 390 | |
| propylamine | 0.05 | 3 | 4 |
| TCEP | 0.01 | 3 | |
| DMF | | 0.95 | 1 |

| reagents | n [mmol] | m [mg] | V [mL] |
|---|---|---|---|
| pHEMA-block-pDMMEP_28 kDa | 0.01 | 281 | |
| propylamine | 0.05 | 3 | 4 |
| TCEP | 0.01 | 3 | |
| DMF | | 0.95 | 1 |

| reagents | n [mmol] | m [mg] | V [mL] |
|---|---|---|---|
| pDMMEP-block-pHEMA_39 kDa | 0.01 | 390 | |
| propylamine | 0.05 | 3 | 4 |
| TCEP | 0.01 | 3 | |
| DMF | | 0.95 | 1 |

| reagents | n [mmol] | m [mg] | V [mL] |
|---|---|---|---|
| pDMMEP-block-pHEMA_28 kDa | 0.01 | 281 | |
| propylamine | 0.05 | 3 | 4 |
| TCEP | 0.01 | 3 | |
| DMF | | 0.95 | 1 |

**Procedure:**

The block copolymer and TCEP were dissolved in DMF. Afterwards the solution was degassed and propylamine was added. The solution was stirred for about 2 h and the product was precipitated in cold diethylether. The sticky polymer was re-dissolved in methanol and precipitated again in cold diethylether for three more times to yield a colorless polymer.

pHEMA-block-pDMMEP:

**$^{1}$H-NMR**: (400 MHz, DMSO-$d_6$) δ (ppm): 4.97-4.62 (br, 1H, -OH), 4.17-3.91 (m, 4H, -O-C$\underline{H}_2$-), 3.94 (s, 2H, -O-C$\underline{H}_2$-), 3.71-3.58 (m, 8H, -C$\underline{H}_2$-OH, 2x -O-C$\underline{H}_3$), 2.29-1.58 (br, 4H, -C$\underline{H}_2$-), 1.13-1.06 (br, 2H, -C$\underline{H}_2$-P), 1.13-0.75 (br, 6H, -C$\underline{H}_3$)

**$^{31}$P-NMR**: (DMSO-$d_6$) δ (ppm): 29.51 (s)

pDMMEP-block-pHEMA:

**$^{1}$H-NMR**: (400 MHz, DMSO-$d_6$) δ (ppm): 4.94-4.58 (br, 1H, -OH), 4.21-3.93 (m, 4H, -O-C$\underline{H}_2$-), 3.92 (s, 2H, -O-C$\underline{H}_2$-), 3.70-3.55 (m, 8H, -C$\underline{H}_2$-OH, 2x -O-C$\underline{H}_3$), 2.29-1.58 (br, 4H, -C$\underline{H}_2$-), 1.13-1.06 (br, 2H, -C$\underline{H}_2$-P), 1.13-0.78 (br, 6H, -C$\underline{H}_3$)

**$^{31}$P-NMR**: (DMSO-$d_6$) δ (ppm): 29.52 (s)

## 2.4 Dopamine-SH[176]

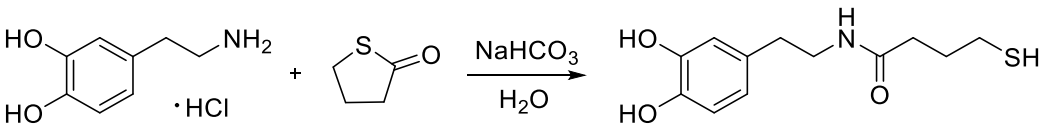


[189.64] [102.15] [255.33]
**dopamine-SH**

| reagents | n [mmol] | m [g] | V [mL] |
|---|---|---|---|
| dopamine-hydrochloride | 21 | 3.98 | |
| γ-thiobutyrolactone | 22.07 | 2.25 | 1.91 |
| sodium hydrogencarbonate | 2.11 | 3.72 | |
| water | | | 40 |

**Procedure:**

Dopamine hydrochloride was mixed with sodium hydrogencarbonate and water in a 100 mL round-bottomed flask equipped with a condenser. Subsequently, γ-thiobutyrolactone was injected very slowly. The reaction mixture was heated at reflux for about 22 h. Hereafter, the solution was transferred into a separatory funnel and washed with brine (40 mL). Thereby, a brown-red solid was precipitated and separated from the product, which was extracted two times with THF. The organic phase was dried with magnesium sulfate, filtered and then evaporated under reduced pressure. A yellow viscous liquid was obtained and dissolved in methanol, whereby a colorless solid was precipitated and removed. The methanol was evaporated to yield a yellow solid.

**Yield:** 5.2 g (97% theoretical yield), yellow viscous liquid

**$R_f$-value** (EE): 0.21 (thiol), 0.44 (disulfide)

**$^1$H-NMR**: (400 MHz, MeOD) δ (ppm): 7.99 (s, 1H, -NH-), 6.70 (d, 1H, $J_1$ = 8.0 Hz, ArH), 6.66 (d, 1H, $J_1$ = 2.1 Hz, ArH), 6.53 (dd, 1H, $J_1$ = 8.0 Hz, $J_2$ = 2.1 Hz, ArH), 3.36 (t, 2H, $J_1$ = 5.8 Hz, $J_2$ = 2.1 Hz, -C$H_2$-NH), 2.65 (t, 2H, $J_1$ = 7.3 Hz, -C$H_2$-Ar), 2.47 (t, 2H, $J_1$ = 7.1 Hz, -C$H_2$-SH), 2.28 (t, 2H, $J_1$ = 7.5 Hz, -C$H_2$-CO), 1.86 (m, 2H, -C$H_2$-C$H_2$-SH), 1.42 (s, 1H, -SH)

**$^{13}$C-NMR**: (100 MHz, MeOD) δ (ppm): 173.9 (-C=O), 145.02 (ArC-OH), 143.61 (ArC-OH), 130.53 (ArC-$CH_2$), 119.52 (ArC), 115.45 (ArC), 114.99 (ArC), 41.33 (-C$H_2$-NH-), 34.51 (-C$H_2$-C$H_2$-NH-), 34.19 (O=C-C$H_2$-), 29.97 (-C$H_2$-C$H_2$-SH), 23.20 (-C$H_2$-SH)

## 2.5 Model reactions[138]

In order to perform the model reactions, **stock solutions** of EDTA, TCEP hydrochloride and HEPES were prepared.

100 mM EDTA was prepared by weighing 931 mg of disodium EDTA dehydrate (EDTA-$Na_2$·2 $H_2O$) into a beaker and adding water to a final volume of 20 mL. A magnetic stiring bar was added and the suspension was stirred while the dropwise addition of NaOH (first 20%, towards the end 2%) to adjust the pH to 7.4 with a pH meter. Aliquots of different size (200 µL, 100 µL, 50 µL) were stored in Eppendorf tubes at -20°C.

1 M HEPES (pH 7.5) (HEPES 1) was prepared by dissolving HEPEs (free acid) in water at a concentration of 238.3 g/L. The suspension was mixed until the solid was completely dissolved. The suspension was stirred while the dropwise addition of NaOH (first 20%, towards the end 2%) to adjust the pH to 7.5 with a pH meter. Half of the total solution was immediately used for preparation of 1 M HEPES (pH 9.6, see next paragraph) while afterwards the remainder of 1 M HEPES (pH 7.5) was divided into aliquots of different size (200 µL, 100 µL, 50 µL) and was stored in Eppendorf tubes at -20°C.

1 M HEPES (pH 9.6) (HEPES 2) was prepared from half of the unused solution of 1 M HEPES (pH 7.5, see previous paragraph) by continuing the addition of 20% NaOH until a pH at 9.6 occurred.

100 mM TCEP hydrochloride was prepared by weighing 100 mg into a beaker and adding water to give a final concentration of 28.7 mg/mL. Aliquots of different size were prepared (100 µL, 50 µL) and was stored at -20°C.

### 2.5.1 Cysteine

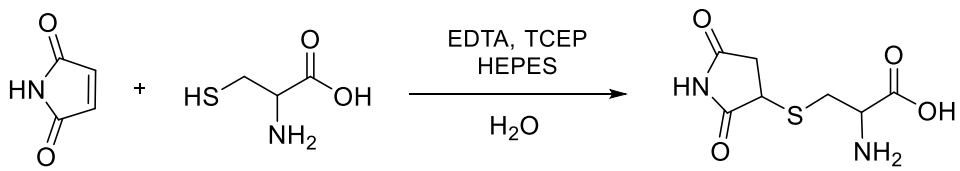


[97.07] [121.15] [218.23]

| experiment | cysteine | | maleimide | |
|---|---|---|---|---|
| | n [mmol] | m [mg] | n [mmol] | m [mg] |
| **A** | 0.25 | 30.29 | 0.05 | 4.85 |
| **B** | 0 | 0 | 4 | 3.88 |

**Procedure:**

For experiment A the thiol-component (cysteine) was weighted into penicillin flasks and transferred with 50 mL of distilled water into a 100 mL round-bottomed flask. For experiment B only 50 mL of distilled water were weighted in the round-bottomed flask. Subsequently the necessary amounts of solutions EDTA, HEPES 1, TCEP and HEPES 2 (see Table 10) respectively were pipetted in that order in both flasks. Afterwards the appropriate amounts of maleimide were added to these flasks. The reaction mixtures were stirred for 3.5 hours at room temperature. Water was removed under high vacuum conditions and the residues were taken up in $D_2O$ for further $^1$H-NMR measurements.

***Table 10: Solutions with the same pH value as in functionalization reactions***

| | pH | c [mol/L] | V [µL] |
|---|---|---|---|
| **EDTA** | 4.7 | 0.1 | 100 |
| **HEPES 1** | 7.5 | 1 | 250 |
| **TCEP** | - | 0.1 | 100 |
| **HEPES 2** | 9.6 | 1 | 100 |

### 2.5.2 Dopamine-thiol

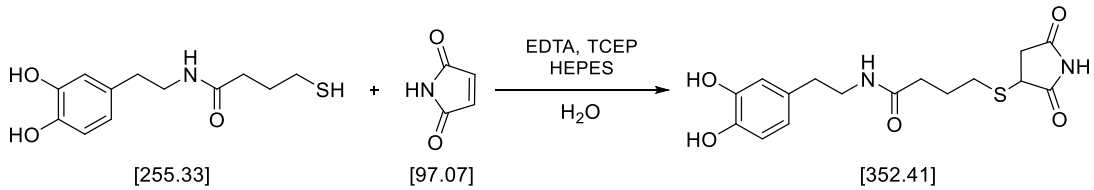


[255.33] [97.07] [352.41]

| experiment | dopamine-thiol | | maleimide | |
|---|---|---|---|---|
| | n [mmol] | m [mg] | n [mmol] | m [mg] |
| **A** | 0.25 | 30.29 | 0.05 | 4.85 |
| **B** | 0 | 0 | 4 | 3.88 |

**Procedure:**

The model reaction with dopamine-thiol was carried out the same way as in 2.5.1.

### 2.5.3 Block copolymer-thiol

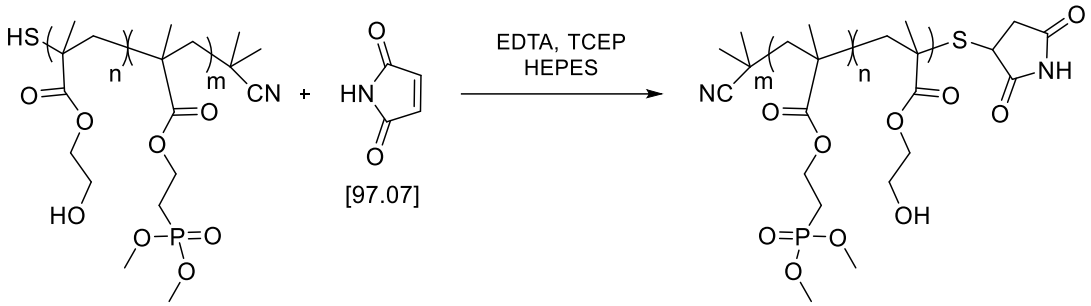


| experiment | HS-pHEMA-co-pDMMEP | | maleimide | |
|---|---|---|---|---|
| | n [mmol] | m [mg] | n [mmol] | m [mg] |
| **A** | 0.25 | 30.29 | 0.05 | 4.85 |
| **B** | 0 | 0 | 4 | 3.88 |

**Procedure:**

The model reaction with HS-pHEMA-co-pDMMEP was carried out the same way as in 2.5.1.

# 3 Single Molecule Force Microscopy

## 3.1 Substrate preparation

The hydroxyapatite (HA) pellet was polished with Buehler Micro Cut Discs. The chronological order, time and roughness of the abrasive papers were listed in Table 11. First the abrasive papers were wetted with water and the forefinger was moved in a figure of eight with constant pressure.

***Table 11: Chronological order of the polishing process of HA***

| chronology | roughness [grit] | time [min] |
|---|---|---|
| 1 | 400 | 5 |
| 2 | 600 | 5 |
| 3 | 800 | 10 |
| 4 | 1200 | 10 |

After the polishing process, the HA pellet was washed with water and sonicated. Furthermore, the surface roughness was checked via microscope. Thereafter, the pellet was dried and glued on a glass slide with epoxy glue.
Besides a mica (muscovite) disc (Agar Scientific Ltd, Stansted, UK) was glued as well. This disc was cleaned by the removal of the topmost layer with an adhesive tape. Afterwards, a PMMA ring was sticked around the two substrates on the glass slide.

In order to prepare the silicon wafer coated with $TiO_2$ and the silicon wafer functionalized with amino groups, the wafers were cut into 0.5 x 0.5 cm pieces. First the two wafers were cleaned by a Boekel UV-cleaner for about 15 min. Afterwards the silicon wafers were chemically cleaned according to a cleaning procedure (see Table 12).

***Table 12: Cleaning procedure for silicon wafers***

| cleaning step | procedure |
|---|---|
| **1** | wafer 2 x 5 min washed with water + ultrasonic bath |
| **2** | wafer washed 5 min with $H_2O$ + 1 N NaOH + ultrasonic bath |
| **3** | wafer washed 5 min with $H_2O$ + ultrasonic bath |
| **4** | wafer washed 5 min with $H_2O$ + ultrasonic bath |
| **5** | wafer washed 5 min with MeOH + 1 N HCl + ultrasonic bath |
| **6** | wafer washed 5 min with $H_2O$ + ultrasonic bath |
| **7** | wafer washed 5 min with acetone + ultrasonic bath |
| **8** | wafer washed 5 min with toluene + ultrasonic bath |
| **9** | wafer washed 5 min with $H_2O$ + ultrasonic bath |
| **10** | drying under argon |

One wafer was coated with **$TiO_2$ nanoparticles** at the Institute of Materials Chemistry by Dr. Alexey Cherevan.

The other wafer was **amino functionalized**. Therefore, it was activated in piranha solution ($H_2SO_4$ : $H_2O_2$ (30%) = 3:1) at 80°C for about 1 h. Afterwards the wafer was dried under argon and washed 5 min with $H_2O$ in an ultrasonic bath. Thereafter, the activated silicon wafer was immersed in 20 mL toluene with 1 v% APTES. After 20 h the silicon wafer was washed with toluene and dried under argon.

The two silicon wafers were characterized via ellipsometry.

## 3.2 Determination of AFM-Cantilever – spring constants

Before tip functionalization and AFM-measurement, the spring constants of the cantilevers have to be determined. The AFM chips were ordered from Bruker NanoInc (AFM Probes). The specification of the AFM chips can be seen in Table 13.

***Table 13: AFM chips specification[86]***

| manufacturer | model | material | nitride thickness [nm] | coating | |
|---|---|---|---|---|---|
| | | | | front side | back side |
| Bruker | MSNL-10 | silicon tip on nitride lever | 600 | none | reflective Au |

The ordered AFM chips have sharp tips with low spring constants displaying six different geometries of cantilevers on it (see Figure 79).

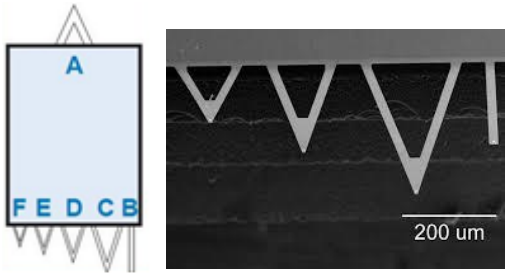


***Figure 79: Cantilever layout of Bruker MSNL AFM chips. Cantilever A is located on the top of the chip and cantilevers B-F are located on the bottom of the chip[206]***

Table 14 below shows the dimensions of different cantilever shapes of Bruker MSNL AFM chips.

***Table 14: Different cantilever shapes and spring constants[206]***

| Shape | Resonant Freq. [kHz] | | Spring Const. [N/m] | | Length [µm] | | Width [µm] | |
|---|---|---|---|---|---|---|---|---|
| | Min. | Max. | Min. | Max. | Min. | Max. | Min. | Max. |
| A triangular | 15 | 30 | 0.025 | 0.140 | 180 | 170 | 17 | 27 |
| B rectangular | 10 | 20 | 0.005 | 0.040 | 205 | 215 | 15 | 25 |
| C triangular | 4 | 10 | 0.005 | 0.020 | 305 | 315 | 15 | 25 |
| D triangular | 10 | 20 | 0.010 | 0.060 | 220 | 230 | 15 | 25 |
| E triangular | 26 | 50 | 0.050 | 0.200 | 135 | 145 | 13 | 23 |
| F triangular | 90 | 160 | 0.300 | 1.400 | 80 | 90 | 13 | 23 |

The AFM chips were clamped in the probe holder and the laser was aligned on each cantilever. The spring constant can be defined on air with the “Sader”-method via thermal noise (see Table 4). These values of the spring constants do not change if the measurement is in air or in liquid. In only the spring constants of the triangular cantilever C were shown. Because the AFM measurements were done with the softest cantilever.

***Table 15: Determined spring constants (K) of cantilever C (Bruker MSNL AFM chips)***

| Type | AFM-Chip | K (mN/m) | | |
|---|---|---|---|---|
| | | min | max | nominal |
| Box II | 1 | 8,044 | 10,87 | 9,463 |
| | 2 | 7,569 | 10,23 | 8,904 |
| | 3 | 8,34 | 7,735 | 9,863 |
| | 4 | 7,715 | 10,43 | 9,076 |
| | 5 | 7,934 | 10,72 | 9,334 |
| | 6 | 7,692 | 10,4 | 9,049 |
| | 7 | 7,147 | 9,659 | 8,407 |
| | 8 | 8,242 | 11,14 | 9,695 |
| | 9 | 6,785 | 9,155 | 7,975 |
| | 10 | 7,809 | 10,23 | 8,908 |
| Box III | 1 | 7.115 | 6.06 | 8.163 |
| | 2 | 7.219 | 6.148 | 8.282 |
| | 3 | 7.332 | 6.244 | 8.673 |
| | 4 | 7.383 | 6.287 | 8.47 |
| | 5 | 7.312 | 6.226 | 8.651 |
| | 6 | 7.322 | 6.235 | 8.401 |
| | 7 | 7.393 | 6.295 | 8.483 |
| | 8 | 7.369 | 6.275 | 8.456 |
| | 9 | 7.63 | 6.497 | 8.753 |
| | 10 | 7.115 | 6.06 | 8.163 |
| Box IV | 1 | 7.531 | 6.413 | 8.641 |
| | 2 | 7.546 | 6.425 | 6.636 |
| | 3 | 3.764 | 3.218 | 4.303 |
| | 4 | 7.622 | 6.49 | 8.746 |
| | 5 | 7.746 | 6.594 | 8.888 |
| | 6 | 7.713 | 6.566 | 8.851 |
| | 7 | 7.677 | 6.537 | 8.809 |
| | 8 | 7.481 | 6.369 | 8.585 |
| | 9 | 7.415 | 6.313 | 8.509 |
| | 10 | 7.536 | 6.416 | 8.647 |
| Box V | 1 | 8.233 | 7.005 | 9.453 |
| | 2 | 8.228 | 7.001 | 9.447 |
| | 3 | 8.293 | 7.055 | 9.522 |

## 3.4 AFM functionalization

In order to measure the adhesion force of the synthesized samples, the AFM chips were functionalized always three days before the measurements. In Table 16 the functionalization step of each AFM chip can be seen.

***Table 16: Different functionalization steps and samples***

| | AFM chip | Functionalization step |
|---|---|---|
| **Box II** | 1 | amino functionalized |
| | 2 | linker functionalized |
| | 3 | DSSEEKC_1 |
| | 4 | DSSEEKC_2 |
| | 5 | DSSEEKC_3 |
| | 6 | D(pS)(pS)EEKC_1 |
| | 7 | D(pS)(pS)EEKC_2 |
| | 8 | D(pS)(pS)EEKC_3 |
| | 9 | naked (not functionalized) |
| | 10 | naked (not functionalized) |
| **Box III** | 1 | amino functionalized |
| | 2 | linker functionalized |
| | 3 | DSSEEKC_4 |
| | 4 | DSSEEKC_5 |
| | 5 | D(pS)(pS)EEKC_4 |
| | 6 | D(pS)(pS)EEKC_5 |
| | 7 | Dopamine-SH_1 |
| | 8 | Dopamine-SH_2 |
| | 9 | Dopamine-SH_3 |
| | 10 | naked (not functionalized) |
| **Box IV** | 1 | naked (not functionalized) |
| | 2 | naked (not functionalized) |
| | 3 | DSSEEKC_6 |
| | 6 | pHEMA-block-pDMMEP (28 kDa)_1 |
| | 7 | pHEMA-block-pDMMEP (28 kDa)_2 |
| | 8 | pHEMA-block-pDMMEP (39 kDa)_1 |
| | 9 | pHEMA-block-pDMMEP (39 kDa)_2 |
| | 10 | pDMMEP-block-pHEMA (28 kDa)_1 |
| **Box V** | 1 | pDMMEP-block-pHEMA (39 kDa)_2 |
| | 2 | pDMMEP-block-pHEMA (28 kDa)_1 |
| | 3 | pDMMEP-block-pHEMA (39 kDa)_2 |

In the first step, prior to functionalization, the Bruker MSNL-10 AFM chips were spontaneous oxidized in ambient atmosphere, resulting in a thin layer of silicon dioxide.

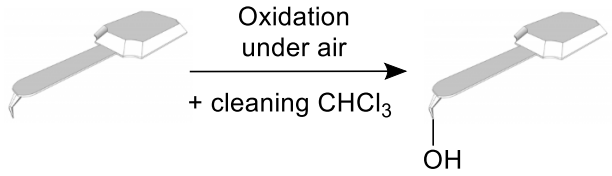


All AFM chips of Table 16 were immersed in chloroform (3 x 5 min) and dried with $N_2$.

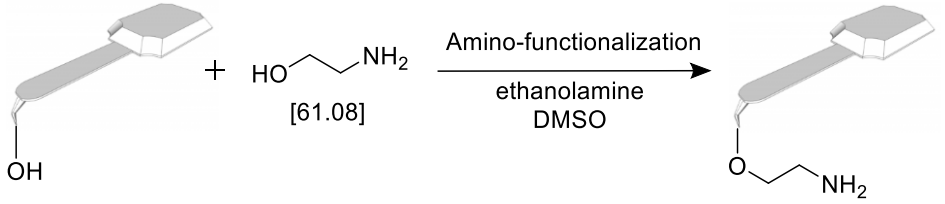


In the second step 3.31 g of ethanolamine were transferred in a crystallizing dish and dissolved in 6.6 mL of DMSO. The solution was heated up to 70 °C for approximately 15 minutes. Afterwards a Teflon disk was immersed, placed in the middle of the dish and molecular sieve beads (4 Å) were added around the disk. After cooling to room temperature, the dissolved air was removed by degassing in a desiccator at 10 mbar for 30 min. The remaining chips were placed on the Teflon disk and incubated in this solution overnight.

After about 16 h, the chips were washed in DMSO (3 x 1 min) and ethanol (3 x 1 min), and dried with $N_2$.

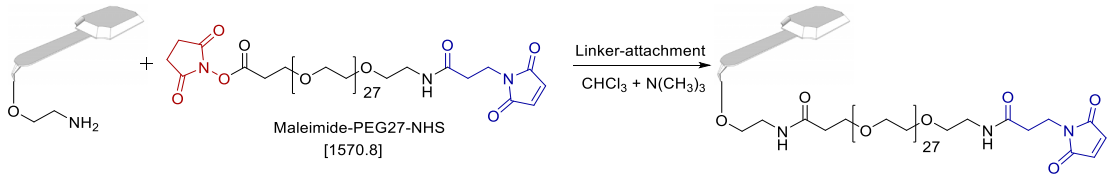


In the third step, 1 mg of Maleimide-PEG-NHS linker was dissolved in 0.5 mL of chloroform in a crimp-sealed vial. Thereafter, 30 µL of trimethylamine were added to the linker solution, which were transferred into four reaction chambers of a Teflon cylinder. This chamber was prepared by drilling four circular holes in a cylinder. The amino-functionalized chips were immersed in this solution (per chamber two chips) and the reaction chamber was covered with a Teflon disk. After two hours of incubation the chips were washed with chloroform (3 x 10 min) and dried with $N_2$.

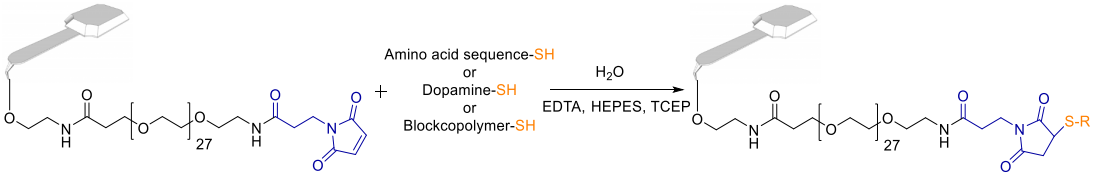


For the last functionalization step, pieces of Parafilm were pressed onto the bottom of polystyrene Petri dishes and the chips which will be functionalized by the same sample were placed onto the Parafilm in a radial arrangement, with the tips in the center and facing upwards.

The weighed portions of the samples (4 mM) (see Table 17) were dissolved in 100 µL deionized water. Then the solution was mixed with 2 µL of EDTA, 5 µL HEPES 1, 2 µL TCEP and 2 µL HEPES 2. Between every step, the solution was vortexed. Afterwards 100 µL of the sample solution were pipetted onto the chips. The reaction was allowed to proceed at room temperature for two hours. The AFM chips were washed in PBS-buffer (3 x 5 min).

***Table 17: Weighed portions of the samples***

| sample | m [mg] |
|---|---|
| DSSEEKC | 0.34 |
| D(pS)(pS)EEKC | 0.40 |
| dopamine-thiol | 0.10 |
| pHEMA-block-pDMMEP (28 kDa) | 11.15 |
| pHEMA-block-pDMMEP (39 kDa) | 15.55 |
| pDMMEP-block-pHEMA (28 kDa) | 11.15 |
| pDMMEP-block-pHEMA (39 kDa) | 15.55 |

All functionalized AFM-chips were stored on small dots of Picodent twinsil® (addition-curing duplicating silicone; mixing ratio 1:1) in sterile filtered PBS-buffer (pH 7.2-7.4) at 7°C in the fridge.

## 3.5 AFM measurement

The AFM measurements were performed in liquid using a NanoWizard ultra speed atomic force microscope (JPK Instruments, Berlin, Germany). The AFM chips were clamped in the probe holder and the laser was aligned on cantilever C (Bruker MSNL-10). The sealed Teflon ring with the prepared substrates was filled with sterile filtered PBS-buffer (pH 7.2.-7.4) The measured spring

constants were entered in the calibration manager in the JPK software and then the cantilever was calibrated by approaching to mica to determine the factor for converting Volts into nm.
All probes were measured in a 10 x 10 µm square with 0 s, 2 s, 4 s and 8 s delay time.

## 3.6 AFM data analysis

***Table 18: Mean adhesion force values and standard deviations of AFM measurements (100 curves per delay time on one substrate)***

| substrate | tip sample | delay time [s] | events | mean value [pN] | standard deviation [pN] | number of curves |
|---|---|---|---|---|---|---|
| mica | naked | 0 | 0 | 25.21 | 1.72 | 50 |
| | | | 1 | 43.79 | 8.34 | 37 |
| | | 2 | 1 | 167.62 | 40.77 | 88 |
| | | 4 | | 204.75 | 43.73 | 90 |
| | | 8 | | 224.76 | 48.85 | 96 |
| | linker | 0 | 1 | 334.98 | 98.89 | 86 |
| | | 2 | | 431.11 | 117.37 | 96 |
| | | 4 | | 453.50 | 115.74 | 93 |
| | | 8 | | 462.12 | 70.29 | 89 |
| | DSSEEKC | 0 | 0 | 27.54 | 4.03 | 27 |
| | | | 1 | 53.61 | 15.85 | 39 |
| | | 2 | 1 | 336.65 | 126.74 | 58 |
| | | 4 | | 438.14 | 152.48 | 59 |
| | | 8 | | 652.01 | 94.86 | 58 |
| | DpSpSEEKC | 0 | 1 | 249.18 | 79.51 | 64 |
| | | 2 | | 445.85 | 85.33 | 79 |
| | | 4 | | 561.03 | 95.61 | 80 |
| | | 8 | | 657.01 | 78.71 | 81 |
| | dopamine | 0 | 0 | 320.50 | 122.66 | 24 |
| | | | 1 | 738.98 | 156.48 | 71 |
| | | 2 | 1 | 1536.34 | 210.31 | 99 |
| | | 4 | | 1612.57 | 212.76 | 85 |
| | | 8 | | 1789.28 | 217.36 | 89 |
| | pDMMEP-block- | 0 | 0 | 76.19 | 19.28 | 38 |
| | | | 1 | 997.30 | 122.21 | 56 |

| | | | | | | |
|---|---|---|---|---|---|---|
| | pHEMA 39 kDa | 2 | 1 | 2162.50 | 306.57 | 52 |
| | | 4 | | 2194.57 | 308.29 | 56 |
| | | 8 | | 2664.50 | 319.49 | 64 |
| | pDMMEP-block-pHEMA 28 kDa | 0 | 1 | 980.57 | 140.64 | 96 |
| | | 2 | | 1877.82 | 221.42 | 98 |
| | | 4 | | 1986.68 | 207.08 | 97 |
| | | 8 | | 2039.00 | 223.53 | 98 |
| | pHEMA-block-pDMMEP 39 kDa | 0 | 1 | 3802.55 | 206.84 | 100 |
| | | 2 | | 4383.27 | 166.08 | 99 |
| | | 4 | | 4339.15 | 130.44 | 100 |
| | | 8 | | 4559.64 | 222.53 | 100 |
| | pHEMA-block-pDMMEP 28 kDa | 0 | 1 | 1252.81 | 236.15 | 96 |
| | | 2 | | 2179.05 | 221.42 | 98 |
| | | 4 | | 2351.91 | 207.08 | 97 |
| | | 8 | | 2433.15 | 223.53 | 98 |
| HA | naked | 0 | 0 | 27.50 | 6.65 | 35 |
| | | | 1 | 46.14 | 14.78 | 10 |
| | | 2 | 0 | 25.93 | 3.28 | 23 |
| | | | 1 | 59.95 | 26.58 | 29 |
| | | 4 | 0 | 34.78 | 10.45 | 52 |
| | | | 1 | 158.25 | 63.46 | 13 |
| | | 8 | 1 | 274.46 | 76.75 | 22 |
| | linker | 0 | 0 | 20.68 | 3.64 | 25 |
| | | | 1 | 199.18 | 62.11 | 19 |
| | | 2 | 1 | 339.65 | 84.41 | 64 |
| | | 4 | | 477.16 | 113.01 | 76 |
| | | 8 | | 526.40 | 141.90 | 53 |
| | DSSEEKC | 0 | 0 | 29.83 | 7.76 | 51 |
| | | | 1 | 46.10 | 14.70 | 12 |
| | | 2 | 0 | 34.52 | 9.01 | 21 |
| | | | 1 | 225.84 | 33.21 | 42 |
| | | 4 | 0 | 42.39 | 13.63 | 20 |
| | | | 1 | 267.36 | 101.58 | 37 |
| | | 8 | 0 | 48.84 | 16.81 | 14 |
| | | | 1 | 338.26 | 138.42 | 31 |
| | | | 2 | 414.68 | 148.20 | 14 |
| | DpSpSEEKC | 0 | 1 | 157.98 | 58.38 | 60 |
| | | 2 | | 692.20 | 187.11 | 64 |
| | | 4 | | 1259.30 | 244.96 | 76 |
| | | 8 | | 1318.16 | 154.50 | 59 |

| | | | | | | |
|---|---|---|---|---|---|---|
| | dopamine | 0 | 1 | 293.39 | 104.82 | 38 |
| | | 2 | 1 | 1230.04 | 231.74 | 62 |
| | | | 2 | 1021.95 | 240.91 | 16 |
| | | 4 | 1 | 1399.08 | 254.82 | 61 |
| | | | 2 | 1183.81 | 308.79 | 13 |
| | | 8 | 1 | 1744.59 | 264.96 | 51 |
| | | | 2 | 1387.87 | 315.27 | 30 |
| | pDMMEP-block-pHEMA 39 kDa | 0 | 1 | 690.23 | 338.35 | 97 |
| | | 2 | | 1242.53 | 365.24 | 90 |
| | | 4 | | 1340.22 | 338.45 | 93 |
| | | 8 | | 1701.64 | 443.03 | 89 |
| | pDMMEP-block-pHEMA 28 kDa | 0 | 1 | 124.03 | 37.61 | 77 |
| | | 2 | | 509.09 | 138.84 | 80 |
| | | 4 | | 599.72 | 193.07 | 76 |
| | | 8 | | 890.31 | 230.73 | 71 |
| | pHEMA-block-pDMMEP 39 kDa | 0 | 1 | 906.77 | 187.87 | 90 |
| | | 2 | | 1254.79 | 314.13 | 81 |
| | | 4 | | 1346.77 | 361.84 | 90 |
| | | 8 | | 1862.95 | 401.30 | 89 |
| | pHEMA-block-pDMMEP 28 kDa | 0 | 1 | 602.65 | 132.79 | 65 |
| | | 2 | | 838.34 | 193.23 | 78 |
| | | 4 | | 970.18 | 189.07 | 62 |
| | | 8 | | 1310.51 | 229.12 | 72 |
| $TiO_2$ | naked | 0 | 0 | 25.22 | 1.75 | 54 |
| | | | 1 | 47.97 | 12.24 | 34 |
| | | 2 | 1 | 165.17 | 44.47 | 97 |
| | | 4 | | 202.67 | 49.51 | 97 |
| | | 8 | | 223.71 | 53.09 | 99 |
| | linker | 0 | 1 | 686.01 | 166.91 | 98 |
| | | 2 | | 814.68 | 143.79 | 98 |
| | | 4 | | 834.07 | 123.00 | 93 |
| | | 8 | | 876.17 | 110.51 | 85 |
| | DSSEEKC | 0 | 1 | 141.64 | 28.94 | 91 |
| | | 2 | 1 | 170.68 | 35.90 | 77 |
| | | | 2 | 166.88 | 35.86 | 17 |
| | | 4 | 1 | 173.79 | 40.00 | 85 |
| | | 8 | | 195.68 | 40.35 | 86 |
| | DpSpSEEKC | 0 | 1 | 620.43 | 157.35 | 91 |
| | | 2 | | 765.18 | 188.13 | 92 |
| | | 4 | | 830.62 | 166.94 | 94 |

| | | | | | | |
|---|---|---|---|---|---|---|
| | | 8 | | 869.90 | 163.29 | 92 |
| | dopamine | 0 | 0 | 154.63 | 53.71 | 20 |
| | | | 1 | 858.58 | 157.24 | 72 |
| | | 2 | 1 | 917.17 | 167.27 | 67 |
| | | 4 | | 1224.64 | 151.80 | 58 |
| | | 8 | | 1389.58 | 188.62 | 60 |
| | pDMMEP-block-pHEMA 39 kDa | 0 | 1 | 1480.70 | 191.77 | 74 |
| | | 2 | | 2203.78 | 167.97 | 91 |
| | | 4 | | 2303.89 | 164.50 | 93 |
| | | 8 | | 2306.84 | 162.02 | 95 |
| | pDMMEP-block-pHEMA 28 kDa | 0 | 1 | 1476.64 | 232.20 | 75 |
| | | 2 | | 1826.73 | 234.00 | 87 |
| | | 4 | | 2153.01 | 266.75 | 97 |
| | | 8 | | 2168.19 | 237.92 | 89 |
| | pHEMA-block-pDMMEP 39 kDa | 0 | 1 | 2204.85 | 275.45 | 104 |
| | | 2 | | 2523.67 | 301.08 | 109 |
| | | 4 | | 2685.97 | 334.32 | 111 |
| | | 8 | | 2728.39 | 369.75 | 124 |
| | pHEMA-block-pDMMEP 28 kDa | 0 | 1 | 1621.58 | 221.88 | 100 |
| | | 2 | | 1996.14 | 254.33 | 100 |
| | | 4 | | 2146.55 | 281.25 | 100 |
| | | 8 | | 2434.25 | 336.21 | 100 |
| $NH_2$ | naked | 0 | 0 | 25.12 | 1.71 | 52 |
| | | | 1 | 45.25 | 11.24 | 41 |
| | | 2 | 1 | 164.55 | 45.12 | 99 |
| | | 4 | | 202.98 | 52.13 | 97 |
| | | 8 | | 222.77 | 51.16 | 99 |
| | linker | 0 | 1 | 618.05 | 186.43 | 99 |
| | | 2 | | 747.04 | 160.63 | 98 |
| | | 4 | | 834.04 | 209.05 | 93 |
| | | 8 | | 851.58 | 175.15 | 95 |
| | DSSEEKC | 0 | 1 | 151.82 | 43.89 | 91 |
| | | 2 | | 218.73 | 46.75 | 89 |
| | | 4 | | 247.43 | 51.91 | 93 |
| | | 8 | | 256.79 | 51.19 | 89 |
| | DpSpSEEKC | 0 | 1 | 644.26 | 149.96 | 76 |
| | | 2 | | 787.91 | 194.93 | 94 |
| | | 4 | | 806.28 | 194.05 | 95 |
| | | 8 | | 823.20 | 197.10 | 87 |
| | dopamine | 0 | 1 | 724.57 | 152.77 | 89 |

| | | | | | | |
|---|---|---|---|---|---|---|
| | | 2 | 1 | 932.86 | 190.63 | 76 |
| | | | 2 | 1024.91 | 196.28 | 18 |
| | | 4 | 1 | 932.21 | 161.80 | 81 |
| | | 8 | 1 | 1035.83 | 199.04 | 71 |
| | | | 2 | 1151.07 | 247.05 | 19 |
| | pDMMEP-block-pHEMA 39 kDa | 0 | 1 | 2061.52 | 245.96 | 95 |
| | | 2 | | 2274.80 | 231.23 | 96 |
| | | 4 | | 2272.35 | 197.48 | 95 |
| | | 8 | | 2344.61 | 193.18 | 94 |
| | pDMMEP-block-pHEMA 28 kDa | 0 | 1 | 2067.35 | 294.11 | 82 |
| | | 2 | | 2694.76 | 222.12 | 93 |
| | | 4 | | 2782.76 | 318.28 | 95 |
| | | 8 | | 2859.67 | 309.48 | 94 |
| | pHEMA-block-pDMMEP 39 kDa | 0 | 1 | 3611.11 | 354.72 | 92 |
| | | 2 | | 3763.44 | 325.99 | 97 |
| | | 4 | | 3948.17 | 298.08 | 96 |
| | | 8 | | 4116.36 | 312.64 | 96 |
| | pHEMA-block-pDMMEP 28 kDa | 0 | 1 | 2947.41 | 351.89 | 94 |
| | | 2 | | 3387.02 | 322.67 | 100 |
| | | 4 | | 3557.80 | 298.08 | 96 |
| | | 8 | | 3737.31 | 312.64 | 96 |

The **statistical analysis** was performed with the statistic software SPSS.
A large number of methods that can be used to investigate mean differences is available. When choosing the method, it is important to note whether the samples are independent or linked. Once this question has been clarified, the question arises how many different variables should be investigated.

The samples in this thesis were independent and the grouping variable was the tip sample. In order to test the significance of the adhesion values of the samples measured on mica, hydroxyapatite, on a $TiO_2$ coated silicon nitride wafer and on a $NH_2$ functionalized silicon nitride wafer, all samples with a delay time of 8 s were chosen.
There are a number of methods by which the mean differences between two or more samples can be examined for significance. If two mean values are to be tested, the t-test for independent samples or the Mann-Whitney U test is used. If more than two means are to be compared, an analysis of variance or

a Kruskal-Wallis test (H-test) is used. If the effect of a third variable is to be controlled, a multi-factorial analysis of variance is possible.

Before testing the significance of the mean values of adhesion the distribution of the data has to be tested in normality tests. Nevertheless, all samples were compared and if one sample is not normally distributed, a distribution-free test has to be chosen. Furthermore, Levene's test was performed on all data of all four substrates. It tests the null hypothesis that the variances in different groups are equal (i.e. the difference between the variances is zero). Due to the fact that the mean of several not normally distributed samples has to be compared, a Kruskal-Wallis test (H-test) was done.

Nevertheless, this test only provides the information that a difference exists and it does not tell exactly where the differences are. One way to see which groups differ is to look at the boxplot (see Figure 87 and Figure 88 in the Appendix). The explanation of a boxplot is shown in Figure 80.

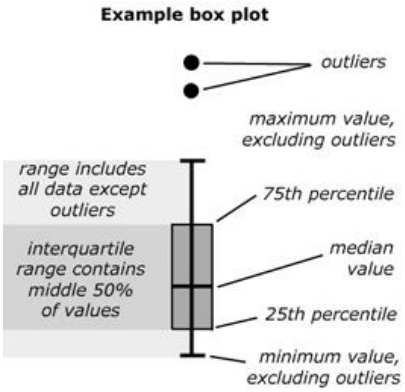


***Figure 80: Boxplot explanation***

The other more statistical way is to perform non-parametric post hoc tests. Therefore, a Dunn-Bonferroni correction on each pair of samples was done. The hypothesis test summary box with the null hypothesis for the Kruskal-Wallis test is shown in Figure 81.

**Hypothesis Test Summary**

| | Null Hypothesis | Test | Sig. | Decision |
|---|---|---|---|---|
| 1 | The distribution of Adhesion [pN] is the same across categories of Tip_Sample. | Independent-Samples Kruskal-Wallis Test | .000 | Reject the null hypothesis. |

Asymptotic significances are displayed. The significance level is .05.

***Figure 81: Hypothesis test summary***

# Summary

In consequence of the increasing life expectancy, larger numbers of injuries and diseases will occur. Due to the rising demand of fixation and adhesion between tissues, implants or scaffolds, adhesive materials need to be developed and optimized. In addition to that, the problem in measuring the adhesion properties of bone glue is to distinguish between cohesive and adhesive behavior and the little information at the molecular level.

The scope of this thesis was to synthesize adhesive block copolymers based on phosphorus-methacrylates, via RAFT polymerization.

Due to the promising properties of 2-hydroxyethylmethacrylate (HEMA)[140] and dimethyl (2-methacryloyloxyethylphosphonate) (DMMEP),[133, 135] this two monomers were chosen for the synthesis of block copolymers. HEMA shows very good biocompatibility, swellability and can act as viscosity regulator. In addition to that, it is easy to modify, stabilizes collagen and immobilizes proteins or cells.[140] pDMMEP tends to self-aggregation[141] and is hydrolysis stable, because of the $C_2$ spacer and the strong P-C bond.[141] Moreover, it shows strong adhesion on titanium and hydroxyapatite surfaces, owing to the interaction between phosphorus ester groups and metal ions. Nevertheless, biocompatibility stands in contrast with an antibacterial effect.[142-144] This means, the higher the biocompatibility, the lower will be the antibacterial effect. Indeed, these properties also may undergo a radical change if they are assembled in the block copolymer.

The blocks in the polymers were designed in the way that once poly-HEMA and one time poly-DMMEP was the starting block. In particular, there can be differences in reaction behavior at RAFT polymerization and in adhesion force because one end will be attached to the AFM tip and the other end is free. Furthermore, the length of DMMEP was varied, because the more phosphorus ester groups, the higher should be the adhesion force. In the end, the RAFT end group was removed to obtain a thiol end group.

Furthermore, a dopamine-thiol compound was synthesized because it can be a very promising adhesive based on the marine mussel, as it was described in in the State of the Art (chapter 1). [122, 124]

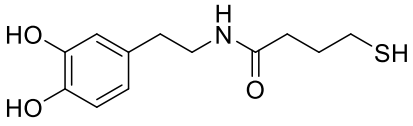


Dopamine-SH

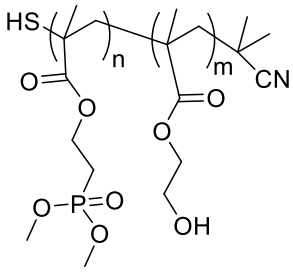


pDMMEP-block-pHEMA

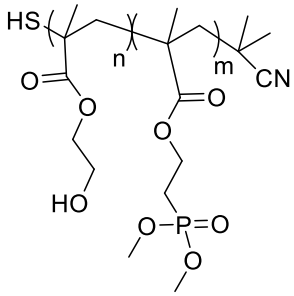


pHEMA-block-pDMMEP

Single-molecule force microscopy (SMFM) is a way of measuring the nano-mechanical behavior of single molecules adhering to specific substrates. The first step was to establish a procedure to essentially graft a single molecule on the tip of an AFM cantilever, as described by Gruber.[138] In order to prove the possibility of tethering one molecule on the apex of the AFM-tip and to perform single molecule atomic force microscopy some calculations concerning the quantification of coupling sites on the used AFM tips were done.[181] The calculations revealed that only one molecule can be tethered to the apex of the used AFM chips. In addition to that, it was possible to attach the amino acid sequences DSSEEKC and DpSpSEEKC to the AFM tip. The adhesion measurements of the synthesized samples and the amino acid sequences were performed on mica (muscovite) with well-known chemical and physical properties, hydroxyapatite (HA) to replicate the mineral part of the bone, a silicon wafer coated with $TiO_2$ nanoparticles to mimic implants and a silicon wafer coated with amino groups to mimic bone proteins.

Prior to analysis, only single rupture events (adhesion events) were taken into account ensuring over 95% probability. The adhesion values at different delay times of the two amino acid sequences were compared to each other and compared to the naked AFM tip and a linker functionalized AFM tip on $TiO_2$.

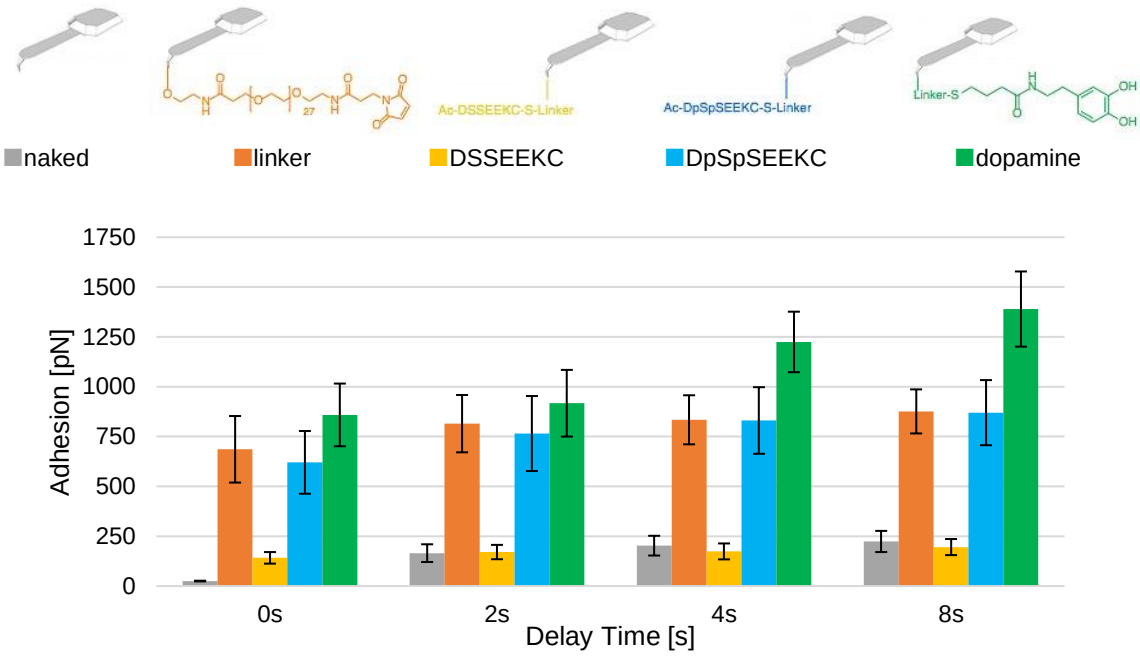


The naked AFM tip showed very low adhesion force and DSSEEKC had lower pull-off force than the linker functionalized tip, which means that the sample attachment was successful. Furthermore, DSSEEKC shows the expected lower adhesion force than DpSpSEEKC. As a result, the phosphorylated serines were responsible for the higher adhesion force on hydroxyapatite and $TiO_2$.

After testing the adhesion of these amino acid sequences and the single functionalization steps, the dopamine-thiol compound was attached to the AFM tip to compare the pull-off forces with literature. [104] The adhesion forces in literature of dopamine-thiol (847 pN ± 157 pN) are in the same range like the forces in this thesis measured with 0 s delay time (859 pN ± 157 pN). The difference between the measurements was a different linker system (reactive and unreactive linker). The pull-off forces with 8 s delay time are even higher (1390 pN ± 189 pN). In addition to that, the block copolymers were tethered to the AFM tip and the adhesion force can be compared to dopamine-thiol.

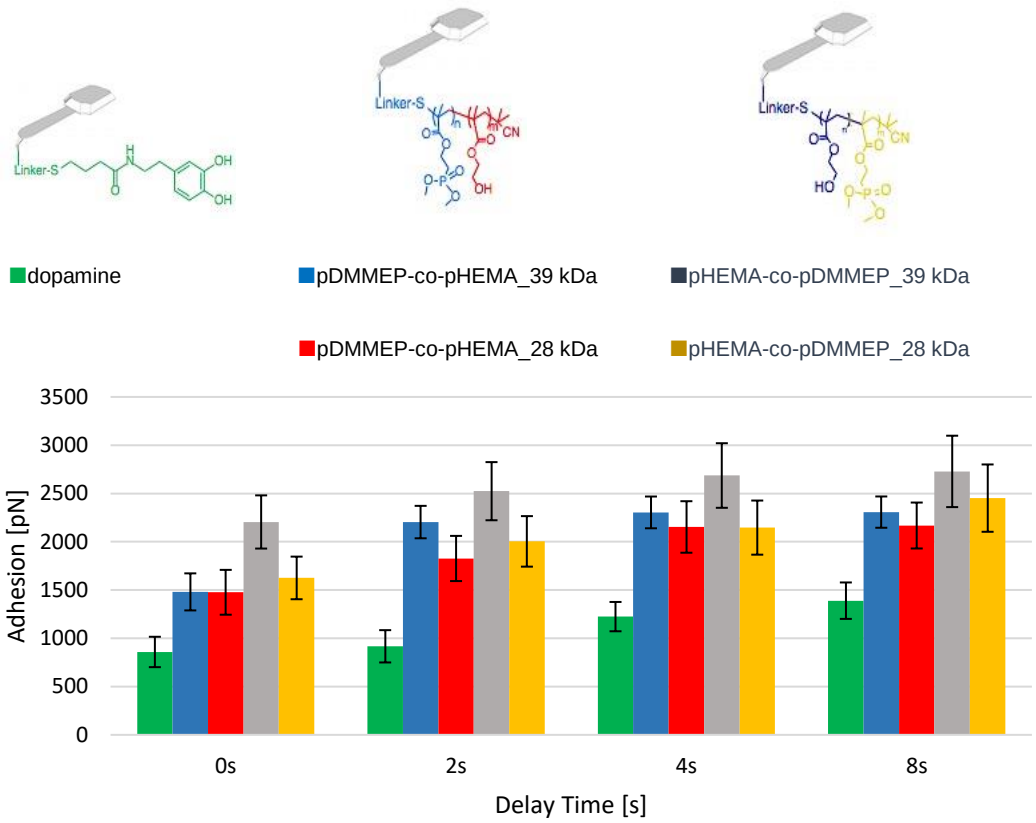


The pull-off forces of the synthesized block copolymers measured on $TiO_2$ were higher than the ones of dopamine. In the Figure above the higher adhesion forces of the polymers with 39 kDa are remarkable, indicating that the block copolymers with 39 kDa contain more DMMEP than the 28 kDa ones. Thereby, the phosphorus ester plays an important role to adhere on these substrates. If the 39 kDa polymers and the 28 kDa polymers were compared among themselves, there can be seen higher adhesion forces of the block copolymers starting with the HEMA block than of the polymers starting with a DMMEP block. In particular, when the HEMA block is attached to the linker system, the DMMEP block is on the free end of the chain and the adhesion force of the phosphorus ester groups with the surface is higher.

By the establishment of a procedure to graft an amino acid sequence on the tip of an AFM cantilever, it was possible to characterize the synthesized block copolymers with different molecular weight and to compare the adhesion force on four different substrates. Due to the comparison with dopamine-thiol, they show great potential towards applications in bone adhesives.

# Materials, Devices and Analyses

| reagent | purity [%] | distributor |
|---|---|---|
| (3-aminopropyl)triethoxysilane (APTES) | 99.0 | Sigma Aldrich |
| 1-methylimidazole | 99.0 | Sigma Aldrich |
| 2-aminoethanol hydrochloride | 98.0 | TCI Chemicals |
| 2-butanone | 99.0 | Fa.Merck |
| 2-hydroxyethyl methacrylate (HEMA) | 99.0 | Sigma Aldrich |
| 4-(2-hydroxyethyl)-1-piperazineethanesulfonic acid (HEPES) | 99.5 | Sigma Aldrich |
| 4,4'-azobis(4-cyanovaleric acid) | 97.5 | Sigma Aldrich |
| 4,4'-azobis(isobutyronitrile) | 98.0 | Sigma Aldrich |
| benzyl chloride | 99.0 | Acros Organics |
| cysteine | 97.0 | Sigma Aldrich |
| dimethyl phosphite | 98.0 | Fa.Merck |
| dimethyl(2-hydroxyethyl)phosphonate | 95.0 | Fluka Chem. Corp. |
| dopamine hydrochloride | 98.0 | Fluka Chem. Corp. |
| DpSpSEEKC | 99.0 | EpochLifeSciences |
| DSSEEKC | 98.0 | EpochLifeSciences |
| ethylenediaminetetraacetic acid (EDTA) | 99.0 | SIgma Aldrich |
| maleic anhydride | 99.0 | Sigma Aldrich |
| maleimide | 99.0 | Sigma Aldrich |
| maleimide-PEG-NHS | 96.0 | Polypure |
| methacrylic anhydride | 94.0 | Sigma Aldrich |
| methacryloyl chloride | 97.0 | Alfa Aesar |
| naphthalin | 98.0 | Fluka |
| PBS-buffer | ster.-filt. | Sigma Aldrich |
| potassium ferricyanide | 99.0 | Sigma Aldrich |
| potassium tert-butoxide | 98.0 | Sigma Aldrich |
| propylamine | 99.0 | Fluka |
| sodium methoxide in methanol | 25 wt% | Sigma Aldrich |
| sulfur | 99.0 | Sigma Aldrich |
| thionyl chloride | 98.0 | Sigma Aldrich |
| triethylamine | 99.0 | Sigma Aldrich |
| tris(2-carboxyethyl)phosphine (TCEP) | 98.0 | TCI Chemicals |
| **γ**-thiobutyrolactone | 98.0 | Sigma Aldrich |

All solvents were applied in a quality common for organic synthesis. All dry solvents were dried following common organic procedures.

**$^{1}$H-NMR** and **$^{13}$C-NMR** spectra were measured with a BRUKER Avance DRX-400 FT-NMR spectrometer. The chemical shift was displayed in parts per million (ppm) (s = singlet, d = doublet, t = triplet, q = quartet, m = multiplet, dd = doublet on doublet, bs = broad singlet). Deuterated chloroform (CDCl3, 99.5% deuteration), deuterated DMSO (DMSO-$d_6$, 99.9% deuteration) and deuterated methanol (MeOD, 99.8% deuteration) from the companies Sigma Aldrich and Eurisotop were used as a solvent

For **thin layer chromatograms** (TLC) TL–aluminum foils coated with silica gel 60 F245 from Merck were used.

**Column chromatography** was conducted on Merck silica gel 60 (0.040–0.063 mm). The silica gel chromatography was performed with a Büchi MPLC-system equipped with the control unit C-620, fraction collector C-660, and UV-photometer C-635.

**Ellipsometric** measurements were carried out using a Sentech SE 500adv which uses a He-Ne as light source and a rotating analyzer. The utilized wavelength was 632.8 nm. Data analysis was done with the supplied instrument software SE400advanced 2.16 which uses the McCracking algorithm. The used optical constants were Si (n = 3.865, k = 0.02), $SiO_2$ (n = 1.465, k = 0), organic layer (n = 1.5, k = 0). The measurements were done at ten different spots on each samples surface, measured twice this spot, and were then averaged.

**ATR-IR** measurements were conducted with a PerkinElmer Spectrum 65 FT-IR Spectrometer equipped with a Specac MKII Golden Gate Single Reflection ATR System.

**AFM measurements** were performed in liquid using a NanoWizard ultra speed atomic force microscope (JPK Instruments, Berlin, Germany). The AFM was operated with the inverted optical microscope Axio Observer, AxioVert 200 (Zeiss, Germany) with a joystick motorized precision stage with 20 × 20 $mm^2$ travel range. The stage offers automatic motion control for precise positioning of the sample relative to optical axis and AFM probe. The NanoWizard is placed on a Halcyonics i4 vibration isolation system (Accurion, Göttingen, Germany). The whole system is located in an acoustic enclosure from JPK which in turn is placed on a stable base (JPK, Berlin, Germany).
Data acquisition and analysis was carried out using SPMControl and JPK data processing software.
Triangular silicon nitride cantilevers MSNL-10 from Bruker were used.

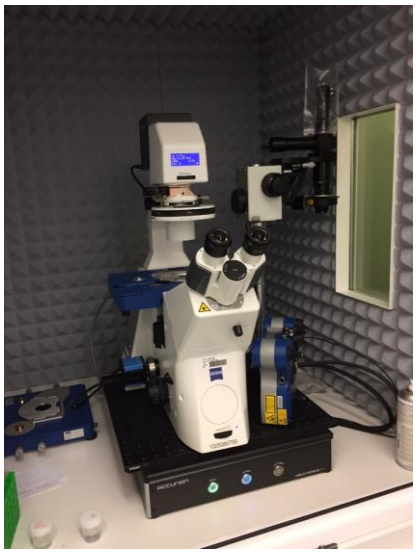

# List of Abbreviations

| | |
|---|---|
| ACVA | 4,4'-azobis(4-cyanovaleric acid) |
| AFM | atomic force microscopy |
| AIBN | 4,4'-azobis(isobutyronitrile) |
| AphS | aminophenyl-trimethoxysilane |
| APTES | (3-aminopropyl)triethoxysilane |
| ATRP | atom transfer radical polymerization |
| BCP | block copolymer |
| BFP | biomembrane force probe |
| BSP | bone sialoprotein |
| CEMA | 2-chlorohydroxyethylmethacrylate |
| CPADB | 4-cyanopentanoic acid dithiobenzoate |
| CPDB | 2-cyanoprop-2-yldithiobenzoate |
| CRP | controlled radical polymerization |
| CTA | chain transfer agent |
| DCM | methylene chloride |
| DMMEP | dimethyl (2-methacryloyloxyethylphosphonate) |
| DMP I | dentin matrix protein |
| DT | degenerative transfer |
| DTBA | sodium dithiobenzoate |
| DTBDS | di(thiobenzoyl) disulfide |
| EDTA | ethylenediaminetetraacetic acid |
| FRP | free radical polymerization |
| GRF | gelatin-resorcinol-aldehyde |
| HA | hydroxyapatite |
| HEMA | 2-hydroxyethylmethacrylate |
| HEPES | 4-(2-hydroxyethyl)-1-piperazineethanesulfonic acid |
| iCMBA | injectable citrate-based inspired bio adhesives |
| ITP | iodine-transfer polymerization |
| L-DOPA | 3,4-dihydroxy-L-phenylalanine |
| MAC3NP2 | propyl N,N-tetramethylbis(phosphonate)-2-hydroxylbismethylenamine methyl methacrylate |

| | |
|---|---|
| MAC3P2 | 2-[2,2-bis(diisopropoxyphosphoryl)ethyoxy]methyl methacrylate |
| Mal-PEG-NHS | maleimide-polyethylene glycol-n-hydroxysuccinimide |
| MDI | 4,4'-diphenylmethane diisocyanate |
| MEMS | micro-electro-mechanical system |
| MPC | methacryloyloxyethyl phosphorylcholine |
| NCP | non-collagenous proteins |
| NMP | nitroxide mediated polymerization |
| OC | osteocalcin |
| ON | osteonectin |
| OP | osteopontin |
| OPD | o-phenylene diamine |
| PCL | polycaprolactone |
| PDI | polydispersity index |
| PEG | polyethylene glycol |
| PMMA | polymethylmethacrylate |
| PRE | persistent radical effect |
| RAFT | reversible addition fragmentation chain transfer polymerization |
| SFRP | stable free radical polymerization |
| SMFM | single-molecule force microscopy |
| SPM | scanning probe microscope |
| TCEP | tris(2-carboxyethyl)phosphin |
| TEA | triethylamine |

# Appendix

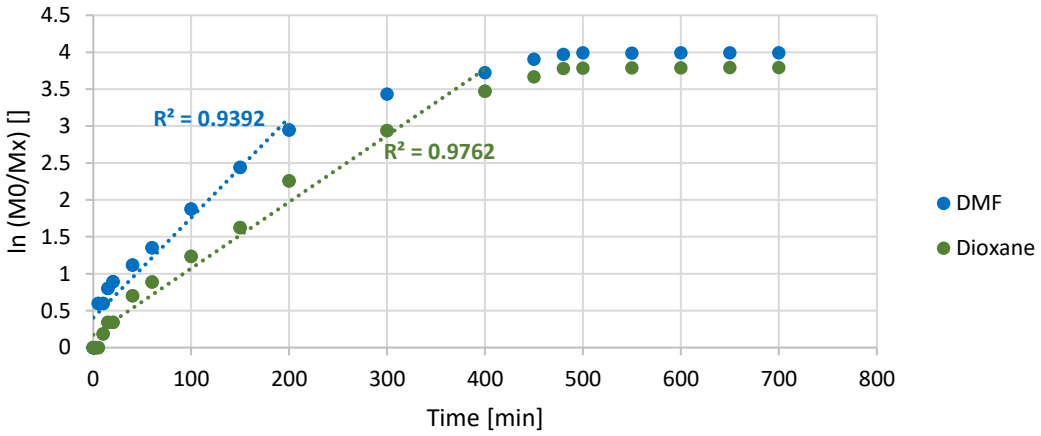


***Figure 82: Pseudo-first order kinetic plot of HEMa 14 kDa with CPDB at 70°C***

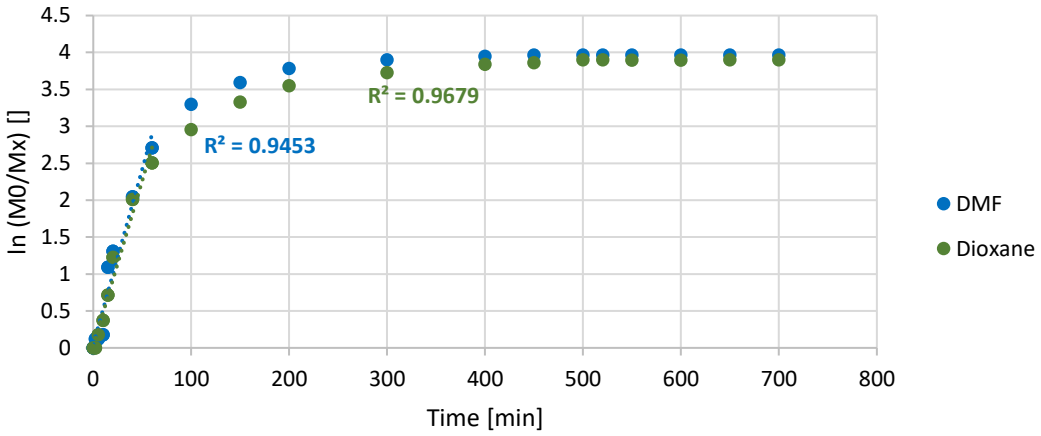


***Figure 83: Pseudo-first order kinetic plot of DMMEP 14 kDa with CPADB at 70°C***

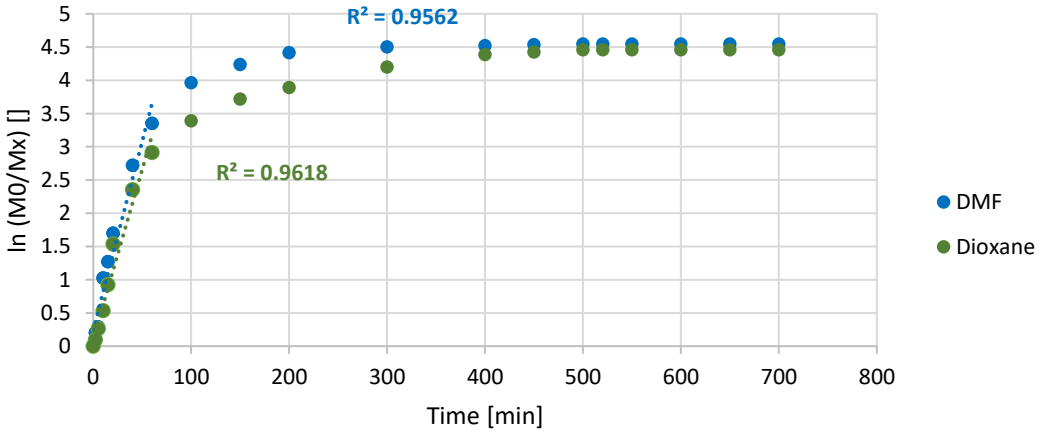


***Figure 84: Pseudo-first order kinetic plot of DMMEP 25 kDa with CPADB at 70°C***

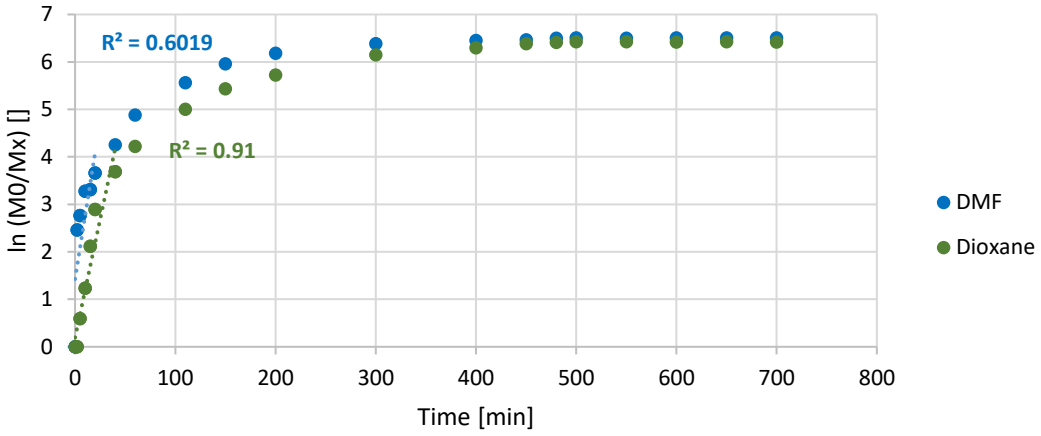


***Figure 85: Pseudo-first order kinetic plot of DMMEP 14 kDa with CPDB at 70°C***

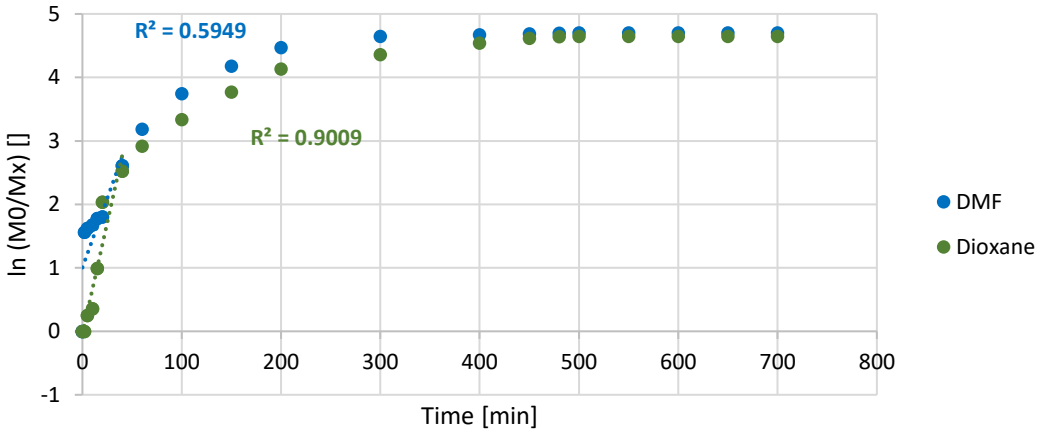


***Figure 86: Pseudo-first order kinetic plot of pDMMEP 25 kDa with CPDB at 70°C***

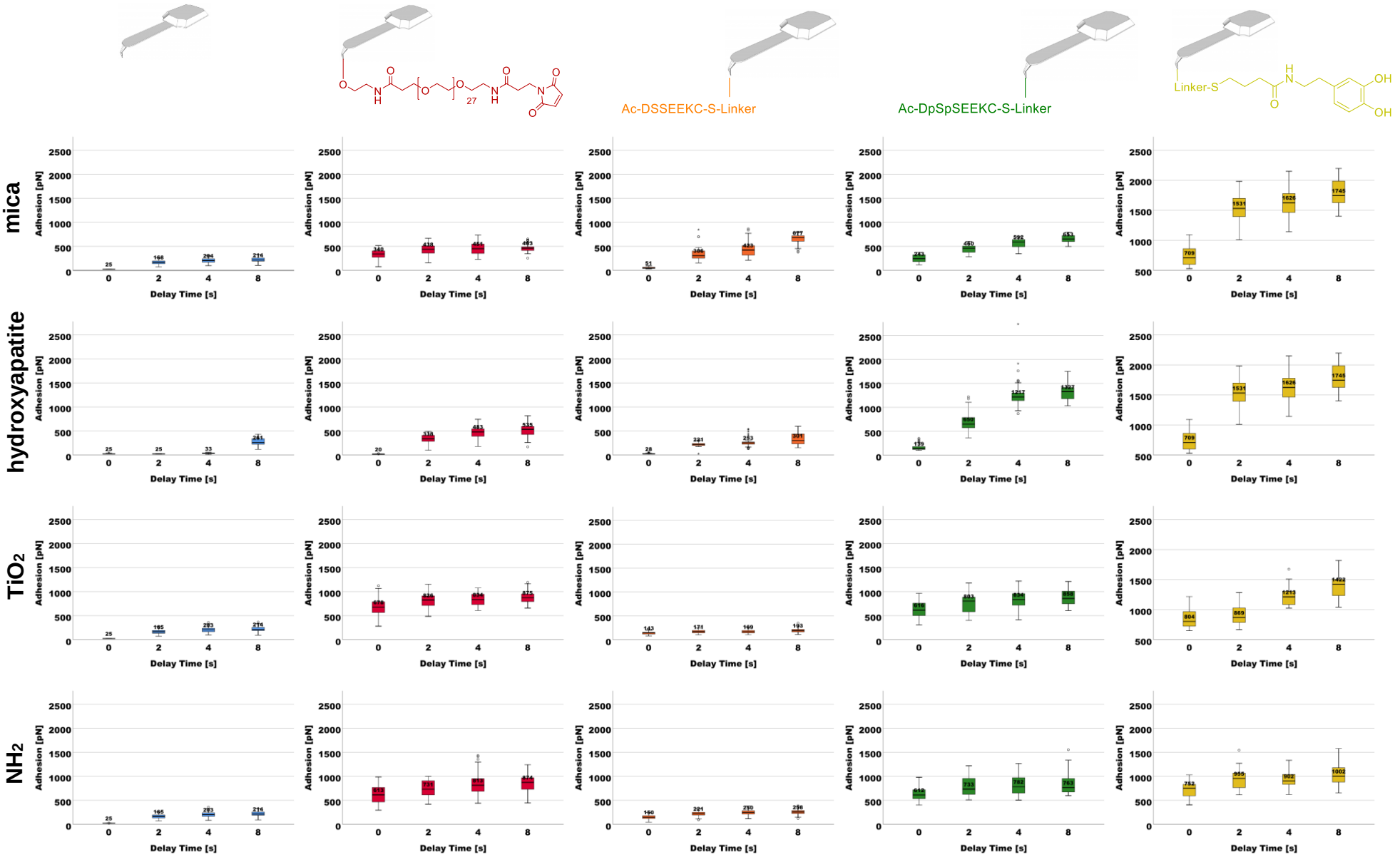


***Figure 87: Boxplot of the naked tip, linker tip, DSSEEKC tip, DpSpSEEKC tip and dopamine tip measured on mica, HA, $TiO_2$ and $NH_2$***

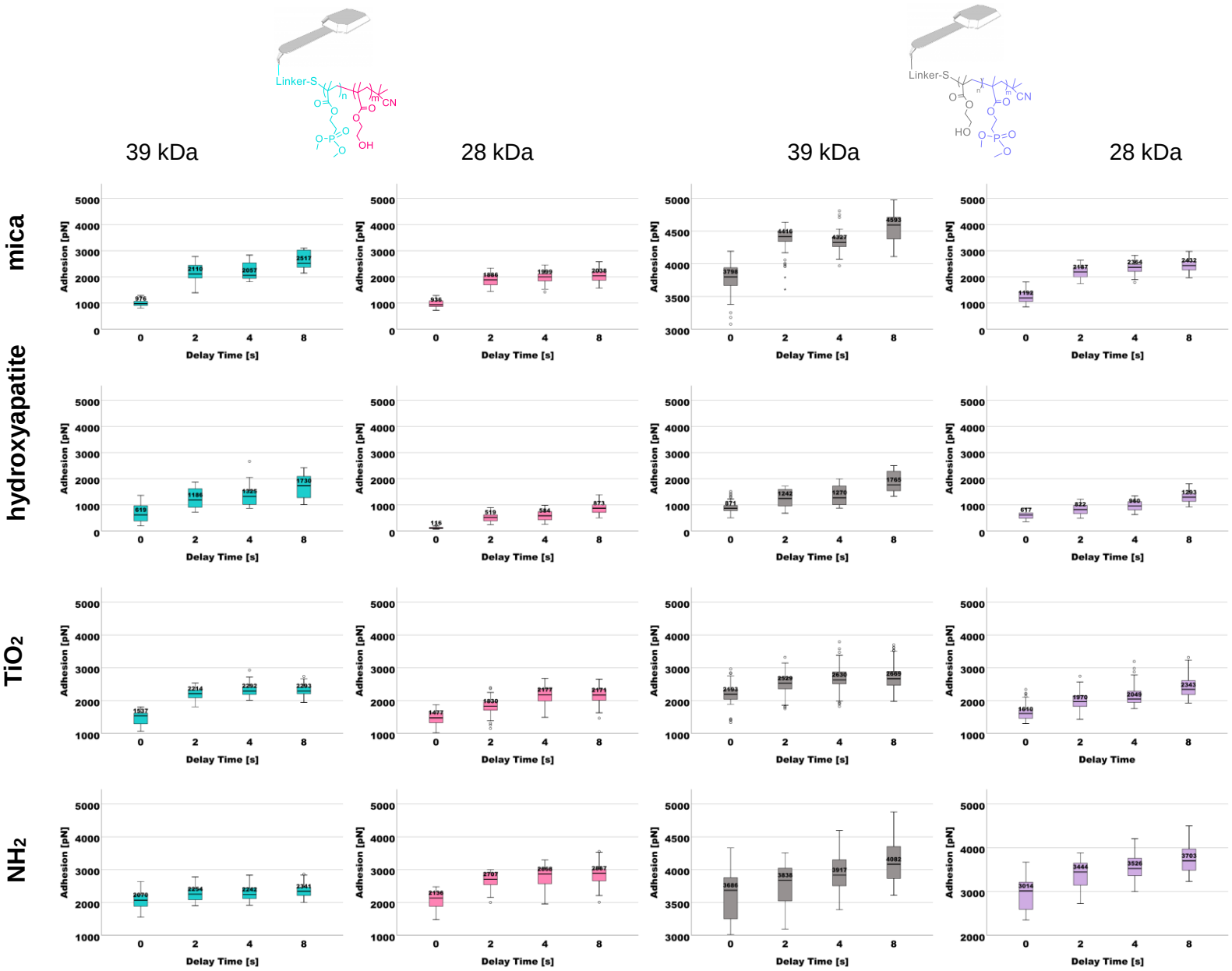


***Figure 88: Boxplot of the tethered block copolymers with different molecular weight***

Table 19 shows the tests of normality to get more information about data distribution on **mica**.

***Table 19: Tests of normality (measurement mica)***

| Tip sample | Mean [pN] | Median [pN] | Kolmogorov-Smirnov[a] | | | Shapiro-Wilk | | |
|---|---|---|---|---|---|---|---|---|
| | | | statistic | df | sig. | statistic | df | sig. |
| naked | 224.76 | 214.26 | 0.101 | 96 | 0.017 | 0.978 | 96 | 0.106 |
| linker | 462.12 | 447.31 | 0.129 | 89 | 0.001 | 0.962 | 89 | 0.010 |
| DSSEEKC | 652.01 | 627.06 | 0.151 | 58 | 0.002 | 0.904 | 58 | 0.000 |
| DpSpSEEKC | 657.01 | 639.61 | 0.089 | 81 | 0.170 | 0.967 | 81 | 0.033 |
| Dopamine | 1789.28 | 1743.49 | 0.104 | 89 | 0.019 | 0.953 | 89 | 0.003 |
| pDMMEP-block-HEMA_39 | 2664.50 | 2584.69 | 0.209 | 64 | 0.000 | 0.824 | 64 | 0.000 |
| pDMMEP-block-HEMA_28 | 2039.00 | 1994.19 | 0.055 | 98 | 0.200* | 0.985 | 98 | 0.314 |
| pHEMA-block-pDMMEP_39 | 4559.64 | 4515.49 | 0.095 | 100 | 0.028 | 0.966 | 100 | 0.012 |
| pHEMA-block-pDMMEP_28 | 2433.15 | 2432.43 | 0.055 | 98 | 0.200* | 0.985 | 98 | 0.314 |

* this is a lower bound of the true significance

a…Lilliefores significance correction

Table 20 shows the results of Levene's test.

***Table 20: Test of homogeneity of variance (Levene's test) on mica***

| | **Levene Statistic** | **df1** | **df2** | **Sig.** |
|---|---|---|---|---|
| Based on Mean | 19.893 | 8 | 764 | 0.000 |
| Based on Median | 17.635 | 8 | 764 | 0.000 |
| Based on Median and with adjusted df | 17.635 | 8 | 429 | 0.000 |
| Based on trimmed mean | 19.946 | 8 | 764 | 0.000 |

Table 21 shows the test statistics of the Kruskal-Wallis test of the samples measured on mica.

***Table 21: Test statistics of the Kruskal-Wallis test (mica)***

| Test Statistics | | | Adhesion [pN] |
|---|---|---|---|
| Kruskal-Wallis H | | | 737.517 |
| df | | | 8 |
| Asymp. Sig. | | | 0.000 |
| Monte Carlo Sig. | Sig. | | 0.000[a] |
| | 99% Confidence Int. | Lower Bound | 0.000 |
| | | Upper Bound | 0.006 |

a…based on 773 samples

In Table 22 the Dunn-Bonferroni correction on certain pairs of samples is shown.

***Table 22: Pairwise comparison of tip samples (mica)***

| Sample 1 - Sample 2 | Test Statistic | Std. Error | Std. Test Statistic | Sig. | Adj. Sig. |
|---|---|---|---|---|---|
| naked - linker | -99.498 | 32.857 | -3.028 | 0.002 | 0.089 |
| linker - DSSEEKC | -100.914 | 37.681 | -2.678 | 0.007 | 0.267 |
| DSSEEKC - DpSpSEEKC | -1.716 | 38.408 | -0.045 | 0.964 | 1.000 |
| Dopamine - pDMMEP-block-pHEMA_39 kDa | -214.879 | 36.596 | -5.872 | 0.000 | 0.000 |
| Dopamine - pDMMEP-block-pHEMA_28 kDa | -63.599 | 32.695 | -1.945 | 0.052 | 1.000 |
| Dopamine - pHEMA-block-pDMMEP_39 kDa | -331.129 | 32.539 | -10.176 | 0.000 | 0.000 |
| Dopamine - pHEMA-block-pDMMEP_28 kDa | -175.803 | 32.695 | -5.377 | 0.000 | 0.000 |
| pDMMEP-block-pHEMA_39 kDa - pDMMEP-block-pHEMA_28 kDa | 151.281 | 35.886 | 4.216 | 0.000 | 0.001 |
| pHEMA-block-pDMMEP_39 kDa - pHEMA-block-pDMMEP_28 kDa | 155.327 | 31.739 | 4.894 | 0.000 | 0.000 |

| | | | | | |
|---|---|---|---|---|---|
| pHEMA-block-pDMMEP_39 kDa - pDMMEP-block-pHEMA_39 kDa | -116.25 | 35.744 | -3.252 | 0.001 | 0.041 |
| pHEMA-block-pDMMEP_28 kDa - pDMMEP-block-pHEMA_28 kDa | -112.204 | 31.899 | -3.518 | 0.000 | 0.016 |

Each row tests the null hypothesis that the sample 1 and sample 2 distributions are the same. Asymptotic significances (2-sided tests) are displayed. The significance level is 0.05.

Table 23 shows the tests of normality to get more information about data distribution on **hydroxyapatite**.

***Table 23: Tests of normality (measurement hydroxyapatite)***

| Tip sample | Mean [pN] | Median [pN] | Kolmogorov-Smirnov[a] | | | Shapiro-Wilk | | |
|---|---|---|---|---|---|---|---|---|
| | | | statistic | df | sig. | statistic | df | sig. |
| naked | 274.46 | 261.07 | 0.149 | 22 | 0.200* | 0.963 | 22 | 0.563 |
| linker | 526.40 | 535.43 | 0.069 | 53 | 0.200* | 0.983 | 53 | 0.639 |
| DSSEEKC | 338.26 | 300.94 | 0.181 | 31 | 0.011 | 0.900 | 31 | 0.007 |
| DpSpSEEKC | 1318.16 | 1326.72 | 0.096 | 59 | 0.200* | 0.969 | 59 | 0.137 |
| Dopamine | 1744.59 | 1633.78 | 0.172 | 51 | 0.001 | 0.879 | 51 | 0.000 |
| pDMMEP-block-HEMA_39 | 1701.64 | 1730.08 | 0.116 | 89 | 0.005 | 0.924 | 89 | 0.000 |
| pDMMEP-block-HEMA_28 | 890.31 | 872.88 | 0.073 | 71 | 0.200* | 0.966 | 71 | 0.052 |
| pHEMA-block-pDMMEP_39 | 1862.95 | 1764.63 | 0.165 | 89 | 0.000 | 0.880 | 89 | 0.000 |
| pHEMA-block-pDMMEP_28 | 1310.51 | 1293.42 | 0.076 | 72 | 0.200* | 0.966 | 72 | 0.051 |

* this is a lower bound of the true significance

a…Lilliefores significance correction

Table 24 displays the results of Levene's test.

***Table 24: Tests of homogeneity of variance (Levene's test) on hydroxyapatite***

| | Levene Statistic | df1 | df2 | Sig. |
|---|---|---|---|---|
| Based on Mean | 13.369 | 8 | 528 | 0.000 |
| Based on Median | 11.929 | 8 | 528 | 0.000 |
| Based on Median and with adjusted df | 11.929 | 8 | 356 | 0.000 |
| Based on trimmed mean | 13.188 | 8 | 528 | 0.000 |

Table 25 shows the test statistics of the Kruskal-Wallis test of the samples measured on mica.

***Table 25: Test statistics of the Kruskal-Wallis test (hydroxyapatite)***

| Test Statistics | | | Adhesion [pN] |
|---|---|---|---|
| Kruskal-Wallis H | | | 413.074 |
| df | | | 8 |
| Asymp. Sig. | | | 0.000 |
| Monte Carlo Sig. | Sig. | | 0.000[a] |
| | 99% Confidence Int. | Lower Bound | 0.000 |
| | | Upper Bound | 0.009 |

a…based on 528 samples

In Table 26 the Dunn-Bonferroni correction on certain pairs of samples is shown.

***Table 26: Pairwise comparison of tip samples (hydroxyapatite)***

| Sample 1 - Sample 2 | Test Statistic | Std. Error | Std. Test Statistic | Sig. | Adj. Sig. |
|---|---|---|---|---|---|
| naked - linker | -52.896 | 39.352 | -1.344 | 0.179 | 1.000 |
| linker - DSSEEKC | 38.945 | 35.084 | 1.110 | 0.267 | 1.000 |
| DSSEEKC - DpSpSEEKC | -233.006 | 34.419 | -6.77 | 0.000 | 0.000 |
| Dopamine - pDMMEP-block-pHEMA_39 kDa | 37.955 | 27.250 | 1.393 | 0.164 | 1.000 |
| Dopamine - pDMMEP-block-pHEMA_28 kDa | 259.295 | 28.481 | 9.104 | 0.000 | 0.000 |
| Dopamine - pHEMA-block-pDMMEP_39 kDa | -13.349 | 27.250 | -0.490 | 0.624 | 1.000 |

| | | | | | |
|---|---|---|---|---|---|
| Dopamine - pHEMA-block-pDMMEP_28 kDa | 140.154 | 28.398 | 4.935 | 0.000 | 0.000 |
| pDMMEP-block-pHEMA_39 kDa - pDMMEP-block-pHEMA_28 kDa | 221.340 | 24.690 | 8.965 | 0.000 | 0.000 |
| pHEMA-block-pDMMEP_39 kDa - pHEMA-block-pDMMEP_28 kDa | 153.503 | 24.595 | 6.241 | 0.000 | 0.000 |
| pHEMA-block-pDMMEP_39 kDa - pDMMEP-block-pHEMA_39 kDa | -51.303 | 23.260 | -2.206 | 0.027 | 0.987 |
| pHEMA-block-pDMMEP_28 kDa - pDMMEP-block-pHEMA_28 kDa | -119.140 | 25.951 | -4.591 | 0.000 | 0.000 |

Each row tests the null hypothesis that the sample 1 and sample 2 distributions are the same. Asymptotic significances (2-sided tests) are displayed. The significance level is 0.05.

Table 27 shows the tests of normality to get more information about data distribution on **$TiO_2$**.

***Table 27: Tests of normality (measurement $TiO_2$)***

| Tip sample | Mean [pN] | Median [pN] | Kolmogorov-Smirnov[a] | | | Shapiro-Wilk | | |
|---|---|---|---|---|---|---|---|---|
| | | | statistic | df | sig. | statistic | df | sig. |
| naked | 223.71 | 213.95 | 0.092 | 99 | 0.038 | 0.983 | 99 | 0.217 |
| linker | 876.17 | 874.54 | 0.044 | 85 | .200* | 0.981 | 85 | 0.229 |
| DSSEEKC | 195.68 | 193.48 | 0.090 | 86 | 0.079 | 0.956 | 86 | 0.005 |
| DpSpSEEKC | 869.90 | 857.54 | 0.067 | 92 | .200* | 0.965 | 92 | 0.015 |
| Dopamine | 1389.58 | 1422.21 | 0.123 | 60 | 0.025 | 0.963 | 60 | 0.064 |
| pDMMEP-block-HEMA_39 | 2306.84 | 2292.66 | 0.062 | 95 | 0.200* | 0.991 | 95 | 0.764 |
| pDMMEP-block-HEMA_28 | 2168.19 | 2170.87 | 0.067 | 89 | 0.200* | 0.980 | 89 | 0.198 |

| | | | | | | | | |
|---|---|---|---|---|---|---|---|---|
| pHEMA-block-pDMMEP_39 | 2806.16 | 2713.76 | 0.151 | 101 | 0.000 | 0.924 | 101 | 0.000 |
| pHEMA-block-pDMMEP_28 | 2436.74 | 2349.74 | 0.155 | 99 | 0.000 | 0.915 | 99 | 0.000 |

* this is a lower bound of the true significance

a…Lilliefores significance correction

Table 28 shows the results of Levene's test.

***Table 28: Tests of homogeneity of variance (Levene's test) on $TiO_2$***

| | Levene Statistic | df1 | df2 | Sig. |
|---|---|---|---|---|
| Based on Mean | 17.950 | 8 | 797 | 0.000 |
| Based on Median | 17.136 | 8 | 797 | 0.000 |
| Based on Median and with adjusted df | 17.136 | 8 | 499.125 | 0.000 |
| Based on trimmed mean | 18.192 | 8 | 797 | 0.000 |

Table 29 shows the test statistics of the Kruskal-Wallis test of the samples measured on mica.

***Table 29: Test statistics of the Kruskal-Wallis test ($TiO_2$)***

| Test Statistics | | | Adhesion [pN] |
|---|---|---|---|
| Kruskal-Wallis H | | | 737.523 |
| df | | | 8 |
| Asymp. Sig. | | | 0.000 |
| Monte Carlo Sig. | Sig. | | 0.000[a] |
| | 99% Confidence Int. | Lower Bound | 0.000 |
| | | Upper Bound | 0.006 |

a…based on 806 samples

In Table 30 the Dunn-Bonferroni correction on certain pairs of samples is displayed.

***Table 30: Pairwise comparison of tip samples ($TiO_2$)***

| Sample 1 - Sample 2 | Test Statistic | Std. Error | Std. Test Statistic | Sig. | Adj. Sig. |
|---|---|---|---|---|---|
| naked - linker | -168.311 | 34.427 | -4.889 | 0.000 | 0.000 |
| linker - DSSEEKC | 200.644 | 35.608 | 5.635 | 0.000 | 0.000 |
| DSSEEKC - DpSpSEEKC | -197.541 | 34.921 | -5.657 | 0.000 | 0.000 |
| Dopamine - pDMMEP-block-pHEMA_39 kDa | -186.279 | 38.392 | -4.852 | 0.000 | 0.000 |
| Dopamine - pDMMEP-block-pHEMA_28 kDa | -137.799 | 38.89 | -3.543 | 0.000 | 0.014 |
| Dopamine - pHEMA-block-pDMMEP_39 kDa | -336.266 | 37.948 | -8.861 | 0.000 | 0.000 |
| Dopamine - pHEMA-block-pDMMEP_28 kDa | -220.375 | 38.091 | -5.786 | 0.000 | 0.000 |
| pDMMEP-block-pHEMA_39 kDa - pDMMEP-block-pHEMA_28 kDa | 48.48 | 34.345 | 1.412 | 0.158 | 1.000 |
| pHEMA-block-pDMMEP_39 kDa - pHEMA-block-pDMMEP_28 kDa | -34.096 | 33.438 | -1.02 | 0.308 | 1.000 |
| pHEMA-block-pDMMEP_39 kDa - pDMMEP-block-pHEMA_39 kDa | -149.987 | 33.275 | -4.507 | 0.000 | 0.000 |
| pHEMA-block-pDMMEP_28 kDa - pDMMEP-block-pHEMA_28 kDa | -82.576 | 34.008 | -2.428 | 0.015 | 0.546 |

Each row tests the null hypothesis that the sample 1 and sample 2 distributions are the same. Asymptotic significances (2-sided tests) are displayed. The significance level is 0.05.

Table 31 shows the tests of normality to get more information about data distribution on **$NH_2$**.

***Table 31: Tests of normality (measurement $NH_2$)***

| Tip sample | Mean [pN] | Median [pN] | Kolmogorov-Smirnov[a] | | | Shapiro-Wilk | | |
|---|---|---|---|---|---|---|---|---|
| | | | statistic | df | sig. | statistic | df | sig. |
| naked | 222.77 | 213.95 | 0.087 | 99 | 0.063 | 0.981 | 99 | 0.163 |
| linker | 851.58 | 873.71 | 0.060 | 95 | 0.200* | 0.991 | 95 | 0.747 |
| DSSEEKC | 256.79 | 257.50 | 0.052 | 89 | 0.200* | 0.993 | 89 | 0.928 |
| DpSpSEEKC | 823.20 | 763.34 | 0.143 | 87 | 0.000 | 0.886 | 87 | 0.000 |
| Dopamine | 1035.83 | 1002.33 | 0.079 | 71 | 0.200* | 0.973 | 71 | 0.125 |
| pDMMEP-block-HEMA_39 | 2344.61 | 2340.83 | 0.071 | 94 | 0.200* | 0.975 | 94 | 0.072 |
| pDMMEP-block-HEMA_28 | 2859.67 | 2887.49 | 0.082 | 94 | 0.133 | 0.985 | 94 | 0.336 |
| pHEMA-block-pDMMEP_39 | 4116.36 | 4082.24 | 0.084 | 96 | 0.088 | 0.959 | 96 | 0.004 |
| pHEMA-block-pDMMEP_28 | 3737.31 | 3703.19 | 0.084 | 96 | 0.088 | 0.959 | 96 | 0.004 |

* this is a lower bound of the true significance

a…Lilliefores significance correction

Table 32 displays the results of Levene's test.

***Table 32: Tests of homogeneity of variance (Levene's test) on $NH_2$***

| | **Levene Statistic** | **df1** | **df2** | **Sig.** |
|---|---|---|---|---|
| Based on Mean | 27.377 | 8 | 812 | 0.000 |
| Based on Median | 23.987 | 8 | 812 | 0.000 |
| Based on Median and with adjusted df | 23.987 | 8 | 515 | 0.000 |
| Based on trimmed mean | 26.765 | 8 | 812 | 0.000 |

Table 33 shows the test statistics of the Kruskal-Wallis test of the samples measured on mica.

***Table 33: Test statistics of the Kruskal-Wallis test ($NH_2$)***

| Test Statistics | | | Adhesion [pN] |
|---|---|---|---|
| Kruskal-Wallis H | | | 778.538 |
| df | | | 8 |
| Asymp. Sig. | | | 0.000 |
| Monte Carlo Sig. | Sig. | | 0.000[a] |
| | 99% Confidence Int. | Lower Bound | 0.000 |
| | | Upper Bound | 0.006 |

a…based on 821 samples

In Table 34 the Dunn-Bonferroni correction on certain pairs of samples is shown.

***Table 34: Pairwise comparison of tip samples ($NH_2$)***

| Sample 1 - Sample 2 | Test Statistic | Std. Error | Std. Test Statistic | Sig. | Adj. Sig. |
|---|---|---|---|---|---|
| naked - linker | -225.877 | 34.060 | -6.632 | 0.000 | 0.000 |
| linker - DSSEEKC | 190.66 | 34.984 | 5.450 | 0.000 | 0.000 |
| DSSEEKC - DpSpSEEKC | -174.714 | 35.754 | -4.887 | 0.000 | 0.000 |
| Dopamine - pDMMEP-block-pHEMA_39 kDa | -132.326 | 37.288 | -3.549 | 0.000 | 0.000 |
| Dopamine - pDMMEP-block-pHEMA_28 kDa | -213.592 | 37.288 | -5.728 | 0.000 | 0.000 |
| Dopamine - pHEMA-block-pDMMEP_39 kDa | -390.872 | 37.120 | -10.530 | 0.000 | 0.000 |
| Dopamine - pHEMA-block-pDMMEP_28 kDa | -331.278 | 37.120 | -8.924 | 0.000 | 0.000 |
| pDMMEP-block-pHEMA_39 kDa - pDMMEP-block-pHEMA_28 kDa | -81.266 | 34.591 | -2.349 | 0.019 | 0.677 |
| pHEMA-block-pDMMEP_39 kDa - pHEMA-block-pDMMEP_28 kDa | 59.594 | 34.229 | 1.741 | 0.082 | 1.000 |

| | | | | | |
|---|---|---|---|---|---|
| pHEMA-block-pDMMEP_39 kDa - pDMMEP-block-pHEMA_39 kDa | -258.545 | 34.411 | -7.514 | 0.000 | 0.000 |
| pHEMA-block-pDMMEP_28 kDa - pDMMEP-block-pHEMA_28 kDa | -117.686 | 34.411 | -3.420 | 0.001 | 0.023 |

Each row tests the null hypothesis that the sample 1 and sample 2 distributions are the same. Asymptotic significances (2-sided tests) are displayed. The significance level is 0.05.

# References


1. http://www.sasserlone.de/zitat/178/albert.einstein/ Porträt Albert Einstein. http://www.sasserlone.de (accessed 11.12.2017).
2. Currey, J. D., *Bones: Structure and Mechanics*. Princeton University Press: 2013.
3. Salgado, A. J.; Coutinho, O. P.; Reis, R. L., Bone Tissue Engineering: State of the Art and Future Trends. *Macromolecular Bioscience* **2004,** *4* (8), 743-765.
4. Oyen, M. L., The Materials Science of Bone: Lessons from Nature for Biomimetic Materials Synthesis. *MRS Bulletin* **2008,** *33* (1), 49-55.
5. Olszta, M. J.; Cheng, X.; Jee, S. S.; Kumar, R.; Kim, Y.-Y.; Kaufman, M. J.; Douglas, E. P.; Gower, L. B., Bone structure and formation: A new perspective. *Materials Science and Engineering: R: Reports* **2007,** *58* (3), 77-116.
6. Wegst, U. G. K.; Bai, H.; Saiz, E.; Tomsia, A. P.; Ritchie, R. O., Bioinspired structural materials. *Nature Materials* **2014,** *14*, 23.
7. Wegst, U. G. K.; Bai, H.; Saiz, E.; Tomsia, A. P.; Ritchie, R. O., Bioinspired structural materials. In *Nature Materials*, Nature Publishing Group, a division of Macmillan Publishers Limited. All Rights Reserved.: 2014; Vol. 14, p 23.
8. Sommerfeldt, D.; Rubin, C., Biology of bone and how it orchestrates the form and function of the skeleton. *European Spine Journal* **2001,** *10* (Suppl 2), S86-S95.
9. Lowry, J., Bone Regeneration and Repair: Biology and Clinical Applications. *Annals of The Royal College of Surgeons of England* **2006,** *88* (3), 334-334.
10. Bilezikian, J. P.; Raisz, L. G.; Martin, T. J., *Principles of Bone Biology*. Elsevier Science: 2008.
11. Giannoudis, P. V.; Einhorn, T. A.; Marsh, D., Fracture healing: the diamond concept. *Injury* **2007,** *38*, S3-S6.
12. Sami, Fracture Healing. OrthoTips: 2015.
13. Donkerwolcke, M.; Burny, F.; Muster, D., Tissues and bone adhesives—historical aspects. *Biomaterials* **1998,** *19* (16), 1461-1466.
14. Heiss, C.; Kraus, R.; Schluckebier, D.; Stiller, A.-C.; Wenisch, S.; Schnettler, R., Bone Adhesives in Trauma and Orthopedic Surgery. *European Journal of Trauma* **2006,** *32* (2), 141-148.
15. Bloch, B., Bonding of fractures by plastic adhesives. *Bone & Joint Journal* **1958,** *40* (4), 804-812.
16. Nigst, H.; Wagener, H.; Bircher, J.; Zuppinger, P., Industrielle Gießharze in der Knochenchirurgie. *DMW-Deutsche Medizinische Wochenschrift* **1960,** *85* (16), 658-660.
17. Giebel, G.; Rimpler, M., Klebungen am Skelettsystem: Klebstoffe, 50 Jahre Hilfsstoffe für den Chirurgen (Teil 1)-Skeletal System Gluing Adhesives, 50 Years of Surgical Aids. Part 1. *Biomedizinische Technik/Biomedical Engineering* **1981,** *26* (3), 35-40.
18. Rietz, K.-A., Polymer osteosynthesis-experimental studies with an epoxy resin. *Acta chirurgica Scandinavica* **1964,** *128*, 387.

19. Mandarino, M.; Salvatore, J. In *Polyurethane polymer (ostamer): its use in fractured and diseased bones; experimental results*, Surgical forum, 1958; p 762.
20. Hulliger, L., Untersuchungen über die Wirkung von Kunstharzen (Palacos und Ostamer) in Gewebekulturen. *Archives of Orthopaedic and Trauma Surgery* **1962,** *54* (5), 581-588.
21. Buchner, H.; Feischl, P., Spätergebnisse bei der Behandlung von Knochenbrüchen mit Polyurethanschaum. *Archiv für orthopädische und Unfall-Chirurgie, mit besonderer Berücksichtigung der Frakturenlehre und der orthopädisch-chirurgischen Technik* **1962,** *54* (1), 48-57.
22. Drompp, B. W., Chemical osteosynthesis of fractures and non-unions of the shafts of long bones of the lower extremity. *The American Journal of Surgery 99* (5), 733-744.
23. Leemann, R. A.; Hedinger, C.; Jenny, M., Experimental animal and histological results in fracture gluing with the polyurethane polymer" ostamer". *Schweizerische medizinische Wochenschrift* **1961,** *91*, 908-914.
24. Buchner, H., Erfahrungen mit Polyurethanschaum (Ostamer) bei der Behandlung von Knochenbrüchen. *Klin Med (Wien)* **1961,** *16*, 264-288.
25. Coover Jr, W., Joyner, FB, Sliearer, NH, J1-., and Weckes, TH, Jr.: A new plastic adhesive. *Soc. Plast. Engineers J* **1959,** *15*, 413.
26. Giebel, M., Adhesives in surgery—Ergebnisse bei Klebungen mit verschiedenen Klebern an verschiedenen Geweben. *Wien Med Akad* **1968,** *1968*, 65-66.
27. Meyer, G.; Muster, D.; Schmitt, D.; Jung, P.; Jaeger, J., Bone bonding through bioadhesives: present status. *Biomaterials, medical devices, and artificial organs* **1979,** *7* (1), 55-71.
28. Charnley, J., The Healing of Human Fractures in Contact With Self-curing Acrylic Cement. *Clinical Orthopaedics and Related Research* **1966,** *47*, 157-164.
29. Breusch, S.; Kühn, K.-D., Knochenzemente auf basis von polymethylmethacrylat. *Der Orthopäde* **2003,** *32* (1), 41-50.
30. Smith, D., Lutes, glues, cements and adhesives in medicine and dentistry. *Biomedical engineering* **1973,** *8* (3), 108.
31. Kort, J., *Klebstoff in der Chirurgie: experimentelle Untersuchungen und klinische Anwendung*. Schattauer: 1971.
32. Currie, L. J.; Sharpe, J. R.; Martin, R., The use of fibrin glue in skin grafts and tissue-engineered skin replacements. *Plast Reconstr Surg* **2001,** *108*, 1713-26.
33. Patel, S.; Rodriguez-Merchan, E.; Haddad, F., The use of fibrin glue in surgery of the knee. *Bone & Joint Journal* **2010,** *92* (10), 1325-1331.
34. Cooper, C.; Falb, R., Surgical adhesives. *Annals of the New York Academy of Sciences* **1968,** *146* (1), 214-224.
35. Bouten, P. J. M.; Zonjee, M.; Bender, J.; Yauw, S. T. K.; van Goor, H.; van Hest, J. C. M.; Hoogenboom, R., The chemistry of tissue adhesive materials. *Progress in Polymer Science* **2014,** *39* (7), 1375-1405.
36. Schnabelrauch, M.; Vogt, S. In *Werkstoffe für die Medizintechnik*, Werkstoffwoche, 1999.
37. No, Y. J.; Roohani-Esfahani, S.-i.; Zreiqat, H., Nanomaterials: the next step in injectable bone cements. *Nanomedicine* **2014,** *9* (11), 1745-1764.

38. Vaishya, R.; Chauhan, M.; Vaish, A., Bone cement. *Journal of Clinical Orthopaedics and Trauma* **2013,** *4* (4), 157-163.
39. Oldfield, F. F.; Yasuda, H. K., ESR study of MMA polymerization by a peroxide/amine system: Bone cement formation. *Journal of Biomedical Materials Research* **1999,** *44* (4), 436-445.
40. Tobita, H., Polymerization Processes, 1. Fundamentals. In *Ullmann's Encyclopedia of Industrial Chemistry*, Wiley-VCH Verlag GmbH & Co. KGaA: 2000.
41. Braunecker, W. A.; Matyjaszewski, K., Controlled/living radical polymerization: Features, developments, and perspectives. *Progress in Polymer Science* **2007,** *32* (1), 93-146.
42. Moad, G.; Rizzardo, E.; Thang, S. H., Toward Living Radical Polymerization. *Accounts of Chemical Research* **2008,** *41* (9), 1133-1142.
43. Fisher, H., The persistent radical effect in controlled radical polymerizations. *J. Polym. Sci.; Part A: Polym. Chem* **1999,** *37*, 1885.
44. Fischer, H., Unusual selectivities of radical reactions by internal suppression of fast modes. *Journal of the American Chemical Society* **1986,** *108* (14), 3925-3927.
45. Zetterlund, P. B.; Kagawa, Y.; Okubo, M., Controlled/living radical polymerization in dispersed systems. *Chemical reviews* **2008,** *108* (9), 3747-3794.
46. Shipp, D. A., Living Radical Polymerization: Controlling Molecular Size and Chemical Functionality in Vinyl Polymers. *Journal of Macromolecular Science, Part C* **2005,** *45* (2), 171-194.
47. Lacroix-Desmazes, P.; Severac, R.; Boutevin, B., Reverse iodine transfer polymerization of methyl acrylate and n-butyl acrylate. *Macromolecules* **2005,** *38* (15), 6299-6309.
48. Moad, G.; Rizzardo, E.; Thang, S. H., Living radical polymerization by the RAFT process–a third update. *Australian Journal of Chemistry* **2012,** *65* (8), 985-1076.
49. Le, T. P.; Moad, G.; Rizzardo, E. Polymerization with living characteristics. US 7,666,962 B2, 23.2.2010, 2010.
50. Chiefari, J.; Chong, Y.; Ercole, F.; Krstina, J.; Jeffery, J.; Le, T. P.; Mayadunne, R. T.; Meijs, G. F.; Moad, C. L.; Moad, G., Living free-radical polymerization by reversible addition− fragmentation chain transfer: the RAFT process. *Macromolecules* **1998,** *31* (16), 5559-5562.
51. Pascale, C.; Dominique, C.; Samir, Z.; Xavier, F.; Ghenwa, B. Method for block polymer synthesis by controlled radical polymerisation from dithiocarbamate compounds. 1999.
52. Charmot, D.; Corpart, P.; Adam, H.; Zard, S.; Biadatti, T.; Bouhadir, G. In *Controlled radical polymerization in dispersed media*, Macromolecular Symposia, Wiley Online Library: 2000; pp 23-32.
53. Matyjaszewski, K.; Müller, A. H., *Controlled and living polymerizations: from mechanisms to applications*. John Wiley & Sons: 2009.
54. Barner-Kowollik, C., Handbook of RAFT Polymerization. In *123Library*, 1 ed.; Wiley-VCH: 2008.
55. Lowe, A. B.; McCormick, C. L., Reversible addition–fragmentation chain transfer (RAFT) radical polymerization and the synthesis of water-soluble (co) polymers under homogeneous conditions in organic and aqueous media. *Progress in Polymer Science* **2007,** *32* (3), 283-351.

56. Moad, G.; Rizzardo, E.; Thang, S. H., Radical addition–fragmentation chemistry in polymer synthesis. *Polymer* **2008,** *49* (5), 1079-1131.
57. Smith, A. E.; Xu, X.; McCormick, C. L., Stimuli-responsive amphiphilic (co) polymers via RAFT polymerization. *Progress in polymer science* **2010,** *35* (1), 45-93.
58. Moad, G.; Rizzardo, E.; Thang, S. H., A RAFT Tutorial. *The Strem Chemiker* 3.2011, 2011, p 56.
59. Keddie, D. J.; Moad, G.; Rizzardo, E.; Thang, S. H., RAFT Agent Design and Synthesis. *Macromolecules* **2012,** *45* (13), 5321-5342.
60. Adelsberger, J.; Kulkarni, A.; Jain, A.; Wang, W.; Bivigou-Koumba, A. M.; Busch, P.; Pipich, V.; Holderer, O.; Hellweg, T.; Laschewsky, A.; Müller-Buschbaum, P.; Papadakis, C. M., Thermoresponsive PS-b-PNIPAM-b-PS Micelles: Aggregation Behavior, Segmental Dynamics, and Thermal Response. *Macromolecules* **2010,** *43* (5), 2490-2501.
61. Du, B.; Mei, A.; Yang, Y.; Zhang, Q.; Wang, Q.; Xu, J.; Fan, Z., Synthesis and micelle behavior of (PNIPAm-PtBA-PNIPAm)m amphiphilic multiblock copolymer. *Polymer* **2010,** *51* (15), 3493-3502.
62. Skey, J.; O'Reilly, R. K., Synthesis of chiral micelles and nanoparticles from amino acid based monomers using RAFT polymerization. *Journal of Polymer Science Part A: Polymer Chemistry* **2008,** *46* (11), 3690-3702.
63. Bernard, J.; Favier, A.; Zhang, L.; Nilasaroya, A.; Davis, T. P.; Barner-Kowollik, C.; Stenzel, M. H., Poly(vinyl ester) Star Polymers via Xanthate-Mediated Living Radical Polymerization: From Poly(vinyl alcohol) to Glycopolymer Stars. *Macromolecules* **2005,** *38* (13), 5475-5484.
64. Barón, M.; Hellwich, K. H.; Hess, M.; Horie, K.; Jenkins, A. D.; Jones, R. G.; Kahovec, J.; Kratochvíl, P.; Metanomski, W. V.; Mormann, W.; Stepto, R. F. T.; Vohlídal, J.; Wilks, E. S., Glossary of class names of polymers based on chemical structure and molecular architecture (iupac recommendations 2009). *Pure and Applied Chemistry* **2009,** *81* (6), 1131-1186.
65. Li, J.; Ren, J.; Cao, Y.; Yuan, W., Synthesis of biodegradable pentaarmed star-block copolymers via an asymmetric BIS-TRIS core by combination of ROP and RAFT: From star architectures to double responsive micelles. *Polymer* **2010,** *51* (6), 1301-1310.
66. Chaffey-Millar, H.; Stenzel, M. H.; Davis, T. P.; Coote, M. L.; Barner-Kowollik, C., Design Criteria for Star Polymer Formation Processes via Living Free Radical Polymerization. *Macromolecules* **2006,** *39* (19), 6406-6419.
67. Chaffey-Millar, H.; Busch, M.; Davis, T. P.; Stenzel, M. H.; Barner-Kowollik, C., Advanced Computational Strategies for Modelling the Evolution of Full Molecular Weight Distributions Formed During Multiarmed (Star) Polymerisations. *Macromolecular Theory and Simulations* **2005,** *14* (3), 143-157.
68. Luzon, M.; Boyer, C.; Peinado, C.; Corrales, T.; Whittaker, M.; Tao, L.; Davis, T. P., Water-soluble, thermoresponsive, hyperbranched copolymers based on PEG-methacrylates: Synthesis, characterization, and LCST behavior. *Journal of Polymer Science Part A: Polymer Chemistry* **2010,** *48* (13), 2783-2792.
69. Wang, W.-J.; Wang, D.; Li, B.-G.; Zhu, S., Synthesis and Characterization of Hyperbranched Polyacrylamide Using Semibatch Reversible

Addition−Fragmentation Chain Transfer (RAFT) Polymerization. *Macromolecules* **2010,** *43* (9), 4062-4069.
70. Ge, Z.; Luo, S.; Liu, S., Syntheses and self-assembly of poly(benzyl ether)-b-poly(N-isopropylacrylamide) dendritic–linear diblock copolymers. *Journal of Polymer Science Part A: Polymer Chemistry* **2006,** *44* (4), 1357-1371.
71. Ge, Z.; Chen, D.; Zhang, J.; Rao, J.; Yin, J.; Wang, D.; Wan, X.; Shi, W.; Liu, S., Facile synthesis of dumbbell-shaped dendritic-linear-dendritic triblock copolymer via reversible addition-fragmentation chain transfer polymerization. *Journal of Polymer Science Part A: Polymer Chemistry* **2007,** *45* (8), 1432-1445.
72. Fairbanks, B. D.; Gunatillake, P. A.; Meagher, L., Biomedical applications of polymers derived by reversible addition–fragmentation chain-transfer (RAFT). *Advanced drug delivery reviews* **2015,** *91*, 141-152.
73. Förster, S.; Konrad, M., From self-organizing polymers to nano-and biomaterials. *Journal of Materials Chemistry* **2003,** *13* (11), 2671-2688.
74. Gody, G.; Maschmeyer, T.; Zetterlund, P. B.; Perrier, S., Rapid and quantitative one-pot synthesis of sequence-controlled polymers by radical polymerization. *Nature Communications* **2013,** *4*, 2505.
75. Rickerby, D. S., A review of the methods for the measurement of coating-substrate adhesion. *Surface and Coatings Technology* **1988,** *36* (1), 541-557.
76. Binnig, G.; Quate, C. F.; Gerber, C., Atomic force microscope. *Physical review letters* **1986,** *56* (9), 930.
77. Eaton, P.; West, P., *Atomic Force Microscopy*. OUP Oxford: 2010.
78. Marti, O.; Elings, V.; Haugan, M.; Bracker, C. E.; Schneir, J.; Drake, B.; Gould, S. A. C.; Gurley, J.; Hellemans, L.; Shaw, K.; Weisenhorn, A. L.; Zasadzinski, J.; Hansma, P. K., Scanning probe microscopy of biological samples and other surfaces. *Journal of Microscopy* **1988,** *152* (3), 803-809.
79. Wolter, O.; Bayer, T.; Greschner, J., Micromachined silicon sensors for scanning force microscopy. *Journal of Vacuum Science & Technology B: Microelectronics and Nanometer Structures Processing, Measurement, and Phenomena* **1991,** *9* (2), 1353-1357.
80. Albrecht, T. R.; Akamine, S.; Carver, T.; Quate, C. F., Microfabrication of cantilever styli for the atomic force microscope. *Journal of Vacuum Science & Technology A: Vacuum, Surfaces, and Films* **1990,** *8* (4), 3386-3396.
81. Tortonese, M.; Barrett, R.; Quate, C., Atomic resolution with an atomic force microscope using piezoresistive detection. *Applied physics letters* **1993,** *62* (8), 834-836.
82. Akamine, S.; Barrett, R.; Quate, C., Improved atomic force microscope images using microcantilevers with sharp tips. *Applied Physics Letters* **1990,** *57* (3), 316-318.
83. Raiteri, R.; Grattarola, M.; Butt, H.-J.; Skládal, P., Micromechanical cantilever-based biosensors. *Sensors and Actuators B: Chemical* **2001,** *79* (2), 115-126.
84. Khushalani, D. G.; Pande, R. S.; Patrikar, R. M., Fabrication and characterization of MEMS cantilever array for switching applications. *Microelectronic Engineering* **2016,** *157* (Supplement C), 78-82.

85. Nanoandmore AFM Chips. https://www.nanoandmore.com/afm-support-chips.php (accessed 11.12.2017).
86. BrukerNanoInc Bruker AFM Probes. https://www.brukerafmprobes.com/p-3710-msnl-10.aspx (accessed 11.12.2017).
87. OlympusCorporation AFM Probes. http://probe.olympus-global.com/en/ (accessed 11.12.2017).
88. Crawford, S. V-shaped AFM cantilevers. http://nanotechweb.org/cws/article/tech/17122 (accessed 11.12.2017).
89. NanoWorld AR5-NCLR. http://www.nanoworld.com/pointprobe-high-aspect-ratio-afm-tip-ar5-nclr (accessed 11.12.2017).
90. NanoWorld NCH. http://www.nanoworld.com/pointprobe-tapping-mode-afm-tip-nch (accessed 11.12.2017).
91. NanoWorld PNP-DB. http://www.nanoworld.com/pyrex-nitride-rectangular-silicon-nitride-cantilever-afm-tip-pnp-db (accessed 11.12.2017).
92. NanoWorld SSS-NCL. http://www.nanoworld.com/pointprobe-super-sharp-silicon-tapping-mode-afm-tip-sss-ncl (accessed 11.12.2017).
93. Hutter, J. L.; Bechhoefer, J., Calibration of atomic-force microscope tips. *Review of Scientific Instruments* **1993,** *64* (7), 1868-1873.
94. Leite, F. L.; Herrmann, P. S. P., Application of atomic force spectroscopy (AFS) to studies of adhesion phenomena: a review. *Journal of Adhesion Science and Technology* **2005,** *19* (3-5), 365-405.
95. Leite, F. L.; Bueno, C. C.; Da Róz, A. L.; Ziemath, E. C.; Oliveira, O. N., Theoretical Models for Surface Forces and Adhesion and Their Measurement Using Atomic Force Microscopy. *International Journal of Molecular Sciences* **2012,** *13* (10).
96. Smith, S. B.; Finzi, L.; Bustamantef, C., Direct mechanical measurements of the elasticity of single DNA molecules by using magnetic beads. *Nov* **1992,** *13*, 1122-1126.
97. Ashkin, A.; Schütze, K.; Dziedzic, J.; Euteneuer, U.; Schliwa, M., Force generation of organelle transport measured in vivo by an infrared laser trap. *Nature* **1990,** *348* (6299), 346-348.
98. Wilson, L.; Matsudaira, P. T.; Sheetz, M. P., *Laser tweezers in cell biology*. Academic Press: 1997; Vol. 55.
99. Neuman, K. C.; Nagy, A., Single-molecule force spectroscopy: optical tweezers, magnetic tweezers and atomic force microscopy. *Nature Methods* **2008,** *5*, 491.
100. Kishino, A.; Yanagida, T., Force measurements by micromanipulation of a single actin filament by glass needles. *Nature* **1988,** *334* (6177), 74-76.
101. Evans, E.; Ritchie, K.; Merkel, R., Sensitive force technique to probe molecular adhesion and structural linkages at biological interfaces. *Biophysical journal* **1995,** *68* (6), 2580-2587.
102. Rief, M.; Oesterhelt, F.; Heymann, B.; Gaub, H. E., Single molecule force spectroscopy on polysaccharides by atomic force microscopy. *Science* **1997,** *275* (5304), 1295-1297.
103. Hinterdorfer, P.; Baumgartner, W.; Gruber, H. J.; Schilcher, K.; Schindler, H., Detection and localization of individual antibody-antigen recognition events by atomic force microscopy. *Proceedings of the National Academy of Sciences* **1996,** *93* (8), 3477-3481.

104. Messersmith, P. B.; Lee, H.; Scherer, N. F., Single-molecule mechanics of mussel adhesion. *Proceedings of the National Academy of Sciences* **2006,** *103* (35), 12999-13003.
105. Roach, H., Why does bone matrix contain non-collagenous proteins? The possible roles of osteocalcin, osteonectin and bone sialoprotein in bone mineralisation and resorption. *Cell biology international* **1994,** *18* (6), 617-628.
106. Ingram, R. T.; Clarke, B. L.; Fisher, L. W.; Fitzpatrick, L. A., Distribution of noncollagenous proteins in the matrix of adult human bone: evidence of anatomic and functional heterogeneity. *Journal of Bone and Mineral Research* **1993,** *8* (9), 1019-1029.
107. Tye, C. E.; Hunter, G. K.; Goldberg, H. A., Identification of the type I collagen-binding domain of bone sialoprotein and characterization of the mechanism of interaction. *Journal of Biological Chemistry* **2005,** *280* (14), 13487-13492.
108. Young, M. F.; Kerr, J. M.; Ibaraki, K.; Heegaard, A.-M.; Robey, P. G., Structure, expression, and regulation of the major noncollagenous matrix proteins of bone. *Clinical orthopaedics and related research* **1992,** *281*, 275-294.
109. Thurner, P. J., Atomic force microscopy and indentation force measurement of bone. *Wiley Interdisciplinary Reviews: Nanomedicine and Nanobiotechnology* **2009,** *1* (6), 624-649.
110. Stayton, P. S.; Drobny, G. P.; Shaw, W. J.; Long, J. R.; Gilbert, M., Molecular recognition at the protein-hydroxyapatite interface. *Critical Reviews in Oral Biology and Medicine* **2003,** *14* (5), 370-376.
111. Gilbert, M.; Shaw, W. J.; Long, J. R.; Nelson, K.; Drobny, G. P.; Giachelli, C. M.; Stayton, P. S., Chimeric Peptides of Statherin and Osteopontin That Bind Hydroxyapatite and Mediate Cell Adhesion. *Journal of Biological Chemistry* **2000,** *275* (21), 16213-16218.
112. Long, J. R.; Shaw, W. J.; Stayton, P. S.; Drobny, G. P., Structure and Dynamics of Hydrated Statherin on Hydroxyapatite As Determined by Solid-State NMR. *Biochemistry* **2001,** *40* (51), 15451-15455.
113. Autumn, K.; Liang, Y. A.; Hsieh, S. T.; Zesch, W.; Chan, W. P.; Kenny, T. W.; Fearing, R.; Full, R. J., Adhesive force of a single gecko foot-hair. *Nature* **2000,** *405* (6787), 681-685.
114. Chisholm, J. R. M.; Kelley, R., Marine ecology: Worms start the reef-building process. *Nature* **2001,** *409* (6817), 152-152.
115. Waite, J. H., Adhesion à la Moule1. *Integrative and Comparative Biology* **2002,** *42* (6), 1172-1180.
116. Waite, J. H.; Tanzer, M. L., Polyphenolic Substance of Mytilus edulis: Novel Adhesive Containing L-Dopa and Hydroxyproline. *Science* **1981,** *212* (4498), 1038.
117. Yu, M.; Hwang, J.; Deming, T. J., Role of l-3,4-Dihydroxyphenylalanine in Mussel Adhesive Proteins. *Journal of the American Chemical Society* **1999,** *121* (24), 5825-5826.
118. Burzio, L. A.; Waite, J. H., Cross-Linking in Adhesive Quinoproteins: Studies with Model Decapeptides. *Biochemistry* **2000,** *39* (36), 11147-11153.
119. Haemers, S.; Koper, G. J. M.; Frens, G., Effect of Oxidation Rate on Cross-Linking of Mussel Adhesive Proteins. *Biomacromolecules* **2003,** *4* (3), 632-640.

120. Monahan, J.; Wilker, J. J., Cross-Linking the Protein Precursor of Marine Mussel Adhesives: Bulk Measurements and Reagents for Curing. *Langmuir* **2004,** *20* (9), 3724-3729.
121. Miller, D. R.; Spahn, J. E.; Waite, J. H., The staying power of adhesion-associated antioxidant activity in <em>Mytilus californianus</em&gt. *Journal of The Royal Society Interface* **2015,** *12* (111).
122. Waite, J. H., Mussel adhesion – essential footwork. *The Journal of Experimental Biology* **2017,** *220* (4), 517.
123. Strausberg, R. L.; Link, R. P., Protein-based medical adhesives. *Trends in biotechnology* **1990,** *8*, 53-57.
124. Waite, J. H., Nature's underwater adhesive specialist. *International Journal of Adhesion and Adhesives* **1987,** *7* (1), 9-14.
125. Vreeland, V.; Waite, J. H.; Epstein, L., Minireview—polyphenols and oxidases in substratum adhesion by marine algae and mussels. *Journal of Phycology* **1998,** *34* (1), 1-8.
126. Matos-Pérez, C. R.; White, J. D.; Wilker, J. J., Polymer composition and substrate influences on the adhesive bonding of a biomimetic, cross-linking polymer. *Journal of the American Chemical Society* **2012,** *134* (22), 9498-9505.
127. Sever, M. J.; Weisser, J. T.; Monahan, J.; Srinivasan, S.; Wilker, J. J., Metal-mediated cross-linking in the generation of a marine-mussel adhesive. *Angewandte Chemie* **2004,** *116* (4), 454-456.
128. Mehdizadeh, M.; Weng, H.; Gyawali, D.; Tang, L.; Yang, J., Injectable citrate-based mussel-inspired tissue bioadhesives with high wet strength for sutureless wound closure. *Biomaterials* **2012,** *33* (32), 7972-7983.
129. Mehdizadeh, M.; Yang, J., Design strategies and applications of tissue bioadhesives. *Macromolecular bioscience* **2013,** *13* (3), 271-288.
130. Senhaji, O.; Robin, J. J.; Achchoubi, M.; Boutevin, B., Synthesis and characterization of new methacrylic phosphonated surface active monomer. *Macromolecular Chemistry and Physics* **2004,** *205* (8), 12.
131. Avci, D.; Albayrak, A. Z., Synthesis and copolymerization of new phosphorus-containing acrylates. *Journal of Polymer Science Part A: Polymer Chemistry* **2003,** *41* (14), 2207-2217.
132. Wyman, P.; Crook, V. L.; Hunt, B. J.; Ebdon, J. R., Improved synthesis of phosphorus-containing styrenic monomers. *Designed Monomers and Polymers* **2004,** *7* (3), 301-309.
133. Monge, S., Polymerization of Phosphorus-Containing (Meth)acrylate Monomers. In *Phosphorus based Polymers*, Monge, S.; Ghislain, D., Eds. 22 May 2014; pp P001-318.
134. Grøndahl, L.; Cardona, F.; Chiem, K.; Wentrup-Byrne, E., Preparation and characterization of the copolymers obtained by grafting of monoacryloxyethyl phosphate onto polytetrafluoroethylene membranes and poly(tetrafluoroethylene-co-hexafluoropropylene) films. *Journal of Applied Polymer Science* **2002,** *86* (10), 2550-2556.
135. Monge, S.; Canniccioni, B.; Graillot, A.; Robin, J.-J., Phosphorus-Containing Polymers: A Great Opportunity for the Biomedical Field. *Biomacromolecules* **2011,** *12* (6), 1973-1982.
136. Heiss, C.; Hahn, N.; Wenisch, S.; Alt, V.; Pokinskyj, P.; Horas, U.; Kilian, O.; Schnettler, R., The tissue response to an alkylene bis(dilactoyl)-methacrylate bone adhesive. *Biomaterials* **2005,** *26* (12), 1389-1396.

137. Grossterlinden, L.; Janssen, A.; Schmitz, N.; Priemel, M.; Pogoda, P.; Amling, M.; Rueger, J. M.; Linhart, W., Deleterious tissue reaction to an alkylene bis(dilactoyl)-methacrylate bone adhesive in long-term follow up after screw augmentation in an ovine model. *Biomaterials* **2006,** *27* (18), 3379-3386.
138. Gruber, H. General information on the functionalization of atomic force microscopy (AFM) tips via long, flexible polyethylene glycol (PEG) chains http://www.jku.at/biophysics/content/e257042/e257047/02_systematic_overview_2016_05_06_eng.pdf (accessed 11.12.2017).
139. Canniccioni, B.; Monge, S.; David, G.; Robin, J.-J., RAFT polymerization of dimethyl(methacryloyloxy)methyl phosphonate and its phosphonic acid derivative: a new opportunity for phosphorus-based materials. *Polymer Chemistry* **2013,** *4* (13), 3676-3685.
140. Montheard, J.-P.; Chatzopoulos, M.; Chappard, D., 2-hydroxyethyl methacrylate (HEMA): chemical properties and applications in biomedical fields. *Journal of Macromolecular Science, Part C: Polymer Reviews* **1992,** *32* (1), 1-34.
141. Francová, D.; Kickelbick, G., Synthesis of methacrylate-functionalized phosphonates and phosphates with long alkyl-chain spacers and their self-aggregation in aqueous solutions. *Monatshefte für Chemie-Chemical Monthly* **2009,** *140* (4), 413.
142. Winkel, A.; Dempwolf, W.; Gellermann, E.; Sluszniak, M.; Grade, S.; Heuer, W.; Eisenburger, M.; Menzel, H.; Stiesch, M., Introducing a semi-coated model to investigate antibacterial effects of biocompatible polymers on titanium surfaces. *International journal of molecular sciences* **2015,** *16* (2), 4327-4342.
143. Pfaffenroth, C.; Winkel, A.; Dempwolf, W.; Gamble, L. J.; Castner, D. G.; Stiesch, M.; Menzel, H., Self-Assembled Antimicrobial and Biocompatible Copolymer Films on Titanium. *Macromolecular bioscience* **2011,** *11* (11), 1515-1525.
144. Lee, M.; Kim, H.; Seo, J.; Kang, M.; Kang, S.; Jang, J.; Lee, Y.; Seo, J.-H., Surface zwitterionization: Effective method for preventing oral bacterial biofilm formation on hydroxyapatite surfaces. *Applied Surface Science* **2018,** *427*, 517-524.
145. D'Alelio, G. F. Halogenated esters of phosphorus-containing acids. 1977.
146. D'Alelio, G. F. Halogenated esters of phosphorus-containing acids. 1975.
147. Misato, A.; Kou, S.; Honma, Y.; Takeda, M.; Konno, K.; Fuka, N. Ethylphosphonate analogs as bactericides and fungicides. 02.11.1976, 1976.
148. Smit, C.; Hennink, W.; De Ruiter, B.; Luiken, A.; Marsman, M.; Bouwma, J. In *RadTech'90 North Am*, Conf Proc, 1990; pp 148-153.
149. Rajalakshmi, K.; Krishnan, P. S. G.; Nayak, S. K., Synthesis of dialkyl 2-(Methacryloyloxyethyl) phosphonates, their characterization and polymerization. *Polymer Science Series B* **2015,** *57* (5), 408-416.
150. Jeanmaire, T.; Hervaud, Y.; David, G.; Boutevin, B., New Phosphonated Methacrylate Monomers with C2/C3 Spacers. *Phosphorus, Sulfur, and Silicon and the Related Elements* **2008,** *183* (9), 2204-2213.
151. Moszner, N.; Zeuner, F.; Fischer, U. K.; Rheinberger, V., Monomers for adhesive polymers, 2. Synthesis and radical polymerisation of hydrolytically stable acrylic phosphonic acids. *Macromolecular Chemistry and Physics* **1999,** *200* (5), 1062–1067.

152. Mitsukami, Y.; Donovan, M. S.; Lowe, A. B.; McCormick, C. L., Water-Soluble Polymers. 81. Direct Synthesis of Hydrophilic Styrenic-Based Homopolymers and Block Copolymers in Aqueous Solution via RAFT. *Macromolecules* **2001,** *34* (7), 2248-2256.
153. Benaglia, M.; Rizzardo, E.; Alberti, A.; Guerra, M., Searching for More Effective Agents and Conditions for the RAFT Polymerization of MMA: Influence of Dithioester Substituents, Solvent, and Temperature. *Macromolecules* **2005,** *38* (8), 3129-3140.
154. Kurzer, F.; Lawson, A., Thiobenzoylthioglycolic Acid. In *Organic Syntheses*, John Wiley & Sons, Inc.: 2003.
155. Kunihiro, H.; Ozaki, T., Zinc chlorinated dithiobenzoates. Google Patents: 1972.
156. Becke, F.; Hagen, H., Production of aromatic dithiocarboxylic acids. Google Patents: 1972.
157. Plummer, R.; Goh, Y.-K.; Whittaker, A. K.; Monteiro, M. J., Effect of Impurities in Cumyl Dithiobenzoate on RAFT-Mediated Polymerizations. *Macromolecules* **2005,** *38* (12), 5352-5355.
158. Aamer, K. A.; Tew, G. N., RAFT polymerization of a novel activated ester monomer and conversion to a terpyridine-containing homopolymer. *Journal of Polymer Science Part A: Polymer Chemistry* **2007,** *45* (23), 5618-5625.
159. Unger, S., Lebende radikalische Polymerisation von (Glyco-)Monomeren mittels reversible Addition-Fragmentation Chain Transfer (RAFT). In *Lebende radikalische Polymerisation*, 2010.
160. Thang, S. H.; Chong, Y. K.; Mayadunne, R. T. A.; Moad, G.; Rizzardo, E., A novel synthesis of functional dithioesters, dithiocarbamates, xanthates and trithiocarbonates. *Tetrahedron Letters* **1999,** *40* (12), 2435-2438.
161. Vega-Rios, A.; Licea-Claveríe, A., Controlled Synthesis of Block Copolymers containing N-isopropylacrylamide by Reversible Addition-Fragmentation Chain-Transfer (RAFT) Polymerization. *Journal of the Mexican Chemical Society* **2011,** *55*, 21-32.
162. Matyjaszewski, K.; Davis, T. P.; Barner-Kowollik, C.; Vana, P., The Kinetics of Free-Radical Polymerization. In *Handbook of Radical Polymerization*, John Wiley & Sons, Inc.: 2002; pp 187-261.
163. Weaver, J. V. M.; Bannister, I.; Robinson, K. L.; Bories-Azeau, X.; Armes, S. P.; Smallridge, M.; McKenna, P., Stimulus-Responsive Water-Soluble Polymers Based on 2-Hydroxyethyl Methacrylate. *Macromolecules* **2004,** *37* (7), 2395-2403.
164. David, G.; Asri, Z. E.; Rich, S.; Castignolles, P.; Guillaneuf, Y.; Lacroix-Desmazes, P.; Boutevin, B., Peculiar Behavior of Degenerative Chain Transfer Polymerization of a Phosphonated Methacrylate. *Macromolecular Chemistry and Physics* **2009,** *210* (8), 631-639.
165. Chen, M.; Moad, G.; Rizzardo, E., Thiocarbonylthio end group removal from RAFT-synthesized polymers by a radical-induced process. *Journal of Polymer Science Part A: Polymer Chemistry* **2009,** *47* (23), 6704-6714.
166. Chong, Y. K.; Le, T. P. T.; Moad, G.; Rizzardo, E.; Thang, S. H., A More Versatile Route to Block Copolymers and Other Polymers of Complex Architecture by Living Radical Polymerization: The RAFT Process. *Macromolecules* **1999,** *32* (6), 2071-2074.

167. Moad, G.; Rizzardo, E.; Thang, S. H., End-functional polymers, thiocarbonylthio group removal/transformation and reversible addition–fragmentation–chain transfer (RAFT) polymerization. *Polymer International* **2011,** *60* (1), 9-25.
168. O'Reilly, R. K.; Chong, Y. K.; Moad, G.; Rizzardo, E.; Thang, S. H., Thiocarbonylthio End Group Removal from RAFT-Synthesized Polymers by Radical-Induced Reduction. *Macromolecules* **2007,** *40* (13), 4446-4455.
169. Xu, J.; He, J.; Fan, D.; Wang, X.; Yang, Y., Aminolysis of Polymers with Thiocarbonylthio Termini Prepared by RAFT Polymerization: The Difference between Polystyrene and Polymethacrylates. *Macromolecules* **2006,** *39* (25), 8616-8624.
170. Lima, V.; Jiang, X.; Brokken-Zijp, J.; Schoenmakers, P. J.; Klumperman, B.; Van Der Linde, R., Synthesis and characterization of telechelic polymethacrylates via RAFT polymerization. *Journal of Polymer Science Part A: Polymer Chemistry* **2005,** *43* (5), 959-973.
171. Boyer, C.; Liu, J.; Bulmus, V.; Davis, T., *RAFT Polymer End-Group Modification and Chain Coupling/Conjugation Via Disulfide Bonds*. 2009; Vol. 62.
172. Patton, D. L.; Mullings, M.; Fulghum, T.; Advincula, R. C., A Facile Synthesis Route to Thiol-Functionalized α,ω-Telechelic Polymers via Reversible Addition Fragmentation Chain Transfer Polymerization. *Macromolecules* **2005,** *38* (20), 8597-8602.
173. Scales, C. W.; Convertine, A. J.; McCormick, C. L., Fluorescent Labeling of RAFT-Generated Poly(N-isopropylacrylamide) via a Facile Maleimide−Thiol Coupling Reaction. *Biomacromolecules* **2006,** *7* (5), 1389-1392.
174. H. Northrop, B.; H. Frayne, S.; U. Choudhary, U., *Thiol-Maleimide "Click" Chemistry: Evaluating the Influence of Solvent, Initiator, and Thiol on the Reaction Mechanism, Kinetics, and Selectivity*. 2015; Vol. 6.
175. Espeel, P.; Du Prez, F. E., One-pot multi-step reactions based on thiolactone chemistry: A powerful synthetic tool in polymer science. *European Polymer Journal* **2015,** *62*, 247-272.
176. Olofsson, K.; Granskog, V.; Cai, Y.; Hult, A.; Malkoch, M., Activated dopamine derivatives as primers for adhesive-patch fixation of bone fractures. *RSC Advances* **2016,** *6* (31), 26398-26405.
177. Gruber, H. Functionalization of AFM tips with Maleimide Linkers. http://www.jku.at/biophysics/content/e257042/e257052/07_AFM_tip_with_maleimide_2016_05_06_eng.pdf (accessed 11.12.2017).
178. Moya, A.; Cherevan, A.; Marchesan, S.; Gebhardt, P.; Prato, M.; Eder, D.; Vilatela, J. J., Oxygen vacancies and interfaces enhancing photocatalytic hydrogen production in mesoporous CNT/TiO2 hybrids. *Applied Catalysis B: Environmental* **2015,** *179* (Supplement C), 574-582.
179. Pasternack, R. M.; Rivillon Amy, S.; Chabal, Y. J., Attachment of 3-(Aminopropyl)triethoxysilane on Silicon Oxide Surfaces: Dependence on Solution Temperature. *Langmuir* **2008,** *24* (22), 12963-12971.
180. Fujiwara, H., Introduction to Spectroscopic Ellipsometry. In *Spectroscopic Ellipsometry*, John Wiley & Sons, Ltd: 2007; pp 1-11.
181. Ebner, A.; Wildling, L.; Zhu, R.; Rankl, C.; Haselgrübler, T.; Hinterdorfer, P.; Gruber, H. J., Functionalization of Probe Tips and Supports for Single-Molecule Recognition Force Microscopy. In *STM and AFM Studies on*

*(Bio)molecular Systems: Unravelling the Nanoworld*, Samorì, P., Ed. Springer Berlin Heidelberg: Berlin, Heidelberg, 2008; pp 29-76.
182. Gruber, H. Amino-functionalization of AFM tips (and supports). http://www.jku.at/biophysics/content/e257042/e257048/03_AFM_tip_aminofunctionalization_2016_05_06_eng.pdf (accessed 11.12.2017).
183. Ebner, A.; Hinterdorfer, P.; Gruber, H. J., Comparison of different aminofunctionalization strategies for attachment of single antibodies to AFM cantilevers. *Ultramicroscopy* **2007,** *107* (10–11), 922-927.
184. Kumar, R.; Ramakrishna, S. N.; Naik, V. V.; Chu, Z.; Drew, M. E.; Spencer, N. D.; Yamakoshi, Y., Versatile method for AFM-tip functionalization with biomolecules: fishing a ligand by means of an in situ click reaction. *Nanoscale* **2015,** *7* (15), 6599-6606.
185. Vadillo-Rodríguez, V.; Busscher, H. J.; Norde, W.; de Vries, J.; Dijkstra, R. J. B.; Stokroos, I.; van der Mei, H. C., Comparison of Atomic Force Microscopy Interaction Forces between Bacteria and Silicon Nitride Substrata for Three Commonly Used Immobilization Methods. *Applied and Environmental Microbiology* **2004,** *70* (9), 5441-5446.
186. Grandbois, M.; Beyer, M.; Rief, M.; Clausen-Schaumann, H.; Gaub, H. E., How Strong Is a Covalent Bond? *Science* **1999,** *283* (5408), 1727.
187. Gabai, R.; Segev, L.; Joselevich, E., Single Polymer Chains as Specific Transducers of Molecular Recognition in Scanning Probe Microscopy. *Journal of the American Chemical Society* **2005,** *127* (32), 11390-11398.
188. Hinterdorfer, P.; Gruber, H. J.; Kienberger, F.; Kada, G.; Riener, C.; Borken, C.; Schindler, H., Surface attachment of ligands and receptors for molecular recognition force microscopy. *Colloids and Surfaces B: Biointerfaces* **2002,** *23* (2–3), 115-123.
189. Haselgruebler, T.; Amerstorfer, A.; Schindler, H.; Gruber, H. J., Synthesis and Applications of a New Poly(ethylene glycol) Derivative for the Crosslinking of Amines with Thiols. *Bioconjugate Chemistry* **1995,** *6* (3), 242-248.
190. Gruber, H. Flexible attachment of antibodies and other sensor molecules to the measuring tips of force microscopes. http://www.jku.at/biophysics/content/e257042/e257046/01_simple_introduction_2016_05_06_eng.pdf (accessed 11.12.2017).
191. Pfreundschuh, M.; Alsteens, D.; Wieneke, R.; Zhang, C.; Coughlin, S. R.; Tampé, R.; Kobilka, B. K.; Müller, D. J., Identifying and quantifying two ligand-binding sites while imaging native human membrane receptors by AFM. *Nature Communications* **2015,** *6*, 8857.
192. Gruber, H. Functionalization of AFM tips with Biotin. http://www.jku.at/biophysics/content/e257042/e257049/04_AFM_tip_with_biotin_2016_05_06_eng.pdf (accessed 11.12.2017).
193. Gruber, H. Functionalization of AFM tips with Acetal Linkers. http://www.jku.at/biophysics/content/e257042/e257051/06_AFM_tip_with_acetal_2016_05_06_eng.pdf (accessed 11.12.2017).
194. Gruber, H. Functionalization of AFM tips with Aldehyde Linkers. http://www.jku.at/biophysics/content/e257042/e257050/05_AFM_tip_with_aldehyde_2016_05_06_eng.pdf (accessed 11.12.2017).
195. Kamruzzahan, A. S. M.; Ebner, A.; Wildling, L.; Kienberger, F.; Riener, C. K.; Hahn, C. D.; Pollheimer, P. D.; Winklehner, P.; Hölzl, M.; Lackner, B.; Schörkl, D. M.; Hinterdorfer, P.; Gruber, H. J., Antibody Linking to Atomic

Force Microscope Tips via Disulfide Bond Formation. *Bioconjugate Chemistry* **2006,** *17* (6), 1473-1481.
196. Yoshimura, S. H.; Takahashi, H.; Otsuka, S.; Takeyasu, K., Development of glutathione-coupled cantilever for the single-molecule force measurement by scanning force microscopy. *FEBS Letters* **2006,** *580* (16), 3961-3965.
197. Wildling, L.; Rankl, C.; Haselgrübler, T.; Gruber, H. J.; Holy, M.; Newman, A. H.; Zou, M.-F.; Zhu, R.; Freissmuth, M.; Sitte, H. H.; Hinterdorfer, P., Probing Binding Pocket of Serotonin Transporter by Single Molecular Force Spectroscopy on Living Cells. *Journal of Biological Chemistry* **2012,** *287* (1), 105-113.
198. Riener, C. K.; Stroh, C. M.; Ebner, A.; Klampfl, C.; Gall, A. A.; Romanin, C.; Lyubchenko, Y. L.; Hinterdorfer, P.; Gruber, H. J., Simple test system for single molecule recognition force microscopy. *Analytica Chimica Acta* **2003,** *479* (1), 59-75.
199. Ikai, A., *The world of nano-biomechanics*. Elsevier: 2016.
200. Evans, E.; Kinoshita, K.; Simon, S.; Leung, A., Long-lived, high-strength states of ICAM-1 bonds to β 2 integrin, I: lifetimes of bonds to recombinant α L β 2 under force. *Biophysical journal* **2010,** *98* (8), 1458-1466.
201. Williams, P. M., Analytical descriptions of dynamic force spectroscopy: behaviour of multiple connections. *Analytica Chimica Acta* **2003,** *479* (1), 107-115.
202. Rankl, C.; Kienberger, F.; Wildling, L.; Wruss, J.; Gruber, H. J.; Blaas, D.; Hinterdorfer, P., Multiple receptors involved in human rhinovirus attachment to live cells. *Proceedings of the National Academy of Sciences* **2008,** *105* (46), 17778-17783.
203. Lamprecht, C.; Plochberger, B.; Ruprecht, V.; Wieser, S.; Rankl, C.; Heister, E.; Unterauer, B.; Brameshuber, M.; Danzberger, J.; Lukanov, P., A single-molecule approach to explore binding, uptake and transport of cancer cell targeting nanotubes. *Nanotechnology* **2014,** *25* (12), 125704.
204. Baumgartner, W.; Hinterdorfer, P.; Schindler, H., Data analysis of interaction forces measured with the atomic force microscope. *Ultramicroscopy* **2000,** *82* (1), 85-95.
205. Oesterhelt, F.; Rief, M.; Gaub, H., Single molecule force spectroscopy by AFM indicates helical structure of poly (ethylene-glycol) in water. *New Journal of Physics* **1999,** *1* (1), 6.
206. BrukerNanoInc Bruker's silicon nitride Probe - Cantilever Layouts. https://www.brukerafmprobes.com/Images/SiN%20Sheet.jpg (accessed 11.12.2017).